The University of Sheffield

Faculty of Engineering

Department of Materials Science and Engineering

Interconnected Pickering Polymerized High Internal Phase Emulsions

Enes Durgut

A thesis submitted in fulfillment of the requirements for the degree of Doctor of Philosophy

September 2023

Abstract

High internal phase emulsions are used as a template to produce highly porous and interconnected polymeric materials. The method simply relies on the solidification of the continuous phase and the removal of the internal phase. Consequently, materials with a porosity correlated with the amount of the internal phase are obtained. If the solidification of the continuous phase involves the polymerization, the resultant material is called Polymerized High Internal Phase Emulsions (PolyHIPE). Since the method relies on the preparation of emulsion, it necessitates the utilization emulsion stabilizer. Surfactants are commonly used stabilizers to obtain interconnected and porous PolyHIPEs. Alternative stabilizers are solid particles, the emulsion stabilized with the colloidal particles are called Pickering emulsions. Although Pickering emulsions offer various advantages over surfactants, the obtained PolyHIPE from Pickering HIPEs do not exhibit interconnected porous structures since they do not exhibit pore throats unlike PolyHIPEs obtained from surfactant stabilized HIPE. On the other hand, the formation of pore throats is still under debate. While Pickering PolyHIPEs are known for their closed cellular structure, there are a few reports demonstrating the interconnected Pickering PolyHIPEs, without mentioning the details of how they are formed. In this study, we investigated the pore throat formation in Pickering PolyHIPEs and proposed a new mechanism in pore throat formation in Pickering PolyHIPEs for the first time. The effect of various parameters on the formation of pore throats is evaluated; particle size, particle concentration, internal phase volume, and particle type. The investigation led us to conclude that the arrested coalescence phenomenon, observed in Pickering emulsion droplets, can be the mechanism. Further, the effect of particle hydrophilicity was evaluated on Pickering PolyHIPE morphology, as well as on HIPE rheology and emulsion interfacial rheology. It is concluded that as the particle hydrophilicity increases, previously observed atypical; large, and interconnected porous Pickering PolyHIPE morphology turns into a typical closed porous Pickering PolyHIPE. Additionally, the closed pores are found to be well-decorated with hydrophilic particles. Furthermore, it is hypothesized that the utilization of both hydrophobic and hydrophilic particles as HIPE stabilizers can lead to the formation of interconnected and hydrophilic particle-decorated porous Pickering PolyHIPE. ZIF-8 is chosen as a functional and hydrophilic co-stabilizer. The efficacy of ZIF-8 decoration on the pores of PolyHIPEs is investigated and it was found that the hydrophobic-hydrophilic particle co-stabilization efficiently produces interconnected and ZIF-8 decorated Pickering PolyHIPEs.

Acknowledgments

I would like to thank and honor every single person, one by one, during my four years of PhD. The selection criteria for the people I will thank are based on the principle that their good actions outweigh the harm they may have caused. I didn't use the 'titles'.

I would like to thank supervisors: **Frederik 'Hocam' Claeyssens**, my primary supervisor, for everything. We have different styles that do not always match, and this mismatch sometimes caused trouble for us. However, we managed to understand each other, especially this year, especially during the period of 'unfortunate events.' I am grateful that he stood behind me like a solid mountain. I admit that I was a PhD student with high expectations, hard to satisfy, and impatient. However, he always handled the situation gracefully. All in all, everything that happened brought us closer, and therefore, I am happy. **Reza Foudazi** for his insights into the hypotheses I proposed. His input both inspired and motivated me. Additionally, he made a significant contribution to our second research chapter. His review article, 'HIPEs to PolyHIPEs,' was inspirational, and I felt like saying, 'I wish I had authored that'. **Jonathan Foster** deserves my thanks for his contribution to the third chapter. I always enjoyed our meetings; he paid great attention to the project and put in a lot of effort, and I am grateful. **Chris Holland** personally conducted my rheology tests and brought an instrument just for my 'perfect' test. During the tests, we had a chance to talk, which I always enjoyed, and I can say I looked up to him as an academic role model.

I want to express my gratitude to my family: **Nevhan 'Misi' Durgut**, **Selen 'Ciko' Durgut**, and **Isa Durgut**. I communicated with my mother almost every day, especially this year. If I managed to get through the 'unfortunate events,' it was mainly thanks to her. She is not only a mother but also the best friend ever, the best de facto psychologist, and the best human being in the world. I am very fortunate to have been raised by her, although it sometimes creates a delusion in me that expecting everyone to be as good as her can lead to significant disappointment in the end. I would also like to thank the rest of the family members: **Ali Ucar**, **Sirpa Ucar**, **Rafet Morgul**, **Ibrahim Ucar**, **Hilal Aksular**, **Biray Karaca**, **Sakir Karaca**, **Suzan 'Cuci' Ucar**, **Selma Ucar**, **Yurdagul 'Gulos' Kilic**, **Bade Kilic**, **Yelda Keles**, **Ruzgar Keles**, **Yeliz Morgul**, and **Firat Albay**.

I would like to thank my friends/colleagues in Sheffield: **Betul Aldemir-Dikici** and **Serkan Dikici** for their warm welcome and huge support, and for being my hidden supervisors. Taking Betul's approval was always an utmost reference for me to believe that what I was doing was good. **Muhammet 'Maho' Ozsoy** and **Semra 'Semus' Tuna** for being amazing friends. Thanks to them, it always felt like 'I am not alone in here.' The majority of the best days I spent in Sheffield were with Muhammet Ozsoy. **Boyang 'Comrade' Liu** for being an amazing friend. I always felt that I was special/different to him. Whenever

I looked for something in the lab, he always left his work and searched with me. Thanks for all the 'gifts from communism'. **Fernanda 'Maria' Valezquez** and **Andy Cooke**, the party people. Although organizing things was generally very hard, the outcome always warranted the effort. **Areli Munive Olarte**, the new gaming night organizer and the new defender of Pickering PolyHIPEs, a small girl with a huge heart. **Nihan 'Niho' Sengokmen-Ozsoz**, for her company and her help, especially during the 'revision period,' handling things with the speed of light. **Giorgos 'Giogio' Tyreas**, a rarely found good person. We became solid friends in a very limited period of time and still are. **Ana Castellanos** and **David Ramos**: We had lots of fun, and they provided amazing support. We are still in touch from miles away for years. **Colin Sherborne**, especially for introducing me to the world of Pickering PolyHIPE and being a good friend. **Emmanual 'Emem' Asare**, or Mr. Emmanuel, always being good to me, inviting me to the baby dedication. **Mina Aleemardani** for being good, always good, pure good. I would also like to thank **Sarah Shafaat**, **Ilkin Ozsoz**, **Sara Memarpour Hobbi**, **Zeming Cheng**, **Meghna Suvarna**, **Anthony Bullock**, **Mahendra Raut**, **Anabelle Fricker**, **Benedict Smith**, **Oguzhan Kivan**, **Jonathan Hinchcliffe**, **Dila Hatun Sal**, **Louis Johnson**, and **Rachel Furmidge**.

I would like to thank my friends outside Sheffield: **Suleyman 'Suly' Gunal**; the hardest person in the world, but an amazing friend. We nearly chatted every day, and he knew everything about what was going on in Sheffield. **Betul 'Bet' Haykir**, although we couldn't manage to see each other, always kept me comfortable from miles away. **Utku Horzum**, our long-lasting heartbroken state just ended this year. We video-called weekly, and he specifically came to Sheffield to support me during the 'unfortunate events.' Many thanks. **Mustafa and Melis Tuncer**, my old friend and his lovely wife, for hosting me, and coming to our wedding from miles away. **Vecdi 'Ustat' Sen**, another pure good person, for our monthly hour-long conversations. I would also like to thank **Volkan 'Volki' Arslan**, **Emrah Acaroz**, **Fulya Akcimen**, **Ezgi Ozkurt**, **Manuel Hoffmann**, **Muvaffak Soydan**, **Tuna Mutlu**, **Bugra Yas**, **Tugce Oruc**, and **Ezgi Bulbul**.

Of course, the contribution of many of the people mentioned above during the 'unfortunate events' was significant. However, in this paragraph, I would like to thank specifically the people who became close to me as a result of their support during the period of 'unfortunate events. **Francesca Cotardo**, the main actress of the period. I guess I am the main actor in her 'unfortunate events.' I am not sure about what to say exactly, but thanks for her support. I hope I was able to provide the support I intended as well. Both **Syed Mohammad Daniel** and **Santosh Tetali** for giving me the truth and ending my unawareness, my stupid concerns, and the state of feeling bad/guilty. I believe we were alienated from each other with Syed Mohammad Daniel. I apologize for adopting someone else's perspective instead of my own and acting accordingly towards him. Thanks for the support, and for all the gifts, teaching me the art of communication through GIFs; they all meant a lot. Similarly, Santosh Tetali for

all the support. I can't define how much I suffered the day that I learned what happened, and I was scared that if something happened to her as a result of defending me, I apologize for inadvertently causing trouble, and I will do my best to seek justice, even though I feel exhausted. Last but not least, **John Glennie** from Mental Health Services, for sincerely siding with me. Even at the very beginning, he stopped the session and, one by one, told me what was going to happen and what I should be doing. Thanks.

I would like to thank people for their technical support: **Vanessa Singleton**, **Cheryl Shaw**, **Oday Hussein**, **Sylwester Mikula**, **Maciej Myszczynski**, **Ian Ross**, and **Le Ma**.

I would like to thank the **Turkish Ministry of Education** for providing me with the scholarship to complete both my MSc and PhD studies.

I would like to thank **Gary Numan** and **Sidewalks and Skeleton** for their performance in Sheffield and Leeds, respectively. **Larian Studios** for developing the game Divinity Original Sin II, which kept me going during lockdown. **Kevin from Copper Pot** and **all the people working at Café Nero** (Division Street).

Academic Outputs

Publication

E. Durgut, C. Sherborne, B. Aldemir-Dikici, GC. Reilly, F. Claeyssens (2022). ''Preparation of Interconnected Pickering Polymerized High Internal Phase Emulsions by Arrested Coalescence. Langmuir. 36, 10953–10962. https://doi.org/10.1021/acs.langmuir.2c01243

E. Durgut, M. Zhou, B. Aldemir-Dikci, R. Foudazi, F. Claeyssens (2024). ''Modifying Pickering Polymerized High Internal Phase Emulsion Morphology by Adjusting Particle Hydrophilicity''. Colloids Surf. A: Physicochem. Eng., 680, 132629. https://doi.org/10.1016/j.colsurfa.2023.132629

Publication in Preparation

E. Durgut, F. Claeyssnes. ''Interconnected Pickering PolyHIPEs''

E. Durgut, J. Foster, F. Claeyssens. ''Surfactant-Free ZIF-8 Decorated and Open Porous Pickering Polymerized High Internal Phase Emulsion''

AM. Olarte, **E. Durgut**, F. Claeyssens, GC, Reilly. ''The Effect of Scaffold Porosity on MSC Proliferation and Osteogenic Differentiation''

Oral Presentation

E. Durgut, F. Claeyssens. ''Pore Throat Formation in Pickering Polymerized High Internal Phase Emulsions''

Table of Contents

List of Abbreviations

AA	Acrylic acid
AAO	Artimisia argyi oil
BET	Brunauer-Emmett-Teller
CNT	Carbon nanotubes
CTAB	Cetlytrimethlyammonium bromide
DVB	Divinyl benzene
EC	Ethyl cellulose
EDX	Energy dispersive X-ray analysis
EHA	2-ehtylhexyl acrylate
FCC	Face-centered cubic
FDTS	1H,1H,2H,2H-perfluorooctyltrichlorosilane
GO	Graphene Oxide
GPC	Gel permeation chromatography
HIPE	High Internal Phase Emulsion
HLB	Hydrophilic-lipophilic balance
IBOA	Isobornyl Acrylate
KPS	Potassium persulfate
LIPE	Low Internal Phase Emulsions
MF	Melamine-formaldehyde
MIPE	Medium Internal Phase Emulsions
MMA	Methyl methacrylate
m-MOP	Melamine-based microporous organic polymers
MO	Methyl orange
MOF	Metal-organic Framework
NMR	Nuclear magnetic resonance
ODS	Octadecyltrimethoxysilane
PCM	Phase change materials
PEG	Polyethylene glycol
P-XRD	Powder X-ray diffraction
SEM	Scanning electron microscope
St	Styrene
TEM	Transmission electron microscope
TEOS	Tetraethyl orthosilicate
TGA	Thermogravimetric analysis
THF	Tetrahydrofuran
TMPTA	Trimethylolpropane triacrylate
uCT	Micro-computed tomography
UV	Ultra-violet
VEO	Vinyl ester oligomer
VER-St	Vinyl ester resin-styrene
ZIF-8	Zeolitic imidazolate framework

List of Figures

List of Tables

Thesis Outline

This thesis presents a new mechanism for pore throat formation in Pickering PolyHIPEs through the arrested coalescence of emulsion droplets and investigates the important parameters affecting pore throat formation. The observed trend is applied to produce functional particle (ZIF-8) decorated and interconnected Pickering PolyHIPEs.

Chapter 1 defines the basic principles of emulsions, HIPE, and PolyHIPEs, with a specific focus on interconnected Pickering PolyHIPEs, as well as the applications of Pickering PolyHIPE. Chapter 2 explains arrested coalescence as a pore throat formation mechanism in Pickering PolyHIPEs and how particle size, concentration, and internal phase volume affect the interconnected morphology. Chapter 3 explores the effect of particle hydrophilicity on Pickering PolyHIPE morphology and HIPE rheology. Chapter 4 investigates the efficiency of ZIF-8 incorporation into the PolyHIPE by using either colloidal particles or surfactant as an emulsion stabilizer.

All chapters of the thesis are intended for publication. Currently, Chapters 1 and 4 are in preparation for publication, Chapter 2 is published, and Chapter 3 is under review. For the consistency of the thesis, all chapters were compiled, and minor modifications were made to the published and under-review chapters. References have been reorganized and provided at the end of the thesis.

I, Enes Durgut, confirm that the thesis is my own work, including data collection, analysis, conceptualization, and writing. The section '3.4.7 Interfacial Rheology' was conducted and written by Muchu Zhou, the second author of the submitted paper. The rest of the authors contributed to the chapters through their supervision, review, and editing.

CHAPTER 1

Interconnected Pickering Polymerized High Internal Phase Emulsions

E. Durgut [a,b], F. Claeyssens [a, b]

[a] Kroto Research Institute, Department of Materials Science and Engineering, University of Sheffield, Sheffield, United Kingdom

[b] Department of Materials Science and Engineering, INSIGNEO Institute for In Silico Medicine, The University of Sheffield, Sheffield, United Kingdom

Abstract

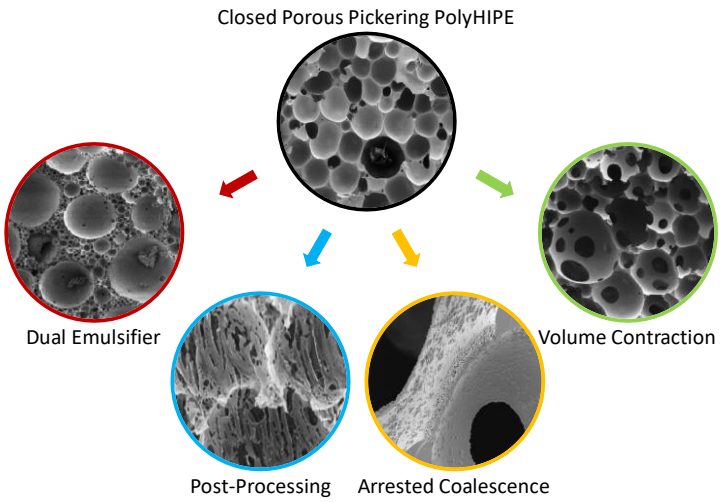

Pickering-polymerized high internal phase emulsions have attracted attention since their successful first preparation 15 years ago, primarily owing to their large pores and the potential for functionalization during production. This review aims to elucidate the fundamental principles of Pickering emulsions, Pickering HIPEs, and Pickering PolyHIPEs while comparing them to conventional surfactant-stabilized counterparts. The morphology of Pickering PolyHIPEs, with a particular emphasis on methods for achieving interconnected structures, is explored and critically assessed. Lastly, the mechanical properties and applications of Pickering PolyHIPEs are presented.

1.1. Scope of the Review

There are several excellent reviews on both polymerized High Internal Phase Emulsions (PolyHIPE) [1–3] and Pickering emulsions [4–6] covering basic principles to current trends in the field. However, a review article specifically focusing on Pickering PolyHIPEs is currently missing in the literature. Therefore, this review article aims to provide the basic principles of emulsions, high internal phase emulsions (HIPEs), and PolyHIPEs. It will then compile reports about Pickering PolyHIPEs, investigating their morphology, properties, and applications, and comparing them with conventional PolyHIPEs where relevant. Although 'poly' in PolyHIPE stands for polymerization, porous materials obtained from HIPE templates without being polymerized are also within the scope of this review and termed as 'HIPE templates'.

1.2. Emulsions

1.2.1. Definitions and Nomenclature

Emulsions are biphasic systems formed by dispersing one immiscible liquid within another. The dispersed phase, in the form of droplets, is known as the internal (or dispersed) phase, while the other phase is the continuous (or external) phase. Emulsions can be classified based on factors such as the hydrophilicity/hydrophobicity of phases, the volume fraction of the internal phase, and the type of stabilizer used.

Water-in-oil (w/o) emulsions involve dispersing the internal water phase in a continuous oil phase, while oil-in-water (o/w) emulsions are the opposite (Fig. 1.1 A, B). Emulsions can also be oil-in-oil (o/o) or water-in-water (w/w). Based on the volume fraction of the internal phase, emulsions fall into three categories: low internal phase emulsion (LIPE) for <33% internal phase, medium internal phase emulsion (MIPE) for 33-74%, and high internal phase emulsion (HIPE) for >74% (Fig. 1.1 A, C).

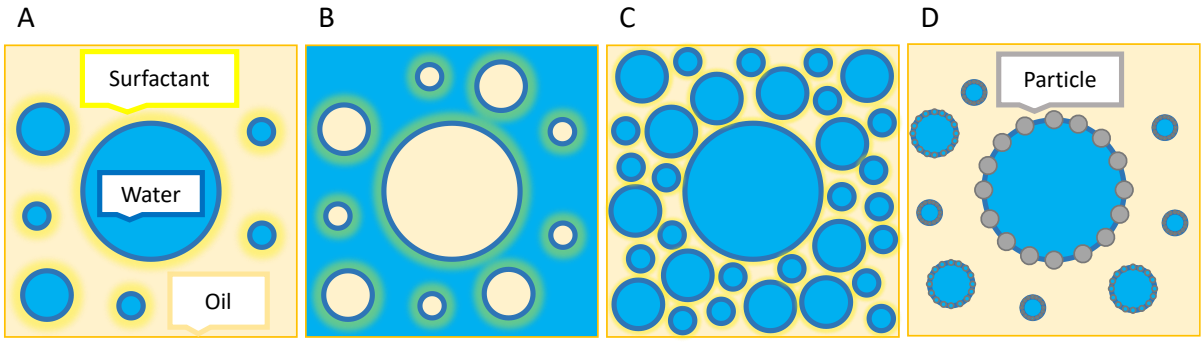

Figure 1.1: The classification of emulsions: surfactant-stabilized (conventional), w/o, LIPE (assuming that the internal phase volume is <33%) (A), o/w counterpart of A (B), HIPE counterpart of A (assuming that the internal phase volume is >74%) (C), Pickering counterpart of A (D).

Furthermore, emulsions can be classified according to the type of stabilizer used—either surfactants or colloidal particles. If the stability is achieved through surfactants, they are termed conventional emulsions. Alternatively, if colloidal particles stabilize the emulsion, it is referred to as a Pickering emulsion (Fig. 1.1 A, D). Emulsions stabilized by both surfactant and Pickering agents are termed dual emulsified emulsions.

1.2.2. Stabilization of Emulsions

An immiscible liquid can be dispersed within another immiscible liquid under shear. When the applied shear is sufficiently high, the internal phase breaks up into droplets within the continuous phase. As emulsion droplets form, the total interfacial area, and consequently, the total interfacial energy, increase within the system. When shear is removed, the dispersed emulsion droplets start to coalesce to reduce the elevated total interfacial energy, ultimately leading the two emulsion phases to separate back into their initial bulk forms. Therefore, to achieve kinetically stable emulsions, emulsion stabilizers are necessary to prevent droplet coalescence.

Conventionally, emulsions are stabilized by surfactants—amphiphilic molecules with both hydrophobic and hydrophilic parts. Due to their amphiphilic nature, surfactant molecules migrate from the generally dissolved continuous phase to the oil/water interface, where the hydrophobic and hydrophilic parts submerge in the oil and water phases, respectively. The type of surfactant determines the type of emulsion formed, either oil-in-water (o/w) or water-in-oil (w/o). Hydrophilic-Lipophilic Balance (HLB), a function of the weight percentage of the hydrophilic portion of the non-ionic surfactant molecule [7], is used to estimate the suitable surfactant for the desired emulsion type. Adsorbed surfactant molecules at the interface reduce interfacial tension between the bulk phases, lowering the energy needed for droplet formation. Emulsion droplets with adsorbed surfactant molecules on the surface are prevented from coalescing with neighboring droplets due to the steric and/or electrostatic barrier effect provided by surfactants [8]. However, surfactant adsorption and desorption at/from the oil/water interface are in thermal equilibrium, and thus, are affected by thermal fluctuations, leading to a loss of emulsion stability and phase separation.

Solid particles in colloid form are another type of stabilizer gaining attention, dating back to Ramsden's [9] and Pickering's [10] pioneering work in 1907. Unlike surfactants, colloidal particles are not necessarily amphiphilic. However, to obtain a stable emulsion, colloidal particles should be wetted in both phases. Similar to surfactants, the phase in which the colloidal particles are dispersed and wetted the most determines the continuous phase of an emulsion—either o/w or w/o. Similar to the HLB value in surfactants, wettability of particles is used to estimate appropriate particles to stabilize the desired emulsion. Because of being wetted by both phases, Pickering agents are adsorbed at the

oil/water interface during emulsification. Emulsion droplets covered with colloidal particles are mechanically protected from coalescence with other droplets. Colloidal particles do not reduce the inherent interfacial tension between two phases; therefore, the formation of emulsion droplets requires higher energy than conventional emulsions. Unlike surfactants, colloidal particles are considered to be adsorbed at the oil/water interface irreversibly [11]. Therefore, long-term emulsion stability is achieved in Pickering emulsions.

Pickering-type stabilizers are considered more efficient than surfactants. The required amount of colloidal particles to obtain stable emulsions is generally less than that of surfactants, in terms of weight percentage. For stable emulsions, full surface coverage of droplets by colloidal particles is not necessary. It was demonstrated that a droplet surface coverage as low as 29% with Pickering agents is sufficient to obtain stable emulsion droplets [12]. Additionally, insufficiently covered emulsion droplets can experience phenomena only observed in Pickering emulsions: particle bridging, limited coalescence, and arrested coalescence (Fig. 1.2). It was claimed that stable emulsions can be achieved below 29% surface coverage as well by particle bridging, which is the separation of two emulsion droplets with a monolayer of particles (Fig. 1.2 B) [13]. Additionally, insufficiently covered emulsion droplets can start to coalesce with each other until sufficient surface coverage is achieved; this phenomenon is called limited coalescence (Fig. 1.2 C). Limited coalescence observed in Pickering emulsion is considered a reason for obtaining a relatively narrow droplet size distribution [14]. Alternatively, two emulsion droplets can start to coalesce, but the coalescence can be arrested by particles collecting at and jamming the coalescing region; this phenomenon is called arrested coalescence or sometimes referred to as partial coalescence (Fig. 1.2 D) [15]. Therefore, stable emulsions can be obtained with a lower concentration of colloidal particles compared to surfactants.

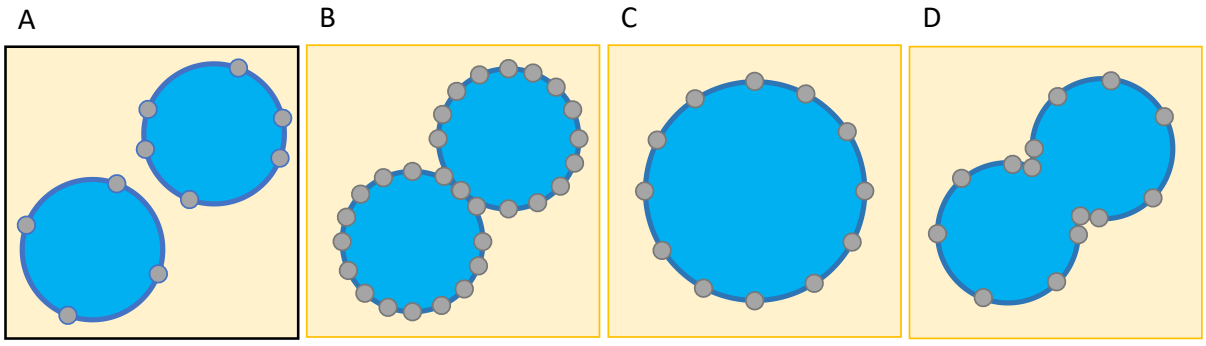

Figure 1.2: Observed phenomena in Pickering emulsions regarding the efficient stabilization of the emulsion; insufficiently covered emulsion droplets (A) can coalesce via: (1) particle bridging, two emulsion droplets are separated from each other by the monolayer of particles (B); (2) limited diffusion where the droplets coalesce until reaching the sufficient surface coverage (C); (3) arrested coalescence of two emulsion droplets, droplets start to coalesce but the coalescence is arrested due to particle jamming at the necking region (D).

Furthermore, depletion attractions can be utilized to enhance emulsion stability. Depletion attraction is an attractive force that occurs between colloidal particles when they are suspended together with smaller depletant molecules. Depletant molecules surrounding the colloidal particles exert pressure, equivalent to osmotic pressure, onto the colloidal particles. When the depletant molecules are excluded from a region between two colloidal particles, the surrounding pressure onto the colloidal particles results in the attractive force between the colloidal particles [16]. The use of depletion interaction to increase the stabilization of Pickering HIPEs has been shown by Kim *et al.* in a simple oil-in-water emulsion stabilized by colloidal silica particles, by adding PEG to the water phase (Fig. 1.3) [17]. It was demonstrated that as long as the depletant molecule (PEG) and the particles (colloidal silica) do not interact with each other strongly and they are well dispersed in the continuous phase, it is possible to obtain a stable emulsion with 90% internal phase with a surface coverage as low as 6%.

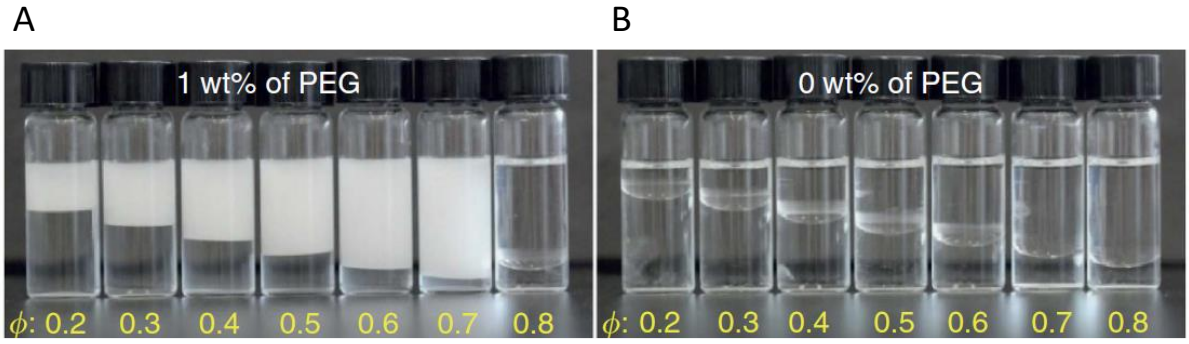

Figure 1.3: The preparation of emulsion by exploiting depletion attraction: The digital images of formation of Pickering HIPE at various internal phase fraction in the presence of depletant PEG (A) and their phase separated counterparts in the absence of depletant agent (B) [17].

1.2.3. Destabilization of Emulsions

The stability of an emulsion is defined as its resistance against changes in physicochemical behavior over time [18]. The physicochemical behaviour of an emulsion is related to the interactions between emulsion droplets, significantly influenced by the nature of the stabilizer and the stabilization mechanism. Emulsion destabilization mechanisms include phase inversion, gravitational separation, Ostwald ripening, and coalescence.

Phase inversion results in a change in emulsion type, shifting from o/w to w/o, or vice versa. Gravitational separation arises from the density mismatch between the continuous phase and the internal phase, categorized into creaming and sedimentation. Creaming occurs when the internal phase has lower density, causing emulsion droplets to migrate and accumulate at the top over time, resulting in two phases within the system, with the continuous phase at the bottom, and the concentrated emulsion on top (Fig. 1.4 C1). Conversely, in the case of sedimentation, if the internal phase has higher density than the continuous phase, the emulsion droplets accumulate at the bottom

(Fig. 1.4 C2). When the emulsion droplets aggregate with each other locally, this destabilization is referred to as flocculation (Fig. 1.4 C3). This is mainly due to the attractive forces between emulsion droplets such as van der Waals or electrostatic interactions, leading them to cluster [19]. Ostwald ripening is the diffusion of smaller emulsion droplets into the larger ones and mainly stems from the difference in internal (Laplace) pressure of emulsion droplets due to size difference [20]. Therefore, emulsions with broader emulsion droplet size distribution are more susceptible to Ostwald ripening (Fig. 1.4 C4). Similarly, coalescence is the merging of emulsion droplets with each other to form larger droplets (Fig. 1.4 C5). The mentioned destabilization mechanisms are interrelated, and the occurrence of one can trigger the other destabilization mechanisms as well. Consequently, as the emulsion experiences these processes, phase separation occurs where the continuous and the internal phase are separated completely from each other (Fig. 1.4 D).

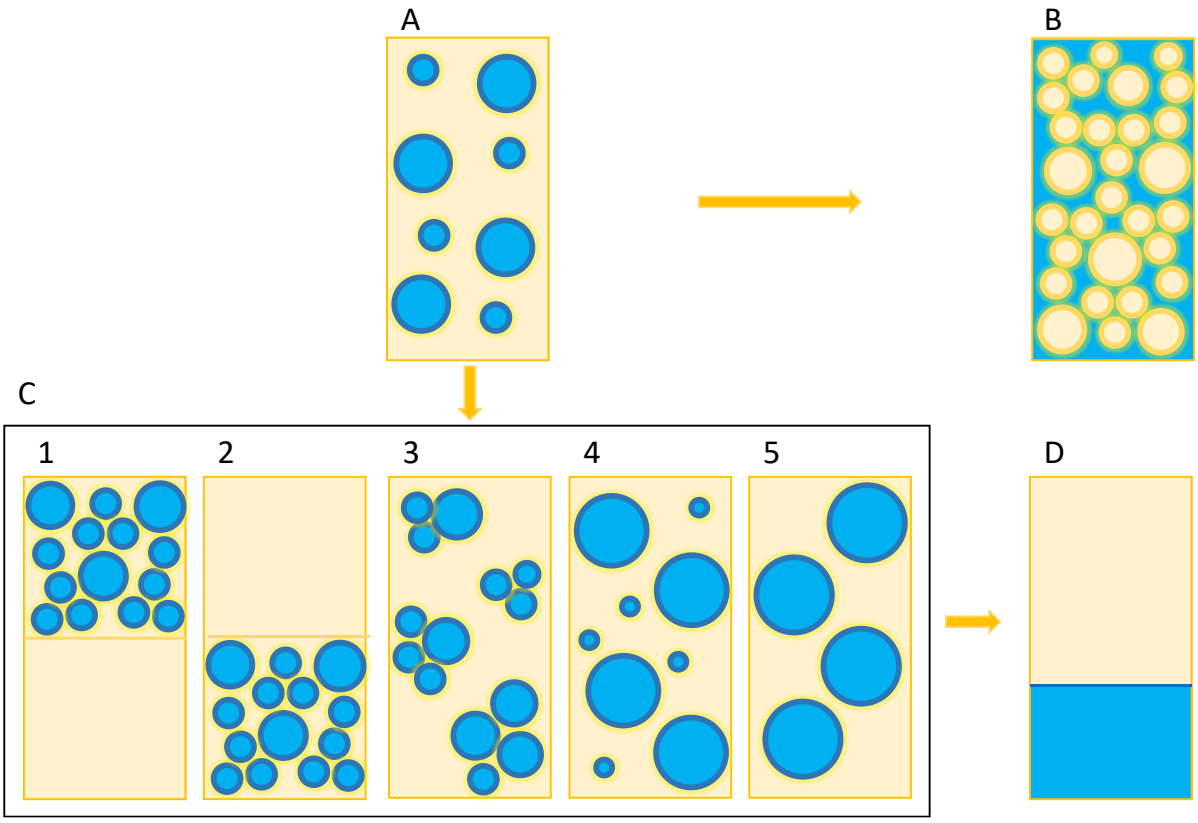

Figure 1.4: The schematic representation of emulsion destabilization mechanisms; The kinetically stabilized emulsion (A), emulsion experiencing phase inversion where the internal water phase becomes continuous phase (B), creaming (C1), sedimentation (C2), flocculation (C3), Ostwald ripening (C4), coalescence (C5) and the phase separated emulsion due to emulsion destabilization (D).

Among the mechanisms involved in emulsion destabilization, Pickering emulsions are resistant to coalescence compared to conventional emulsions. Particles are considered to adsorb to the oil/water interface irreversibly since the energy required to remove particles from the interface is a few orders of magnitude higher than the thermal energy. Therefore, the emulsion droplets are mechanically

shielded by the particles located at the o/w interface forming a physical barrier around emulsion droplets preventing the coalescence of neighbouring droplets.

The superior stability of Pickering emulsions can be a problem when the application necessitates a controlled destabilization of the emulsion or when the application results in the production of Pickering emulsion unintendedly as a by-product. Therefore, methods to destabilize Pickering emulsions are also an active area of research. Melle *et al.* applied an external magnetic field to Pickering emulsions stabilized by magnetic particles, observing that the strong magnetic field de-attaches particles from the oil/water interface to destabilize the emulsion Similarly, the application of an external electric field was reported to destabilize Pickering emulsions, not by detaching particles from the interface, but by relocating already adsorbed particles on the emulsion droplet so that the droplets can access each other to coalesce [21]. Griffith *et al.* demonstrated the destabilization of o/w Pickering emulsion by adding more hydrophobic particles to the system, causing oil droplets to preferentially wet the hydrophobic particles rather than maintaining their droplet form [22]. Kumar *et al.* reported a versatile method to induce destabilization of Pickering emulsions by induced liquid-liquid phase separation due to the addition of a solute which is soluble in both phases of the emulsion [23].

1.3. HIPE

As mentioned in the previous sections, emulsions can be classified based on the internal phase fraction, with High Internal Phase Emulsions (HIPEs) typically defined as emulsions containing over 74% internal phase. This threshold is derived from the maximum packing density of face-centered cubic, non-deformable monodisperse spheres. Theoretically, beyond a 74% internal phase fraction, monodisperse spheres are compelled to deform into polyhedra, leading to restricted mobility of internal phase droplets. These alterations are accompanied by changes in the emulsion's physical properties, particularly its rheological behaviour. Thus, the key factor distinguishing HIPEs from emulsions with lower internal phase fractions is the shift in rheological properties. Although this change is generally proportional to the internal phase fraction, a sudden increase in emulsion viscosity can be observed at volumes of internal phase lower or higher than 74%, given that emulsion droplets are typically no longer non-deformable monodisperse spheres. The HIPE-like behaviour of the emulsion is contingent upon the deformability of the liquids and the polydispersity of the emulsion droplets. Consequently, the definition of HIPEs is a subject of debate, and an alternative definition considers emulsions with an internal phase volume fraction higher than the maximally random jammed packing concentration.

HIPEs demonstrate viscoelastic behaviour due to their closely packed emulsion droplets, behaving like an elastic solid above the applied critical stress (yield stress) and a viscous liquid below it [24]. This

unique rheological property makes HIPEs suitable for applications such as 3D printing inks, as they exhibit desirable viscosity and shear-thinning behaviour [25]. Additionally, owing to their self-supporting physical state and high capacity for encapsulating molecules in the internal phase, especially with their high internal phase volume, HIPEs are attractive in the food, pharmaceutical, and cosmetic industries [26]. In the realm of material science, HIPEs serve as templates for producing highly porous materials, a topic that will be detailed in the following chapters.

1.3.1. The HIPE Preparation Process

Conventional HIPEs have been in use since 1966 [27], but the first successful preparation of Pickering HIPE and its utilization as a template were reported in 2007 by Menner *et al.* [28]. The late emergence of Pickering HIPEs can be attributed to a few factors. First, early studies reported an inversion in Pickering emulsions at high internal phase; indeed, in 1999, Binks *et al.* demonstrated that Pickering emulsions experience catastrophic phase inversion, without any sign of hysteresis during the inversion when the volume of the internal phase reaches ~70% [29]. This catastrophic phase inversion was demonstrated for both water-in-oil (w/o) and oil-in-water (o/w) emulsions. Additionally, this was supported by a thermodynamic model developed by Kralchevsky *et al.* in 2005, which predicted catastrophic phase inversion above 50% internal phase in Pickering emulsions [30]. The difference in proposed internal phase volumes between the experimental (70%) and predicted model (50%) was attributed to kinetic effects. On the other hand, advances in material science and chemistry, particularly the fast advance in inorganic nanoparticle manufacture in the early 2000s, likely contributed to the broadening of particle options as a stabilizer. This, in combination with the use of surface modification techniques, enabled obtaining particles with the desired wettability in both phases.

Similar to lower internal phase emulsions, two immiscible liquids, a suitable stabilizer, and mechanical shear are required to form an HIPE. The mechanical shear should be high enough to enable droplet break-up, and the stabilizer should locate themselves fast enough at the newly formed interface to stabilize emulsion droplets before they recoalesce. As the internal phase volume increases within the emulsion, the accompanied increase in viscosity reduces the mixing efficiency and homogeneity. Therefore, droplet break-up becomes no longer possible. Since viscosity is a limiting factor for the preparation of the HIPE, diluent solvents can be used to thin the initial phases of the emulsion.

Conventionally, the internal phase is added dropwise to the continuous phase under shear to prepare an HIPE (Fig. 1.5 A). Rather than adding the internal phase dropwise, combining all the ingredients in a container followed by simple hand shaking was reported to form an HIPE as well [31]. Alternative methods were also reported to obtain HIPEs either by using phase inversion or forced sedimentation

(Fig. 1.5 B). Sun *et al.* reported that it is possible to turn a particle-stabilized oil-in-water low internal phase emulsion (LIPE) into a water-in-oil HIPE via phase inversion by simply changing the pH or salt concentration of the water phase. This changes the colloidal ionizable poly(styrene-co-methacrylic acid) particle wettability and the stability of the HIPE [32]. This was further illustrated via using other ionizable particles (sulfonated polystyrene) [33] and CO_2-responsive block copolymer [34], which wettability can be tuned by either changing the salt/pH and CO2 concentration of the emulsion, respectively, so that the particles favourably stabilize the inverted emulsion. Alternatively, LIPEs or MIPEs can be forced to sediment (i.e., by centrifugation) so that the excess continuous phase is separated from the highly concentrated part of the emulsion [35–37].

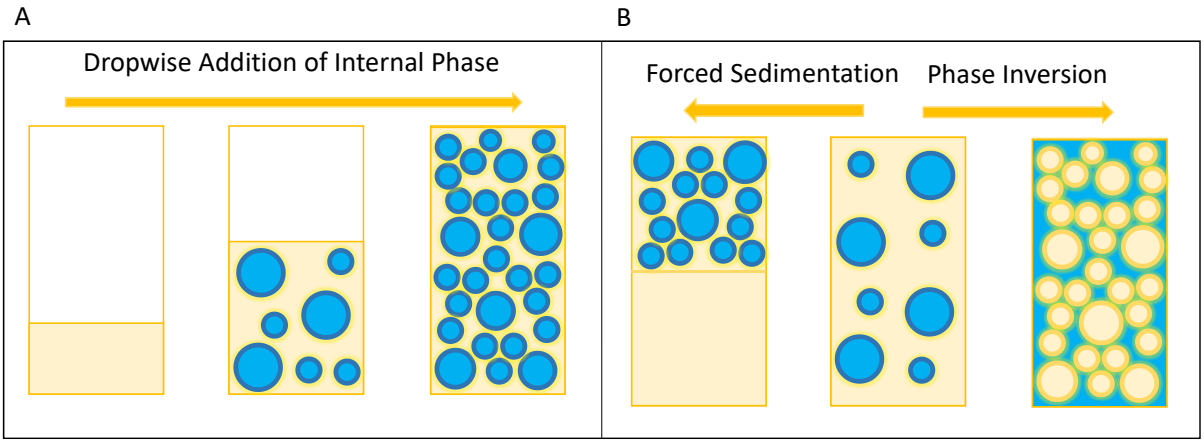

Figure 1.5: The methods to prepare HIPE is schematically represented: Conventional preparation of HIPE where the internal phase is being added dropwise and slowly while the emulsion is being mixed (A) and the production of HIPE from dilute emulsions either by forced sedimentation or phase inversion (B).

1.3.2. Rheology of HIPE

As mentioned in the previous section, (HIPEs) exhibit viscoelastic properties, displaying elastic solid and viscous liquid-like behaviour depending on the applied shear stress. In a wide range of oscillation frequencies, HIPEs exhibit constant elastic and loss modulus, with the elastic modulus being a few orders of magnitude higher than the loss modulus, indicating the viscoelastic behaviour of HIPEs [38]. The viscoelastic properties, including viscosity, elastic modulus, and yield stress, are mainly determined by the interfacial tension between the phases, mean emulsion droplet size and size distribution [39], the internal phase volume, the viscosity of the continuous and internal phase [40] and the inter-droplet interactions [41]. However, the parameters affecting HIPE rheology have a complex and significant effect on each other.

In the case of Pickering HIPEs, they exhibit a higher elastic modulus than that of conventional HIPEs. The increased elasticity of the Pickering HIPEs is attributed to a rigid interfacial layer due to attractive interactions between solid particles (Fig. 1.6 A) [42]. Recently, Kaganyuk *et al.* revealed the effect of

excluded effective internal phase volume due to the size difference between surfactants and colloidal particles (Fig. 1.6 B) and attractive lateral capillary interactions among particles on Pickering HIPE rheology (Fig. 1.6 C) [43].

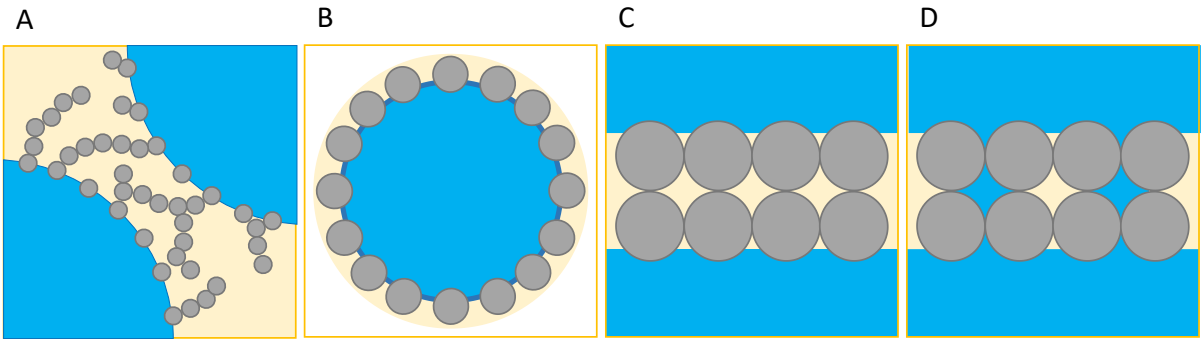

Figure 1.6: The schematic representation of mechanisms involved in increased Pickering HIPE elastic modulus: Interparticle interaction forming 3D network in interfacial area (A), excluded volume effect (B), lateral capillary interactions between particles (C, D).

1.3.3. Emulsion Droplets of HIPE

Theoretically, polyhedral-shaped emulsion droplets are expected when the internal phase volume exceeds the maximum packing density of monodisperse emulsion droplets. However, droplets can be spherical even at internal phase fractions reaching 90-98.5% when the emulsion droplets are polydisperse [44,45] , as the theoretical maximum packing density of polydisperse spheres can be higher than 74%. Alternatively, when the emulsion droplets are relatively small and the interfacial tension is high, emulsion droplets resist being deformed into polyhedra due to their high Laplace pressure, the pressure difference between the inside and outside of the droplet [26]. Therefore, the emulsion droplet size and distribution, as well as interfacial tension, are the main parameters determining the emulsion droplet shape in HIPEs.

The droplet size of the final emulsions is mainly determined by the interfacial tension between the phases, induced shear stress during emulsification, internal phase volume, and stabilizer-associated parameters, which will be focused on in this section. In terms of conventional HIPEs, the concentration of surfactant is inversely proportional to the obtained final droplet size. This is mainly due to the reduced interfacial tension parallel to increased surfactant concentration and the abundance of surfactant molecules, allowing a larger interfacial area to be stabilized. The typical conventional HIPE droplet size is between 1-50 µm.

In the case of Pickering HIPE, the emulsion droplet size correlates with the particle size. Levine *et al.* reported that the particle size should be an order of magnitude lower than the desired final emulsion droplet size [46]. Similar to surfactant, increased particle concentration results in smaller emulsion

droplets. However, depending on the interactions, either inter-particle or between emulsion phases and particles, a further increase in particle concentration can result in the enlargement of the HIPE droplet size. This is due to increased continuous phase viscosity due to being suspended in a higher concentration of particles, therefore increased emulsion viscosity as the internal phase fraction of the emulsion increases. Additionally, particles can flocculate due to inter-particle interactions, leading to a reduction of the effective stabilizer amount in the continuous phase. Overall, a typical Pickering HIPE droplet size is larger than in conventional HIPEs, ranging between 100-500 µm.

1.4. PolyHIPEs

HIPEs can be employed as a template to produce highly porous materials. If the continuous phase of the HIPE consists of polymerizable monomers and in the presence of an appropriate polymerization initiator, the 3D network surrounding the internal phase droplets can be polymerized. Subsequent removal of the internal phase leaves behind porous polymers, where the polymerized continuous phase forms the skeleton of the material, and the internal phase forms the pores (sometimes referred to as voids or cavities). This technique, utilizing HIPE as a template, is known as emulsion templating/HIPE templating. The material obtained via the polymerization of the continuous phase is known as a PolyHIPE (Fig. 1.7).

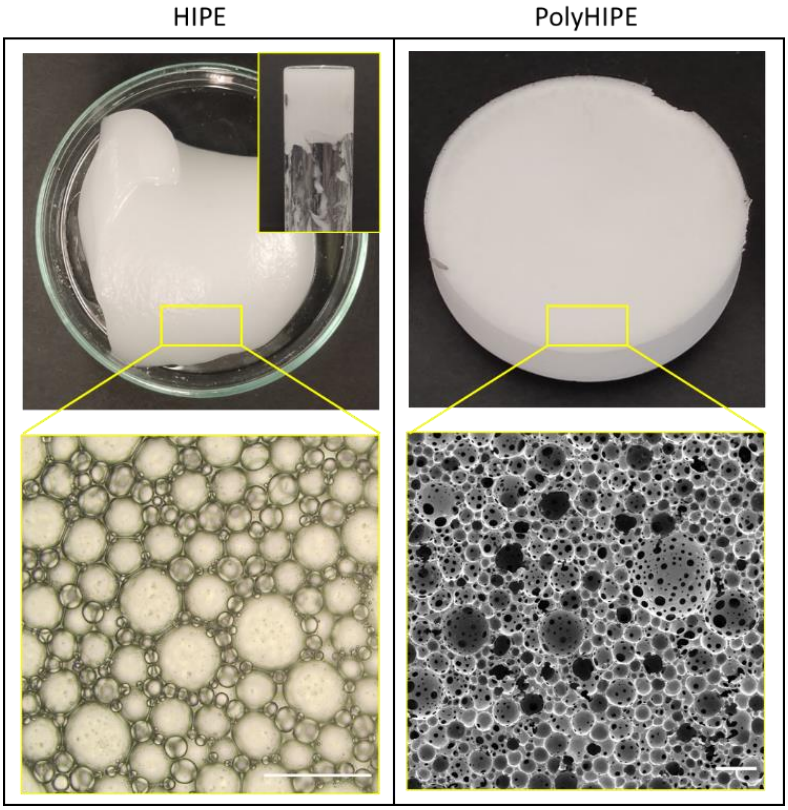

Figure 1.7: The digital images of highly viscous, self-supporting HIPE and its optical micrographs (left). The photopolymerized 3D PolyHIPE and its SEM image of the internal structure. Scale bars are 200 µm

Alternatively, the continuous phase of the HIPE can be solidified without being polymerized to obtain porous materials. Although, by definition, these are not PolyHIPEs but HIPE templates, porous materials obtained by the solidification of the continuous phase are also sometimes referred to as PolyHIPE in the literature. The comparison of conventional and Pickering PolyHIPE is presented in Figure 1.8.

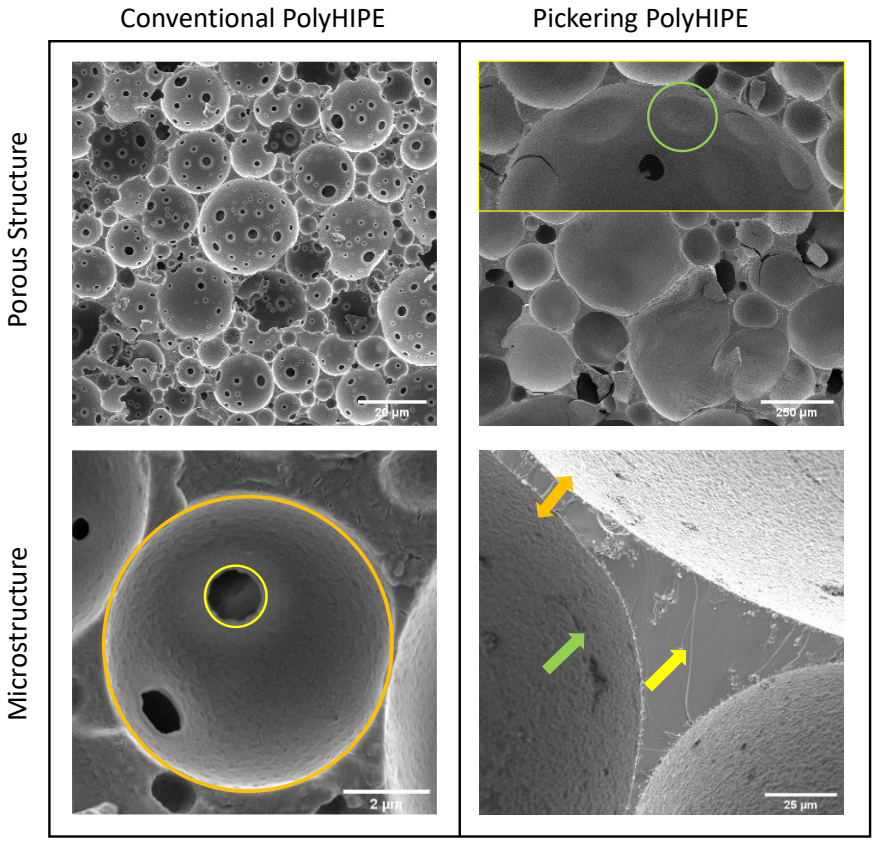

Figure 1.8: SEM Images of typical PolyHIPEs obtained by surfactant-stabilized (conventional PolyHIPEs) or colloidal particle-stabilized HIPEs (Pickering PolyHIPEs). Overall porous structure of a conventional PolyHIPE; pores and pore throats are 10 and 1 um, respectively. The orange circle highlights a pore, an imprint of HIPE droplets after being polymerized and internal phase removal. The yellow circle highlights a typical pore throat. Overall porous structure of a typical Pickering PolyHIPE with ~100 um pores without interconnecting pore throats. The green circle highlights the thin polymeric film covered pore throats. The orange arrows show the interfacial polymeric film separating two neighbouring pores, the green arrow show the pore surface and the yellow arrow show the polymerized trigonal region (Plateau border), the intersect of three pores.

In conventional PolyHIPEs, pores are interconnected through pore throats (sometimes referred to as void cavities or interconnects) on the pore surface. Pore throats, generally proportional to pore size, allow mass transfer through the material. Therefore, PolyHIPEs find applications in various fields due to their ease of manufacturing, cost efficiency, and tunable properties such as porosity, pore size and shape, interconnectivity, surface area, and mechanical properties. They are commonly used as catalyst supports, scaffolds for tissue engineering, and absorbents.

However, there are several concerns associated with conventional PolyHIPEs obtained from surfactant-stabilized HIPE. Firstly, the obtained pore size and pore throat size are small, approximately 10-50 and 1-5 µm, respectively. Such small pore size may limit their suitability for 3D tissue culture scaffolds due to restricted cell infiltration. This pore size allows for cell integration and 3D tissue culture but may impede vascularization when used for implantation, which typically requires pore sizes larger than 100 µm [47]. Secondly, the use of surfactants increases the production cost of the method, as the surfactant concentration required for producing HIPEs and PolyHIPEs is typically high (10-30 wt% of the monomer concentration [48–50]) although there are reports demonstrating <3% of surfactant can effectively produce HIPE [51–53]. Third, surfactants are associated with health and environmental toxicity. If the final product needs to be cleared from the surfactant, then this can only be achieved in a labor-intensive manner, necessitating the usage of organic solvents. Additionally, even after being washed, the leftover surfactant on the PolyHIPE can leach out. The remnants of surfactants also function as a plasticizer, reducing the mechanical properties of conventional PolyHIPE.

Pickering PolyHIPEs offer an alternative to conventional PolyHIPEs. Firstly, any surfactant-associated concerns are eliminated. Secondly, larger pore sizes can be obtained with Pickering PolyHIPEs. Colloidal particles can add interesting functionalities; they can function not only as HIPE stabilizers but also as crosslinkers. Rough pore surfaces can be obtained due to embedded particles within the pore surface, and similarly, these particles can be magnetic, light-responsive, or catalytic, enabling the production of functional PolyHIPEs in a one-pot synthesis. Third, since Pickering HIPEs exhibit superior stability, they can resist destabilization when exposed to polymerization-associated conditions, such as elevated temperature. However, Pickering PolyHIPEs exhibit one major drawback: they do not exhibit pore throats. This drawback eliminates their usage in applications where mass transfer is needed. Therefore, in this section, the morphology and applications of Pickering HIPEs will be reviewed with a focus on the methods to produce interconnected Pickering PolyHIPEs.

1.4.1. Pores

The pore size and distribution of the PolyHIPE are mainly determined by the emulsion droplets. Tuning the emulsion droplets would directly affect the pore size and distribution of the PolyHIPE. However, the deviation between droplet and pore size can occur during polymerization. This can be due to changes in emulsion stability depending on the cure rate [54] or due to volume shrinkage either by monomer-to-polymer conversion or capillary stress induced by the drying process of the material [55]. Both conventional and Pickering PolyHIPEs can experience the mentioned deviation of droplet to pore size in a similar manner. On the other hand, polymerization can affect the final PolyHIPE morphology

significantly depending on the type of initiator, in which phase the initiator is dissolved, and/or the partition coefficient of the initiator.

Polymerization of HIPE requires the initiator to be dissolved either in the continuous phase or in the internal phase. When the initiator is dissolved in the continuous phase, the polymerization starts within the polymer phase. However, if the initiator is dissolved in the internal phase, the polymerization starts from the interface, specifically from the continuous phase film surrounding the emulsion droplet. The locus of initiation affects the pore shape, the thickness of the pore walls, and the interconnectivity of the PolyHIPE. Continuous phase initiation leads to the formation of spherical and interconnected pores, while interfacial initiation results in polyhedral-shaped closed pores in conventional PolyHIPEs (Fig. 1.9).

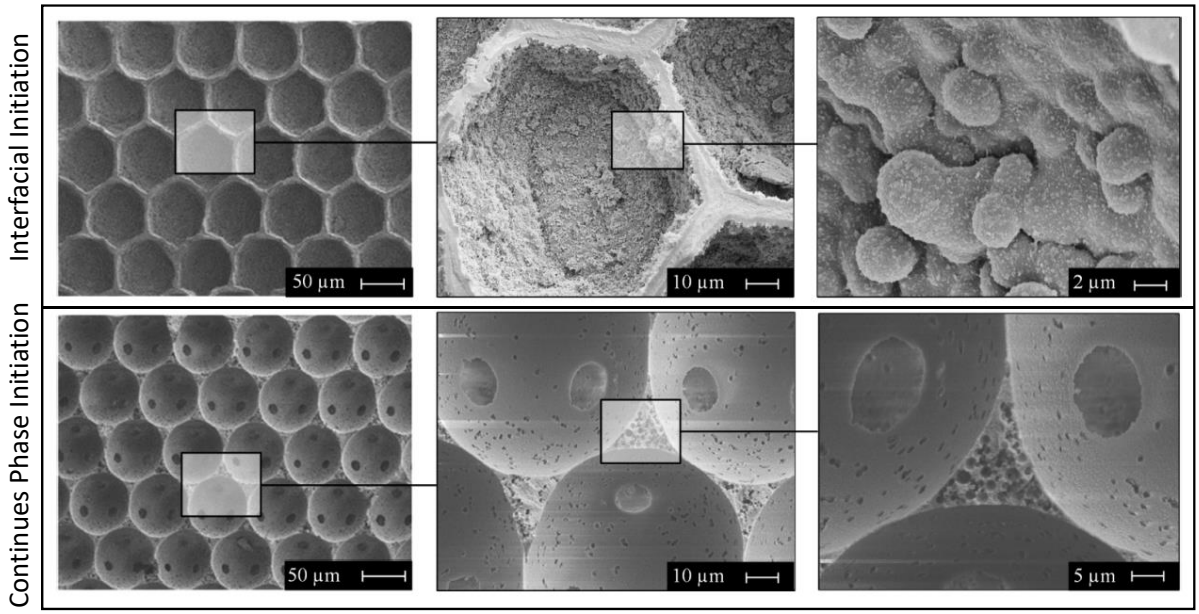

Figure 1.9: The changes in conventional PolyHIPE morphology caused by the difference in locus of initiation; closed polyhedral pores with rough pore surface are obtained in interfacial initiation, while spherical interconnected pores with a smooth pore surface are obtained in continues phase initiation [56].

Traditionally, the morphological difference observed in interfacial initiation is attributed to locking-in the emulsion droplets since the polymerization occurs at the continuous phase films covering the emulsion droplets. As the polymerization continues on the interface, the osmotic pressure difference between the interface and the Plateau border leads to the migration of monomers from the Plateau border to the interface, resulting in a thicker polymer wall separating two emulsion droplets. Conversely, when the polymerization initiates from the continuous phase, this allows the diffusion of monomers from the interface to the Plateau border, resulting in a thinner continuous phase film between neighboring droplets that is prone to rupture and allows the formation of pore throats as well [57]. However, emulsion droplets that are originally spherical turn into a polyhedron during

interfacial polymerization, rather than keeping their original shape. This is questioned by Koch *et al.*, and the osmotic pressure difference as a mechanism to induce polyhedral closed cellular morphology in interfacial-initiated conventional PolyHIPE is refuted [58] and a new mechanism explaining the pore shape transition is provided (Fig. 1.10) [59]. According to the mechanism, as the polymerization continues from the interface, the surfactant molecules migrate either to the interface or to the inside of the polymer film where the surfactant is more soluble. This accumulation of surfactant at the interfacial continuous phase leads to an increase in the interfacial area and, therefore, a transition from a spherical to a polyhedral pore shape. Additionally, the surfactant trapped inside the polymer film can be washed out, revealing a porous inner layer after production.

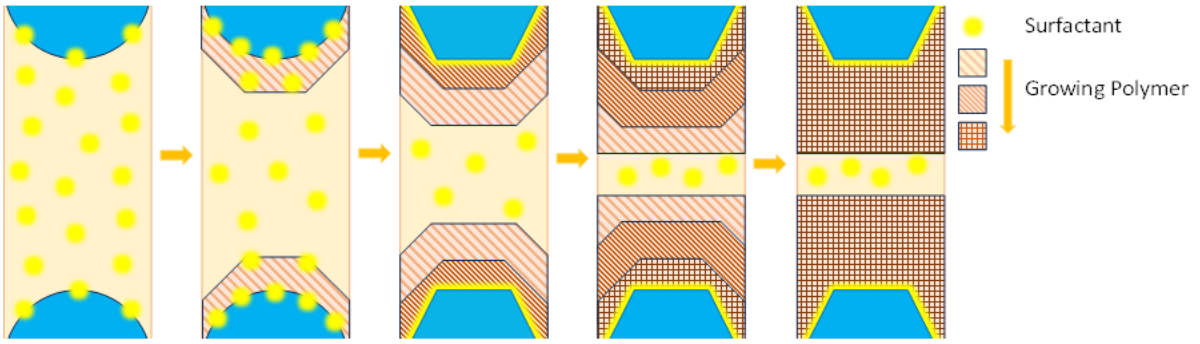

Figure 1.10: Schematic representation of pore shape changes from spherical to hexagonal in during the interfacial polymerization of HIPE (redrawn from [59]).

A similar pore shape transition is observed in Pickering PolyHIPEs as well. Continuous phase initiation yields a spherical, particle-decorated pore surface. Conversely, the interfacial initiation of polymerization results in polyhedral pores. Additionally, during polymerization, the diffusion of monomers toward the internal phase, in other words, beyond the stabilizing particles located at the oil/water interface, was observed. So that the particles were not observed on the pore surface; instead, particles were trapped in the polymer wall (Fig. 1.11) [60]. By locating the particles within the polymer, it is possible to hypothesize the monomer diffusion toward the internal phase during polymerization. It might be the case for conventional PolyHIPE as well since it is impractical to observe such a diffusion in conventional PolyHIPE, and this phenomenon might contradict the mechanism proposed by Koch *et al.* The apparent difference between the mechanisms for the formation of interfacial-initiated Pickering and conventional PolyHIPEs merits further detailed investigation and comparison.

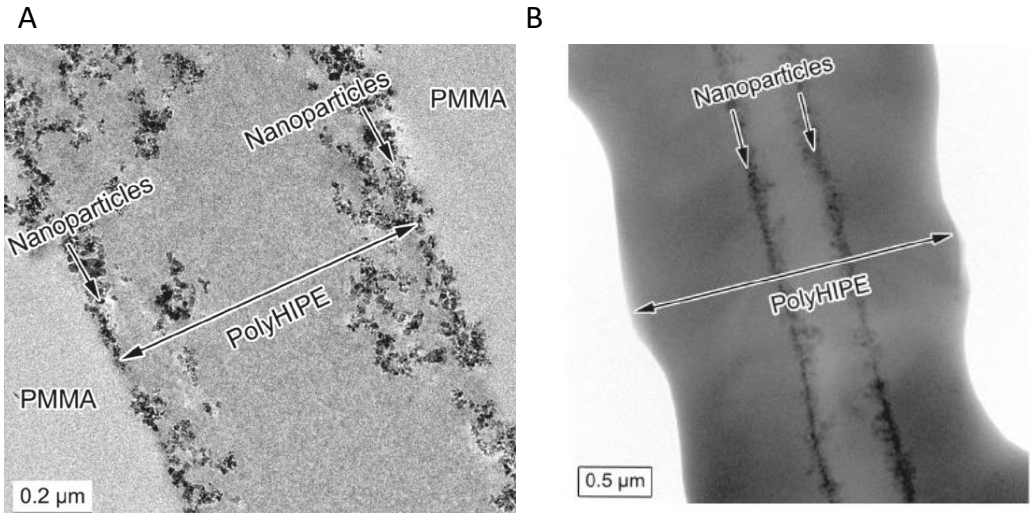

Figure 1.11: TEM images of PolyHIPEs demonstrating the location of particles. Continuous phase initiated PolyHIPE where the particles are at the interface (A), interfacial initiated PolyHIPE where the particles are located within the interfacial polymer film due to monomer diffusion towards the internal phase during polymerization (B) [60].

Similarly, Kim *et al.* investigated three photoinitiators, ranging from hydrophobic to hydrophilic as determined by their decane/water partition coefficients, and the light intensity to induce polymerization on both conventional and Pickering PolyHIPE morphology [61]. As the hydrophilicity of the initiator increases, the pores of Pickering PolyHIPE transform from a spherical to polyhedral shape. In parallel to Gurevitch *et al.* [60], the diffusion of monomers to the interface was observed when interfacial polymerization occurs; therefore, nanoparticles were embedded within the polymer wall. While the partition coefficient does not affect the interconnectivity of the pores in Pickering PolyHIPEs, the pores in conventional PolyHIPEs are significantly affected both in shape and interconnectivity as the hydrophilicity of the photoinitiator increases. Additionally, the effect of light intensity on Pickering PolyHIPE morphology was insignificant, while a significant effect was observed on conventional PolyHIPE, where the open cellular morphology is achieved when the light intensity was high in the interfacially initiated HIPE.

1.4.2. Pore Throats

1.4.2.1. The Formation of Pore Throats in PolyHIPEs

In this section, (i) the prevailing views on pore throat formation in conventional PolyHIPEs, (ii) recently proposed pore throat formation mechanisms, (iii) the mechanism behind the closed-cellular morphology in Pickering PolyHIPEs and (iv) the methods induce pore throat formation in Pickering PolyHIPEs will be reviewed. It is important to note that the pore throat formation in PolyHIPEs is a subject still under debate.

Cameron *et al.* investigated HIPE morphology at different stages of polymerization through CryoSEM. In this study, pore throat formation was observed at the thin interfacial area between two neighboring droplets at the gel point of the HIPE, the transition between viscous emulsion to gel network (Fig. 12 A) [62]. Therefore, polymerization-induced volume contraction was proposed as a governing factor of pore throat formation. On the other hand, Menner *et al.* argued that pore throat formation occurred because of mechanical action, which caused the rupture of the thinnest parts of the interfacial films between two droplets (Fig. 12 B) [63]. This thin polymer film between neighboring pores is considered a susceptible region to rupture during post-processing of PolyHIPE, such as washing and drying, and produces pore throats. The study also highlights that similar pore throats can be observed in Pickering PolyHIPEs.

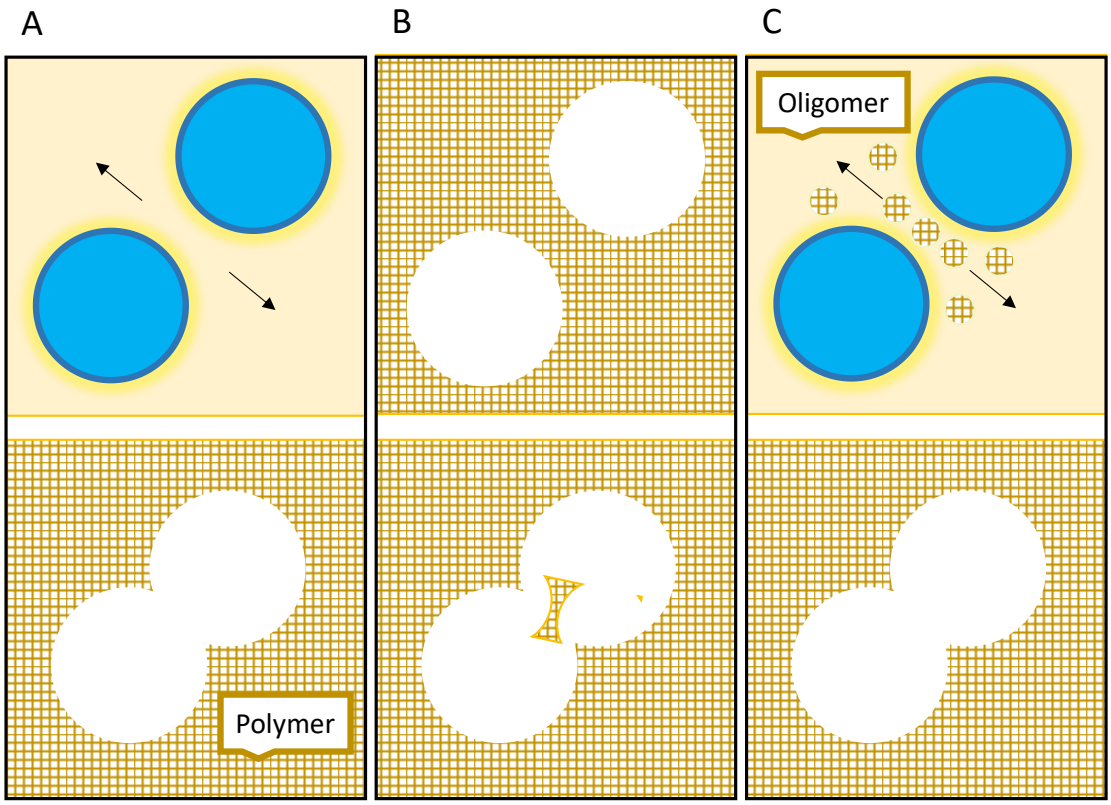

Figure 1.12: The three proposed pore throat formation mechanisms in conventional PolyHIPEs: The drainage or rupture of the thin interfacial continuous film during polymerization (arrows indicates drainage from interface to Plateau border) (A), the thin polymer film between the pores of the PolyHIPE is being ruptured during the post processing of the material (B), the growing oligomer chains at the interfacial area migrate to the Plateau border where this migration induces depletion forces so that the emulsion droplets semi-coalesce during the polymerization (arrows indicate the migration of the oligomers) (C).

Recently, Foudazi highlighted an alternative viewpoint on pore throat formation due to volume contraction [64]. He states that if volume contraction during polymerization were the governing factor of pore throat formation, the locus of polymerization initiation should not affect the openness of the

final product since the extent of volume contraction is the same as long as the continuous phase is the same. Because of this, he proposed an alternative mechanism; pore throat formation due to droplet/pore coalescence driven by depletion attraction (Fig. 12 C). According to this mechanism, the growing oligomer chains at the interfacial area detach and migrate to the Plateau border, the edge between three adjacent water droplets. The migration of prepolymer induces a depletion attraction to allow droplets to partially coalesce during polymerization. Pore throats are formed at the partially coalesced regions of droplets if the migration rate of detached oligomers from the interface to the Plateau border is faster than the rate of polymerization. Alternatively, Pawar *et al.* reported that emulsion droplets can be stable at a partially coalesced state if further coalescence is arrested due to particle jamming at the contact region. In parallel with Foudazi's proposed mechanism, Durgut *et al.* proposed arrested coalescence as a mechanism to induce pore throats in Pickering PolyHIPEs [65]. The claim was supported by the observation of a dense particle layer surrounding the pore throats as well as pore-pore junctions. The proposed mechanisms for pore throat formation in PolyHIPEs are represented in Figure 1.12.

1.4.2.2. Closed Porous Morphology of Pickering PolyHIPEs

Pickering PolyHIPEs are known for their closed porous morphology, unlike surfactant-stabilized HIPE templates [66,67,76–78,68–75]. The closed porous structure of Pickering PolyHIPEs is attributed to the higher thickness and/or stability of the interfacial continuous film, which resists rupturing during polymerization or post-processing of the material, according to the commonly accepted pore throat formation mechanism. The increased stability of the interfacial film arises from the layers of particles surrounding the emulsion droplets and the formed particle network in the interfacial continuous phase [66,75]. Therefore, the stable interfacial film withstands the thinning of the interface during polymerization, preventing rupture and producing a thicker polymer interface without a significant amount of pore throats. The closest point between the pores manifests itself as pore throats covered with the thin polymer film, which would normally be expected to produce pore throats.

Alternatively, the closed-porous morphology in Pickering PolyHIPEs is attributed to the strong adsorption of Pickering agents at the oil/water interface compared to surfactants. Droplet coalescence is hindered during polymerization due to the effective mechanical barrier formed around the emulsion droplets by Pickering agents, while small surfactant molecules can be dispersed in either of the phases when exposed to polymerization-induced forces, allowing droplets to coalesce [69]. Therefore, to introduce interconnected pores in Pickering PolyHIPEs, methods to reduce interfacial stability and the thickness of the interfacial film, as well as the induction of droplet coalescence, are utilized.

1.4.2.3. Interconnected Pickering PolyHIPEs

While Pickering PolyHIPEs typically exhibit a closed-pore morphology, there are several reports demonstrating interconnected Pickering PolyHIPEs. The methods presented in these reports are reviewed in this section. It is important to note that the applicability of these methods to induce pore throat formation is limited to the given experimental conditions.

1.4.2.3.1. Dual Emulsifiers

The utilization of both surfactant and Pickering agents, referred to as "dual emulsifiers," is commonly employed to introduce interconnected pores in Pickering PolyHIPEs [45,66,84–87,68,71,75,79–83]. PolyHIPEs obtained through dual emulsification exhibit intermediate pore sizes [66,71,75,79,80] and larger pore throat sizes than those emulsified solely by either of the emulsifiers [66,75]. Furthermore, hierarchical porous structures have been reported using this method, where the PolyHIPEs exhibit both Pickering-like large and closed pores and conventional-like small and interconnected pores [45,68,79]. Dual emulsification is also employed to enhance HIPE stability [45,79,83,85] or to form a HIPE when the sole use of either emulsifier fails [45,71,81,84,86,88]. The amount of surfactant used in a dual emulsification system is generally less than the amount used to stabilize a HIPE as a sole emulsifier, reducing concerns associated with surfactant use. Alternatively, reactive surfactants as secondary emulsifiers can be used to minimize the possibility of surfactants leaching out from the final product [87]. On the other hand, both synergistic [45,71,79,86] and antagonistic effects [88] of dual emulsifiers on emulsion stabilization are reported (Fig. 1.13).

As highlighted in the previous sections (see Figure 1.6), the formation of a particle network at the interface due to excess particles increases the viscosity of the interfacial film, thus enhancing interfacial film stability. The stable interfacial film resists rupturing during polymerization/post-processing, providing closed pores in PolyHIPE, according to the prevailing view. Ikem *et al.* reported that the addition of Hypermer 2296, which cannot stabilize the HIPE at the given concentration solely, to a premade silica-stabilized HIPE disaggregated the excess particles. Disaggregated particles are well dispersed in the continuous phase, resulting in reduced continuous phase viscosity [66,71]. The reduced continuous phase viscosity allows interfacial film drainage due to the sedimentation of a less concentrated emulsion, thus thinning the interfacial film where the pore throats are formed. Surfactant molecules also adsorb onto the emulsion droplets, reducing the interfacial tension between two phases [66,79]. Together with the reduced continuous phase viscosity and the interfacial tension, this process allows emulsion droplets to be further broken down under shear, producing smaller droplets/pores [66].

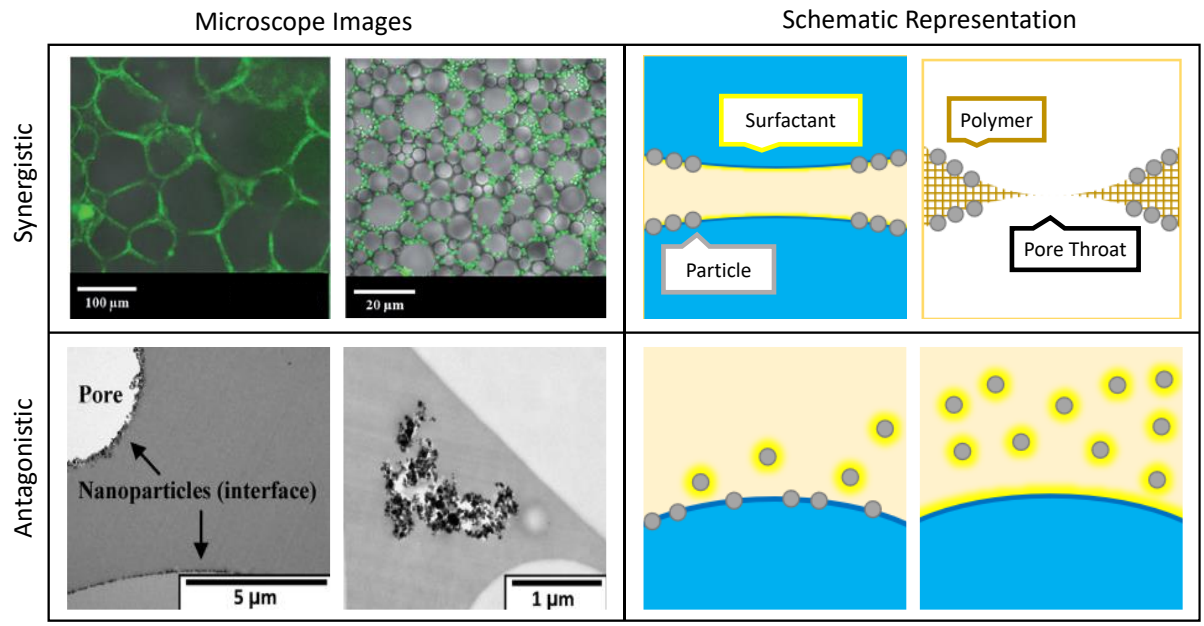

Figure 1.13: Representation of proposed synergistic and antagonistic effect of dual emulsifier system. Synergistic effect demonstrated with confocal microscopy where the green fluorescent particles as a sole stabilizer covering the emulsion droplets (left), when the surfactant is used as co-emulsifier, particles are found at the highly curved regions of the emulsion droplets (right). The synergistic effect is schematically represented, where the surfactant molecules are located at the less curved region of droplets (left). These regions are susceptible to thin film rupture during polymerization, leading to the formation of pore throats (right). Alternatively, antagonistic effect of dual emulsifier system is represented in TEM images of PolyHIPE. particles as a sole HIPE stabilizer localize at the interface (left) however, when the surfactant is used, the particles are observed within the polymer in a an aggregated form (right). The antagonistic effect is schematically represented where the surfactant is adsorbed on the particle surface first and de-attaches them from the interface (left) and surfactant function a s stabilizer only when the particle surfaces are saturated with surfactant (right).

Rather than adding surfactant to the premade emulsion, dual emulsifiers are initially dispersed in the continuous phase when the HIPE is formed. The location of the particles was investigated either by TEM [79] or fluorescent microscopy and it was observed that particles are located at highly curved regions of droplets/pores—either the surface of spherical droplets/pores separated by a thick continuous phase or the droplet/pore surface neighboring the Plateau border—rather than at less curved droplet/pore surfaces where the droplets are jammed/flattened. This observation is explained by the competition between emulsifiers to localize at the oil/water interface. Surfactant molecules can rapidly localize at the oil/water interface at the less curved surface due to their small size. The pressure difference between the Plateau border and the interface due to the interfacial tension leads to the migration of unattached particles from the interface to the Plateau border while the continuous phase film is being drained. Therefore, particles locate themselves at the oil/water interface when they are not subjected to continuous film drainage. Therefore, the competition between emulsifiers to adsorb onto the oil/water interface is suggested [71,79]. On the other hand, Vilchez *et al.* argued for the synergistic (competitive) stabilization of dual emulsifiers mechanism and claimed an antagonistic effect

on emulsion stabilization [88]. It was demonstrated that the surfactant (Hypermer 2296) preferentially adsorbs onto the particle surface (iron oxide), affecting their wettability. The addition of surfactant to the HIPE, which is stabilized by particles, causes phase separation. Enhanced emulsion stability is observed when the surfactant is combined with the particle, which is too hydrophilic to form emulsion solely. They concluded that surfactant acts as an emulsifier only after particle surfaces are saturated with the surfactant.

The dual emulsifier method is employed to obtain a hierarchical porous structure by either dissolving the surfactant in both phases [68] or only in continuous phase [45,79]. Wong *et al.* demonstrated that the addition of Hypermer B246SF results in the co-existence of large closed pores typical for Pickering PolyHIPEs (400 µm) and small interconnected pores typical for conventional PolyHIPEs (13-17 µm) (Fig. 1.14 A-C) [68].

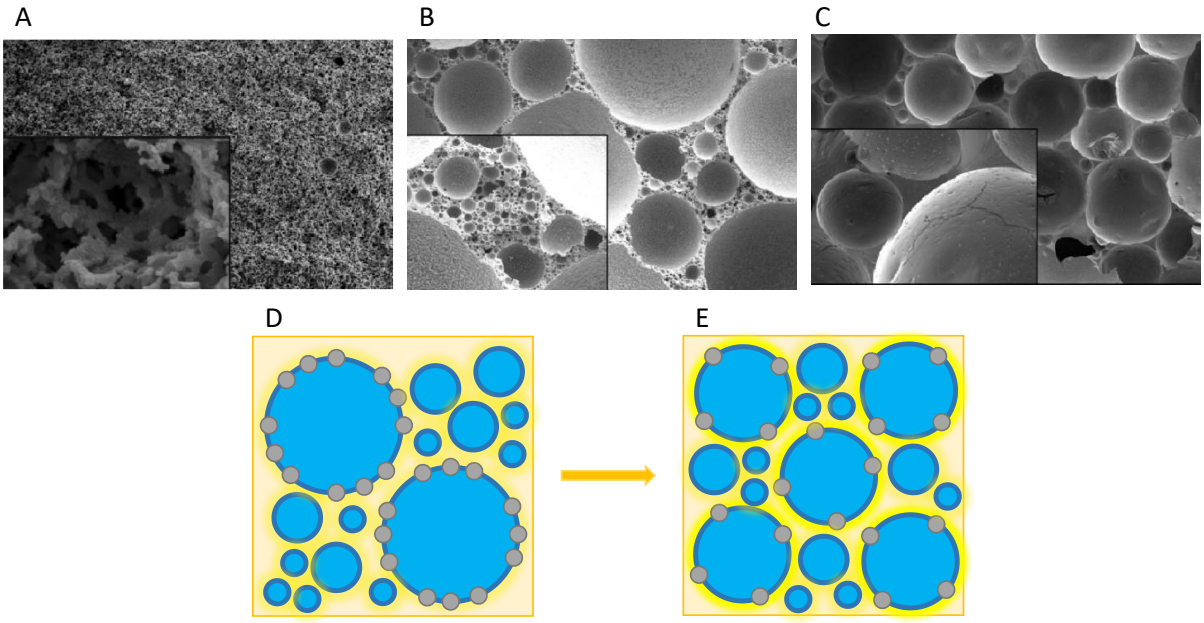

Figure 1.14: SEM images of PolyHIPEs (A-C): PolyHIPEs obtained from HIPE stabilized by surfactant (A), dual emulsifier (B) and colloidal particles (C). The hierarchical porous structure is obtained when both surfactant and colloidal particles are used to stabilize HIPE (B) [68]. Schematic representation of interplay between surfactant and colloidal particle concentration on the HIPE/PolyHIPE morphology: When the particle/surfactant ratio is high, large pores are mainly stabilized by colloidal particles (D), when the particle/surfactant ratio is low, average droplet/pore size reduces (E) [45].

Interestingly, increasing the titanium concentration reduced the pore size of large pores and increased the pore size of small pores, while the surfactant concentration (0.8-8.4% wt) did not affect either pore size. On the other hand, the increase in surfactant concentration was observed to increase the number of pore throats per pore. Furthermore, surfactants are also found to adsorb onto the particle surface and cause them to be dispersed in the PolyHIPE polymer matrix. Further increase in surfactant

concentration (17 wt%) results in the loss of the hierarchical porous structure, and the emulsion was mainly stabilized by surfactant, and the particles were dispersed in the continuous phase. A similar transition from total Pickering to conventional-like morphology as the Pickering agent to surfactant ratio is reduced is reported as well (Fig. 1.14 D-E) [45,71,79,82,83]. Such a transition in morphology is interpreted as an antagonistic effect of dual stabilizers on pore structure by Yin *et al.* [82].

According to these reports, the utilization of dual emulsifier provides an interconnected porous morphology unless all the available surfactants adsorb onto the particle surface, causing particles to completely disperse within the continuous phase, leaving the system without an effective stabilizer. On the other hand, the preferential affinity of surfactant to the particles and/or droplet interface has not yet been investigated. Additionally, at which step of the emulsification the surfactant is added or in which phase the surfactant is dissolved might be another parameter affecting HIPE/PolyHIPE morphology. Furthermore, the effect of depletion attraction on pore throat formation is generally overshadowed: disaggregated particles by surfactant adsorption might function as a depletant to induce pore throat formation due to depletion attraction. Alternatively, the recently hypothesized pore throat formation due to arrested coalescence can be considered; since the introduction of surfactant reduces the viscosity of the continuous phase, the reduced viscosity might facilitate the migration of particles to the necking regions of two semi-coalesced droplets to arrest droplet coalescence.

1.4.2.3.2. Inducing the Volume Contraction During Polymerization

Since polymerization-induced volume shrinkage is one of the proposed mechanisms for pore throat formation, interconnected pores are introduced in Pickering PolyHIPEs by inducing volume shrinkage either by increasing the crosslinker content [76,89] or the addition of a secondary monomer to the continuous phase that undergoes relatively higher shrinkage during polymerization [90].

Pore throat formation is observed in vinyl ester resin-styrene (VER-St) PolyHIPE when the crosslinker vinyl ester oligomer (VEO) content in the continuous phase is between 20-40% [89]. Furthermore, no pore throat formation was observed when the crosslinker content is between 0-10%. Therefore, the interconnected porous structure of the Pickering PolyHIPE is, in this case, attributed to increased volume contraction during polymerization. On the other hand, no pore throat formation is reported when the continuous phase consists of methyl methacrylate (MMA) rather than styrene, with 20% crosslinker VEO. This is interesting since in another study, MMA was incorporated as a secondary monomer in the continuous phase together with the styrene to utilize the high volume shrinkage of MMA during polymerization to induce pore throat formation [90]. While the Styrene PolyHIPE does not exhibit pore throats, the addition of 20% MMA induces pore throat formation, and the gas permeability of the PolyHIPE increases as the MMA content is further increased (Fig. 1.15).

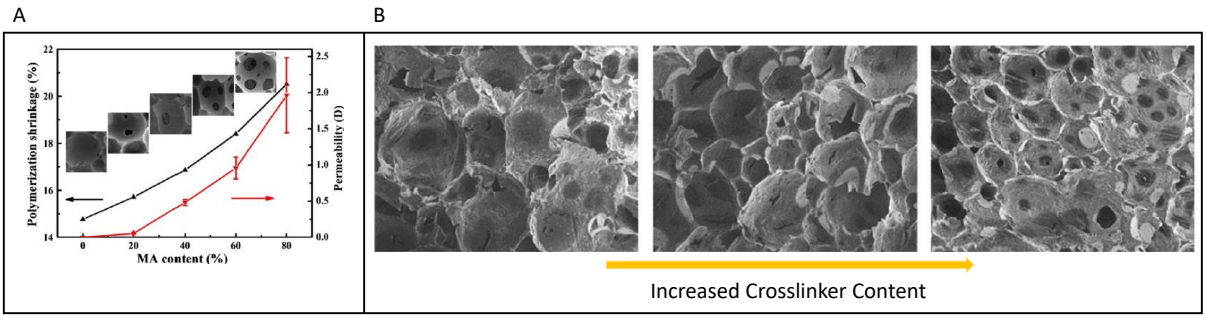

Figure 1.15: The utilization of volume shrinkage to induce pore throat formation. The increase in MMA content within organic phase resulted in pore throat formation due to its high volume shrinkage during polymerization (A). The increase in crosslinker content resulted in formation of pore throat (B) [90].

While inducing volume contraction is reported to obtain an interconnected porous structure in Pickering PolyHIPEs, the method is not versatile. Additionally, the method necessitates a high amount of crosslinker, which might result in undesirable mechanical properties of the PolyHIPE, given that high crosslinking ratios typically produce brittle polymers. On the other hand, depending on the chemistry of the crosslinker and/or secondary monomer, the localization of particles at the interface might be affected. For instance, MMA is more hydrophilic and soluble in water compared to styrene. The mixture would most probably affect the particle wettability in both phases. Therefore, pore throat formation might be much more influenced by the particle location at the interface rather than the effect of polymerization-induced volume contraction.

1.4.2.3.3. Thinning the Interfacial Continuous Phase Film

A thin interfacial, continuous phase, or polymer film between neighboring pores is the common point of the two commonly accepted pore throat formation mechanisms. Thinning the interfacial film generally results in interconnected porous Pickering PolyHIPEs according to the literature. Various methods to thin the interfacial film are reviewed in this section.

Increasing the internal phase fraction is one straightforward way to thin the interfacial film. The increased internal phase fraction leads to shrinkage of the continuous phase both from the Plateau border and interface. It was observed that increasing the internal phase fraction leads to the formation of pore throats, whereas a lower amount of internal phase produces a closed porous morphology [76]. Additionally, increased interconnectivity is also observed for the Pickering PolyHIPEs that were interconnected at lower internal phase fractions [90,91]. On the other hand, there are findings that even at a 90% internal phase fraction, Pickering PolyHIPEs exhibit a closed morphology [69]. Furthermore, incorporating a higher amount of internal phase is generally impractical in Pickering PolyHIPEs: the dispersion of Pickering agents in the continuous phase increases viscosity. As the internal phase is added, the viscosity is further increased, preventing the incorporation of internal

phase due to inefficient mixing of the system. Menner *et al.* tackled this problem of increased viscosity of the continuous phase due to Pickering agent dispersion by using Pickering agents in both phases: hydrophobic carbon nanotubes (CNT) in the continuous oil phase and the hydrophilic CNT in the internal water phase to prepare PolyMIPE (Fig. 1.16) [92].

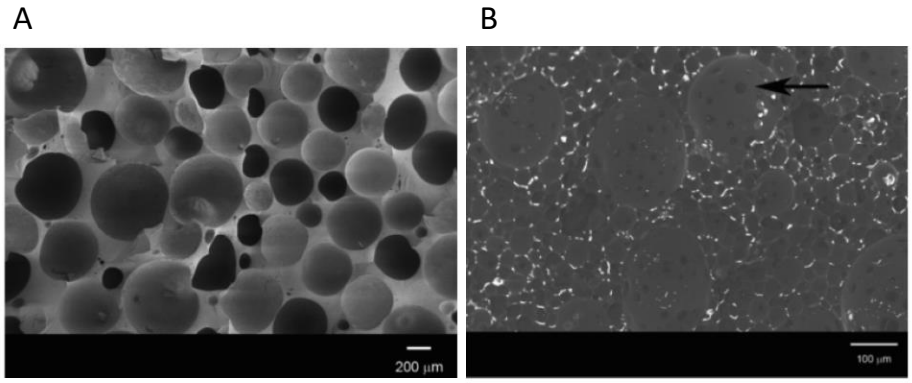

Figure 1.16: Closed cellular PolyMIPE when the CNT is the sole emulsion stabilizer (A), open cellular PolyMIPE obtained by HIPE stabilized by CNT dispersed in the oil phase and the oxidized CNT dispersed in the water phase (black arrow indicates the pore throat) (B) [92].

An alternative way to thin the interface is through the extraction of the continuous phase from the interface by particles or the structures formed by particles. It was observed that non-crosslinked styrene particles as a stabilizer result in interconnected Pickering PolyHIPEs, while crosslinked styrene does not [72]. The pore throat formation was attributed to the swelling of non-crosslinked styrene particles by the continuous phase at the interface, resulting in a thinned interfacial continuous film. Further increase in interconnectivity is achieved by etching the non-crosslinked particles located at the pore wall with THF treatment. Alternatively, Zheng *et al.* reported interesting differences between octadecyltrimethoxysilane (ODS) modified silica particle-stabilized PolyHIPEs when the particles are dispersed in either the water or the oil phase [93]. Only when the particles were dispersed in the internal water phase, did the Pickering PolyHIPE exhibit an interconnected structure. It was observed that particles effectively disperse in the continuous phase but form aggregates when dispersed in the internal phase. These aggregates form micelle-like structures, where the shell is hydrophilic but the core is hydrophobic. Therefore, the interfacial continuous phase diffuses into the micelle-like silica aggregate, resulting in a thinned interfacial film and throat formation.

1.4.2.3.4. The Effect of Particles: Localization and Interaction

Pickering agents, functioning as an effective barrier around the emulsion droplets and their strong adsorption at the interface, are considered the main reasons for obtaining a closed porous morphology in Pickering PolyHIPEs. From this perspective, methods to tune the particle localization at the oil/water interface or re-localization/migration of Pickering agents from the interface during polymerization can

be exploited to obtain pore throat formation. Therefore, papers reporting close to open porous morphology due to particle localization are reviewed in this section.

Pickering agents are generally subjected to surface modifications to tune their wettability to obtain a stable HIPE. The wettability affects the localization of particles at the interface. Several papers investigate the effect of surface modification of Pickering agents on the morphology of Pickering PolyHIPEs. For example, in graphene oxide (GO) nanosheet-stabilized HIPEs, the degree of CTAB modification on graphene oxide nanosheets is reported to affect the openness of the acrylic acid Pickering PolyHIPE [73]. Non-modified GO nanosheets produce closed-cell PolyHIPEs, while an increase in the degree of cetyltrimethylammonium bromide (CTAB) modification introduces pore throats. Decomposed CTAB from the nanosheet surface might be a factor affecting the interconnectivity, but the study demonstrates that a further increase in CTAB modification reduced the interconnectivity. While the author attributed the pore throat formation to the geometry and the atomic scale thickness of the nanosheets (thinner than common Pickering agents), CTAB-modified GO nanosheets were also used in another study to prepare styrene PolyHIPEs that exhibit a closed porous morphology [94]. Additionally, pore throats were rarely observed. This was attributed to the decomposed CTAB from the nanosheet surface. Considering the difference in the hydrophobicity of the organic phase and the sensitivity of the Pickering PolyHIPE openness to the degree of surface modification, the pore throat formation might be more relevant to the localization of Pickering agents rather than atomic scale thickness of the stabilizer. As mentioned in the previous section, the degree of ODS modification of silica particles affected the openness of styrene Pickering PolyHIPE when dispersed in the internal water phase initially. While the mechanism is attributed to the monomer extraction due to silica aggregates, the reduced amount of ODS modification resulted in a closed porous morphology even if it is dispersed in the internal phase [93].

An interconnected porous structure was observed in melamine-formaldehyde (MF) Pickering PolyHIPE where lignin particles were the stabilizer. Pore throats were only formed if the concentration of pre-MF in the continuous water phase is above 25%. The mechanism of the pore throat formation was attributed to the reaction between the lignin particles and pre-MF, which provides the force to draw particles from o/w interface to Plateau border [69]. Consequently, the pore throats are formed either due to droplet/pore coalescence or a sufficient thinning the interface to rupture since the barrier separating two neighboring droplets is removed during polymerization. The closed to open porous morphology was also observed in MF Pickering PolyHIPEs where the stabilizer was dialdehyde cellulose-aniline with various aldehyde to aniline molar ratios [95]. Pore throats were observed when the aldehyde to aniline molar ratio was 20:1, and a closed porous morphology was obtained at reduced aldehyde to aniline molar ratios. On the other hand, the pore throat formation was attributed to

obtained smaller pore size, rather than monomer-particle interaction or the wettability of Pickering agents. Alternatively, sulfonated polystyrene particles in tetrahydrofuran solution were used as an emulsion stabilizer to obtain either styrene or butyl acrylate PolyHIPEs [96]. While the styrene PolyHIPEs exhibit a closed porous morphology, an interconnected porous structure was obtained in butyl acrylate PolyHIPEs.

1.4.2.3.5. Other

Interconnected Pickering PolyHIPEs were reported when non-crosslinked Styrene-Methyl Methacrylate-Acrylic Acid (St-MMA-AA) particles were used as a stabilizer in the study of Hua et al [97]. In this system, there was no monomer to polymerize; and the particles functioned as a stabilizer as well as building blocks forming the material's skeleton. Particles were dispersed in the internal phase, and a water-in-toluene emulsion (anti-Finkle, the dispersion of stabilizer in the internal phase) was obtained. Since toluene dissolves the non-crosslinked particles, the dissolved polymer formed the skeleton, and yet-to-be-dissolved particles functioned as a stabilizer. The interconnectivity of the samples was observed to be strictly dependent on the standing time of the emulsion before solidification. As the standing time increased, more particles were being dissolved, which reduces the interconnectivity of the HIPE template (Fig. 1.17 A). In parallel, chitin nanofibrils were used as a stabilizer as well as the skeletal material of HIPE templates from a cyclohexane-in-water HIPE. Subsequent removal of both the continuous and the internal phase from the emulsion left behind an interconnected chitin HIPE template [98]. In this system, nanofibrils were not subjected to dissolution. Polyurethane/vinyl ester oligomer nanoparticles were utilized in a similar fashion; to stabilize cyclohexane-in-water HIPE and to form the skeleton. On the other hand, the PolyHIPE did not exhibit pore throats but an open morphology with aligned pore walls due to the unidirectional freezing of the HIPE and subsequent lyophilization [99]. It was reported that the increased particle concentration negatively affects the channel formation through the pores because of preventing the ice crystal formation during the unidirectional freezing (Fig. 1.17 B).

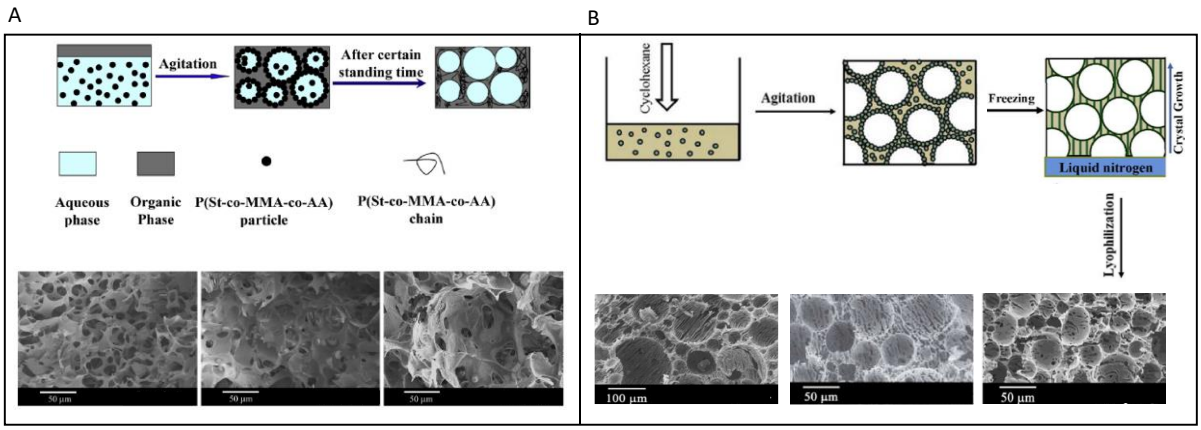

Figure 1.17: The schematic representation of the formation of anti-Finkle emulsion where the stabilizing particles are dispersed in the internal phase initially (A). As the particles interact with the continuous phase where they are soluble, particles disintegrate into polymeric chain and forming the material skeleton. The SEM images of the anti-Finkle emulsion templates demonstrating the loss of interconnectivity of the HIPE template as the standing time of the HIPE increase; 0, 24 and 48 h after preparation from left to right [97]. A schematic representation of the channel formation in Pickering emulsion template by unidirectional freezing (B). The SEM images of the obtained templates and the effect of the increasing particles concentration (15, 25 and 30 %wt particle concentration from left to right) on the channel formation [99].

1.4.3. The Morphological Characterization of PolyHIPEs

1.4.3.1. Porosity

The internal phase of the HIPE represents itself as pores in PolyHIPEs. Therefore, the volume fraction of HIPE's internal phase is equal to the total pore volume of the PolyHIPE, theoretically. However, this value may vary in practice. HIPE can experience destabilization after being prepared or during polymerization, especially when subjected to elevated temperatures for a long time during thermal polymerization. Depending on the material used, the monomer-to-polymer conversion during polymerization may result in shrinkage in PolyHIPE. Alternatively, the porous structure of the PolyHIPE can collapse during post-processing due to capillary stress induced during washing/drying steps.

The cost-effective method to deduce the porosity of the PolyHIPE is using the difference between the skeletal (ρ_{sd}) and bulk density (ρ_c) of the PolyHIPE [100,101]. Assuming that the samples are in known geometrical shape, both ρ_{sd} and ρ_c can be obtained from simple mass and volume measurements of the bulk polymer and the PolyHIPE, respectively. d_s can be deduced from obtaining the volume of the PolyHIPE via the graduated cylinder method (aka liquid displacement method) as well [102,103]. Alternatively, ρ_{sd} and ρ_c can be measured via dedicated devices; pycnometer and envelope density analyzer, respectively [53].

Porosity as well as the specific surface area can be measured through mercury porosimeter [104–106] as well as N_2 adsorption/desorption test. The isotherms obtained from N_2 adsorption/desorption are

analyzed with the Barret-Joyner-Halenda method [105]. The isotherms can be further used to calculate the specific surface area of the PolyHIPE when analyzed with the Brunauer-Emmett-Teller (BET) method [107,108].

Except for the utilization of density difference between ρ_{sd} and ρ_c, the methods necessitate access to the pores, such as N_2, mercury, etc. Therefore, these methods are only reliable if the PolyHIPE exhibits an open porous structure. To evaluate the fraction of dead-end pores, Mravljak *et al.* calculated static porosity by measuring both wet and dry mass as well as wet volume of the PolyHIPE and measured the flow through the porosity pulse experiment measuring conductivity [109]. The difference between the static and flow-through porosity represents the volume fraction of the dead-end pores.

1.4.3.2. Cellular Structure

The cellular structure of a PolyHIPE includes pore size, shape, and distribution; pore throat size and distribution; as well as strut thickness and aspect ratio. Therefore, the evaluation of the cellular structure is mainly dependent on imaging techniques and further analysis through software.

Assuming that the effect of polymerization-induced forces is minimal, pore size and distribution can be deduced from the evaluation of HIPE droplets by acquiring micrographs through light microscopy or methods like dynamic light scattering or laser diffraction. It has been previously demonstrated that PolyHIPE itself can be imaged through light microscopy but necessitates labor-intensive sample preparation [102]. To directly image the PolyHIPE, scanning electron microscopy (SEM) is the commonly used method. The micrographs acquired through SEM can be used to analyze all the microfeatures of the PolyHIPE. Since the samples are sectioned, the imaged pores do not represent the actual sizes of the pores (Fig. 1.18). Therefore, a statistical correction factor is applied to the measured pore sizes, assuming that all the pores are sectioned from R/2 distance from the middle of the pores. The statistical correction factor is found to be $2/\sqrt{3}$ [105], or $4/\pi$ [109] if the equation is integrated through the actual radius of the pore. Additionally, X-Ray microcomputed tomography (µCT) is used to evaluate the PolyHIPE in 3D after reconstructing the collected 2D images (Fig. 1.19) [110,111].

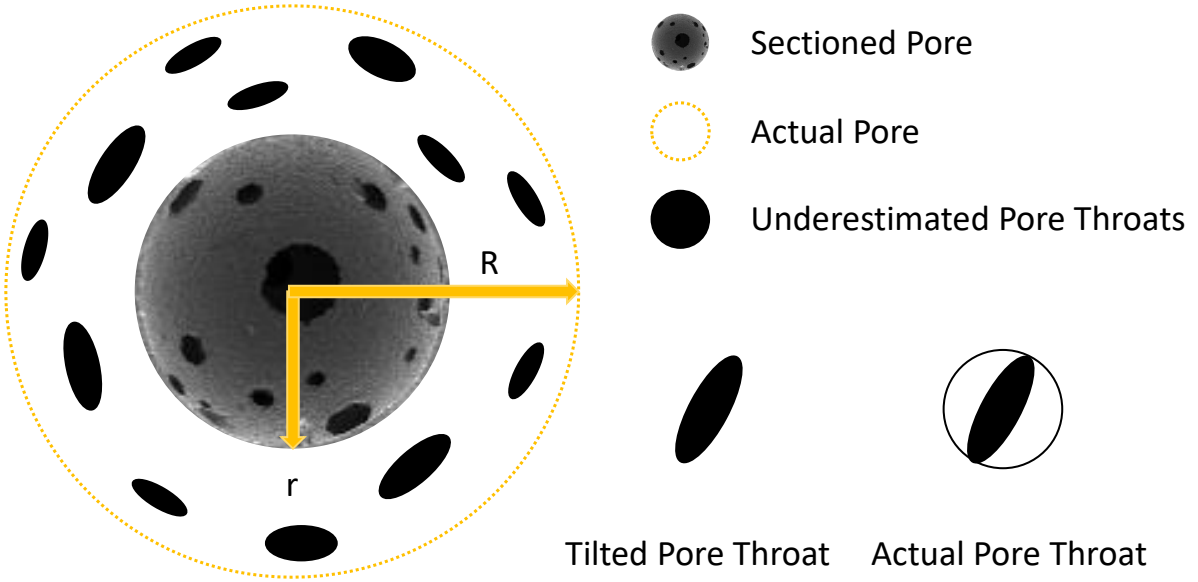

Figure 1.18: Schematic representation of uneven sectioning of PolyHIPEs. R and r represents the actual and the sectioned radius of the pores.

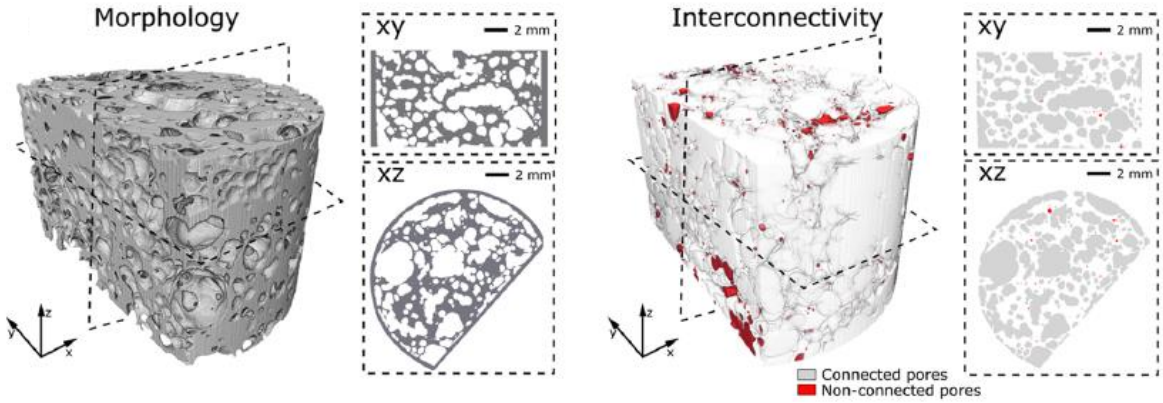

Figure 1.19: The reconstructed 3D image and the 2D images from two different planes of a PolyHIPE obtained from µCT [110].

The pore throat size and distribution are crucial for evaluating the degree of interconnectivity and openness of the pores. SEM micrographs can be used to deduce the average pore throat size and distribution. Since the pore throats are distributed on the hemispherical pores in the micrographs, their size is affected by the angle at which they are viewed [101]. Therefore, the pore throats are considered as ellipsoids, and the long axis of the ellipsoid is used as the pore throat diameter. Counting the number of pore throats per pore, and thus the overall open surface on the pore, is affected by the uneven sectioning of the pores as well. Therefore, the number of pore throats counted on SEM micrographs is multiplied by 4 [109].

Two terms are generally used to report the pore throat/pore relationship of PolyHIPEs; the degree of interconnectivity [102,112] which is the ratio between the average pore throat size to the average pore

size, and the degree of openness [113] which is the ratio between the overall pore throat area to the pore surface area. Alternatively, the permeability of the PolyHIPE provides data to compare the openness of the PolyHIPEs [68]. Instead of using SEM, mercury porosimetry provides the size and distribution of the pore throats of PolyHIPEs by gathering the accessed volume at increased pressure. The higher the pressure, the smaller the pore throats that have been accessed. Normally, mercury porosimetry is a method to acquire the porosity/pore size of porous samples. However, in PolyHIPEs, it provides pore throat size data rather than pore size since the mercury flows through pore throats [105].

1.5. Mechanical Properties of Pickering PolyHIPEs

PolyHIPEs, being highly porous, are known for their inferior mechanical properties, limiting their applications on an industrial scale. Therefore, understanding the governing parameters affecting the mechanical properties of these highly porous materials and improving their mechanical properties are crucial research areas. The intrinsic mechanical properties of the materials forming the skeleton of the PolyHIPE, such as isobornyl acrylate PolyHIPE and 2-ethylhexyl acrylate PolyHIPE exhibiting 50 and 1 MPa Young's modulus, respectively, can be tuned by adjusting the composition of constituent monomers [114]. Pore volume is another determinant of PolyHIPE mechanical properties, directly related to foam density, where an increase in pore volume leads to a reduction in mechanical properties [55,84,114–119]. Since the higher porosity is the integral part of PolyHIPEs, reducing the total pore volume is not a feasible method to produce PolyHIPE with superior mechanical properties. Therefore, the effect of pore organization, distribution, and HIPE stabilizers (surfactants or colloidal particles) on the mechanical properties of PolyHIPEs is reviewed in this section.

Both pore size and distribution influence the mechanical properties, with larger average pore sizes improving properties due to thicker polymeric struts [120]. Additionally, the hierarchical organization of pores were reported to improve the mechanical properties of PolyHIPEs [68,121]. Wong *et al.* demonstrated that the PolyHIPE with large-closed and small-open hierarchical pore organization exhibit improved Young's modulus (~24 MPa) compared to both large-closed (~12 MPa) and small-open (~1 MPa) porous PolyHIPEs [68]. Additionally, interconnectivity of the pores is another morphological feature affecting the mechanical properties. The structural integrity of the pores are negatively affected by the openness of the pores, resulting in the decreased mechanical properties [48,122].

Adjusting the stabilization mechanism, whether using a surfactant or Pickering agent, is considered another approach to tune the mechanical properties of PolyHIPEs. However, changing the type of stabilizer is accompanied by morphological differences in PolyHIPE. Therefore, understanding the

direct effect of stabilizer type on mechanical properties can be challenging. Nevertheless, the type of stabilizer can influence mechanical properties in a more complex manner. For instance, Kovacic *et al.* investigated the effect of surfactant (Pluronic L-121) loading, ranging from 0% to 10%, on PolyHIPE mechanical properties and observed a significant decrease in Young's modulus when surfactant loading exceeded 5% [123]. The observed change in Young's modulus did not correlate simply with the decreasing pore and pore throat size. The study claimed that the remaining surfactant on the polymer wall, which cannot be purified from the material, acts as a plasticizer, negatively affecting mechanical properties. Further increases in surfactant lead to the production of monomer-filled micelles, which are polymerized within the monomer and washed out of the material skeleton, resulting in a further reduction of foam density.

Colloidal particles, when used as a filler rather than a stabilizing agent, have demonstrated the ability to improve the mechanical properties, including Young's modulus and crush strength, of PolyHIPEs when covalently bound to the polymer [115,117,118]. Additionally, colloidal particles, when employed as a stabilizer, have shown similar improvements in mechanical properties [55,71,99,124,125]. The impact of colloidal particles on the mechanical properties of PolyHIPEs is generally attributed to their distribution on the pore surface. Enhanced mechanical properties are observed when pore surfaces are evenly covered with particles, creating an efficient network for stress transfer from the polymer to the particles [126]. However, an increase in particle concentration beyond the optimum loading concentration leads to a reduction in mechanical properties due to particle aggregation, which acts as stress concentration points [66,124,125,127].

1.6. Applications of Pickering PolyHIPEs

Due to their highly interconnected porous structure and consequently large surface area, conventional PolyHIPEs find applications in various fields such as catalyst support, tissue engineering scaffolds, and adsorbents. Pickering PolyHIPEs can be considered a more environmentally friendly alternative to conventional PolyHIPEs by either eliminating or reducing the usage of surfactants, leading to reduced production costs. From a morphological perspective, the intrinsic large pores and rough pore surfaces of Pickering PolyHIPEs can offer improved performance depending on the application, despite some contradictory reports. The enhanced mechanical properties of Pickering PolyHIPEs can be particularly beneficial for applications that require durable materials. Importantly, the integration of particles on the pore walls adds intrinsic functionality to Pickering PolyHIPEs. In this section, we will review reports demonstrating the applications of Pickering PolyHIPEs.

1.6.1. Catalyst Support

One of the most common applications of Pickering PolyHIPEs is their utilization as a catalyst support. Catalytic activity can be achieved by decorating the pore walls with functional colloidal particles. Alternatively, colloidal particles can be subsequently used to tether functional nanoparticles to the PolyHIPE surface. For example, Yi *et al.* used synthesized tadpole-like single-chain polymer Janus nanoparticles, where the tail and the head are composed of polyMMA and poly(4-vinylpyridine), respectively [91]. The nanoparticles were used as the sole stabilizer to produce open-porous St/DVB PolyHIPE. Due to the strong interaction between the poly(4-vinylpyridine) head of the stabilizer and metal nanoparticles, the PolyHIPE was successfully loaded with palladium nanoparticles and further used as a catalyst for the Suzuki-Miyaura carbon-carbon coupling reaction.

TiO2 is one of the most commonly used Pickering agents. Due to its photocatalytic activity, Pickering emulsion templates stabilized by TiO2 are mainly used as photocatalyst support. Li *et al.* produced TiO2-decorated PolyHIPEs by templating an o/w HIPE stabilized by TiO2 and poly(isopropylacrylamide-co-methyl methacrylate) microgels [128]. After sintering the material, the photocatalytic activity of the template was evaluated by the photodegradation of Rhodamine B and reported that the template exhibits better performance compared to commercially available P25 samples. Zhu *et al.* used TiO2 to produce acrylamide Pickering PolyHIPE beads and demonstrated its photocatalytic activity by degrading methyl orange (MO) [129]. While the polymer beads were not as effective as pure TiO2 at the beginning of the test, after 2.5 h of treatment, 99.4% of MO was found to be degraded, similar to pure TiO2 nanoparticles. Additionally, there was no reduction in the photocatalytic performance of the porous beads until 9 cycles of usage. On the other hand, there was no significant difference in photocatalytic performance between the porous beads prepared with a different amount of TiO2 particles due to the limited UV penetration into the beads to excite remaining TiO2 particles within the polymer matrix rather than a pore surface. On the other hand, Yuce *et al.* demonstrated that the loading of TiO2 increases the photocatalytic degradation of 4-nitrophenol of the surface-modified TiO2 particle stabilized emulsion template of polydicyclopentadiene [130].

In addition to TiO2, various functional colloidal particles decorated Pickering PolyHIPEs have been used for various catalytic activities. Lee *et al.* used silver-incorporated melamine-based microporous organic polymers (m-MOP/Ag) as the sole stabilizer to obtain a hydrophilic and open-porous acrylamide PolyHIP [131]. The resultant monolith was utilized as a heterogeneous catalyst to reduce 4-nitrophenol in an aqueous medium. It is reported that the rate constant of the reaction is 7 times faster with the PolyHIPE compared to the bulk m-MOP/Ag composite, suggesting that the catalytic sites are accessible due to the interconnected porous nature of the PolyHIPE. Sun *et al.* prepared a zeolitic imidazolate framework (ZIF-8) porous HIPE template by utilizing ZIF-8 as a stabilizer and the material to form the

skeleton by bonding ZIF-8 nanoparticles within the continuous phase [132]. The ZIF-8 monolith was used as a catalyst for the flow-through Knoevenagel reaction, and it was observed that the monolith reacts with benzaldehyde with a conversion rate of 100%. Gao *et al.* produced an open-porous solid acid by sulphonation of Pickering Poly(DVB-sodium p-styrene sulfonate) and demonstrated its catalytic activity by converting cellulose into 5-hydroxymethylfurfural [133]. Pan *et al.* further improved the system by increasing the surface area of the PolyHIPE through hypercrosslinking and demonstrated its superior catalytic activity [70]. While the obtained PolyHIPE lacked pore throats, it exhibited mesopores due to hypercrosslinking.

1.6.2. Sorbent

Due to their high porosity and high surface area, PolyHIPEs are used as sorbent. The utilization of Pickering emulsion templates as an adsorbent is highlighted in an excellent review by Zhu *et al* [134]. In the case of Pickering PolyHIPEs, large porous structure is beneficial since it allows the efficient mass transport. Since PolyHIPEs as a sorbent material necessitates the interconnected porous structure, they are generally prepared from surfactant/particle dual emulsified HIPEs. Additional selectivity toward specific target such as pollutants or oil/water and metal ions can be achieved due to functional particles decorating the pore walls. For example, Yang *et al.* demonstrated the Cu^{2+} adsorption capacity of interconnected lignin stabilized melamine formaldehyde HIPE template from $CuSO_4$ solution up to 73 mg g^{-1} [69]. Similarly, acrylamide Pickering PolyHIPE hydrogels were demonstrated to adsorb Cu^{2+} up to 280 mg g^{-1}, thanks to ionic functional groups on the material [73]

The efficacy of Pickering PolyHIPEs as a sorbent material in CO_2 capture were demonstrated in several reports. Metal-organic-frameworks (MOFs) are commonly used functional stabilizer in Pickering PolyHIPEs for CO_2 capture due their unsaturated metal centres which can interact with CO_2 [135,136]. Alternatively, He *et al.* prepared 4-vinylbenzyl chloride PolyHIPEs and used them as CO_2 adsorbent after the introduction of quaternary ammonium chloride groups to PolyHIPE [80]. It was observed that surfactant/Pickering dual emulsified emulsion templates exhibit better CO_2 capture compared to both solely surfactant stabilized emulsion templates and commercially available Excillion membranes. The better performance of surfactant/Pickering PolyHIPE system is attributed to the larger pore size of the PolyHIPE. The larger pore size of the PolyHIPE allows efficient mass transfer which facilitates air transport through the material and efficient quaternization/ion exchange, increasing the OH^- groups on the polymer. Wang *et al.* utilized polyethyleneimine enveloped TiO_2 nanoparticles and Span 80 as a stabilizer to produce a St/DVB Pickering PolyHIPE for CO_2 capture [125]. The CO_2 adsorption capacity of Pickering PolyHIPE was approximately 15% higher than that of PolyHIPE prepared by Span 80 only.

The superior performance of Pickering PolyHIPE is attributed to the increased surface area of amine groups on the pore surface due to embedded TiO_2 particles which where enveloped with PEI.

Sulfonated polystyrene was used as a stabilizer to obtain butyl acrylate Pickering PolyHIPE for oil spill recovery application [137]. Various fuels/solvent-water mixture was used as a spilled oil model and it was observed that absorption capacity of the PolyHIPE ranging between 11.2 to 37.5 g g^{-1}. Similarly, Azhar *et al* used iron oxide nanoparticles together with a fluorinated surfactant to obtain hexafluorobutyl Pickering PolyHIPEs with magnetic properties [83]. Pickering PolyHIPEs demonstrated to absorb 14 g g^{-1} and 10.25 mg g^{-1} of DCM and methylene blue, respectively. The oil adsorption capacity of Pickering PolyHIPE was double the capacity of conventionally prepared PolyHIPE. The magnetic property of the PolyHIPE is also beneficial to guide the material to collect oil simply by magnet. Ehtyl cellulose (EC) nanoparticles were HIPE templated and demonstrated it is application to oil/water separation [138]. A droplet of n-decane-in-water emulsion was separated upon contact with the EC porous material due to adsorption of n-decane by EC. Similarly, the ZIF-8 Pickering PolyHIPE was used as oil adsorbent and exhibited high absorption rate, reaching the equilibrium as fast as in 5 s, compared to bulk ZIF-8 [132]. Abebe *et al.* used methylcellulose/tannic acid stabilized alginate/polyacrylic acid Pickering PolyHIPE as an amphiphilic adsorbent, for the removal of methylene blue and quinoline from aqueous and non-aqueous environment, respectively [139]. Both the skeleton of the PolyHIPE and the particles on the pore walls were responsible for methylene blue removal from an aqueous solution, while only the particles contribute the removal of quinine from non-aqueous solution since the PolyHIPE material itself was hydrophilic. Al_2O_3 stabilized acrylic acid HIPE template was used as superabsorbent [76]. The obtained PolyHIPE exhibit superabsorbent ability, absorbing above 40 g g^{-1} water and saline solutions. The crosslinking density of the material is shown to affect the absorption capacity, since a lightly crosslinked polymer wall can absorb water more efficiently than highly crosslinked counterparts. Fe_3O_4 nanoparticle stabilized acrylamide HIPE templates used as water absorbent and demonstrated its efficiency of separating water phase from a surfactant stabilized emulsion [140].

1.6.3. Encapsulation

The closed pores of Pickering PolyHIPEs are used to encapsulate materials for further applications. Depending on the application, closed cellular morphology of conventional Pickering PolyHIPEs can be advantageous if the release of the encapsulated material is not intended [77,141,142]. Alternatively, open-celullar Pickering PolyHIPEs are generally preferred if the encapsulated materials, such as drugs, are expected to be released [55,71,143].

Elastomer-filled hydrophilic PolyHIPEs were prepared by templating either surfactant or nanoparticle-stabilized HIPE, and their water adsorption capacities were compared [141]. In the synthesis, the continuous phase consisted of the hydrophilic monomer, sulfonated styrene, and the internal phase consisted of 2-ethylhexyl acrylate. The obtained PolyHIPE pores were filled with crosslinked EHA elastomer, regardless of the stabilizer used. Interestingly, a significant difference in water absorption capacity, up to three times, between the produced PolyHIPEs was observed. The inferior water absorption capacity of conventional PolyHIPEs was attributed to the copolymerization of SS in the continuous phase and the EHA in the internal phase. The incorporation of hydrophobic EHA into the macromolecular structure reduced the hydrophilic character of the PolyHIPE. Such copolymerization was not observed in Pickering PolyHIPEs due to the efficient barrier effect of particles preventing the interaction of two phases with each other. Similarly, elastomer-filled Pickering PolyHIPEs are demonstrated to exhibit shape memory foams [142]. The PolyHIPE skeleton is composed of semi-crystalline, long side-chained polyacrylates, and the nanoparticles are used as both emulsion stabilizer and crosslinker. Interestingly, the material demonstrated to exhibit dual lock-in shape memory; when the PolyHIPE is subjected to water above the melting temperature of the polymer composing the skeleton, the crystalline structure melts, the hydrogel structure plasticizes and allows the elastomer to recover the original shape of the material. When the PolyHIPE is synthesized with the surfactant and conventional crosslinker, copolymerization takes place between the monomers within both phases, and this copolymerization reduces the side chain mobility, therefore, reducing the shape recovery behavior of the material.

Pickering PolyHIPEs have recently been employed for encapsulating phase change materials (PCMs) for thermal energy storage. Both organic PCMs, such as octadecane[144,145] and dodecanol [146] and inorganic PCMs like calcium chloride hexahydrate [147] were successfully encapsulated within the pores of Pickering PolyHIPEs, serving as the internal phase during HIPE preparation. The intrinsic closed-cellular morphology of Pickering PolyHIPEs, combined with interfacial initiation of polymerization, facilitates efficient PCM encapsulation within the pores while minimizing PCM leakage. Despite the inherent low thermal conductivity of polymers, a crucial property in thermal energy storage and release, enhanced thermal conductivity is achieved through the incorporation of particles with good thermal conductivity. Lu *et al.* not only demonstrated the heat storage capacity of PCM-encapsulated PolyHIPE but also its light-to-heat conversion efficacy. They achieved this by using carboxylated carbon nanotubes (CNT) as a HIPE stabilizer to decorate the pores (Fig. 20 A) [145]. Conversely, due to the low thermal conductivity of polymers, a cellulose-based Pickering PolyHIPE was demonstrated for thermal insulation, leveraging its intrinsic low thermal conductivity, closed porous morphology, and low density (Fig. 20 B) [148].

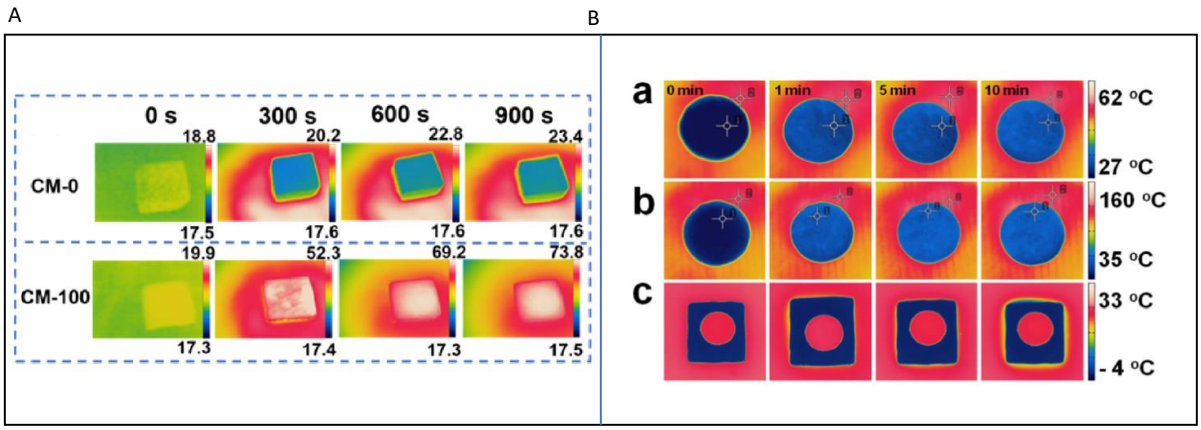

Figure 1.20: The infrared images of PolyHIPE (CM-0) and carboxylated CNT incorporated Pickering PolyHIPE (CM-100) captured at different times under light irradiation, demonstrating to light-to-heat conversion of CNT incorporated Pickering PolyHIPE (A) [145]. The infrared images of PolyHIPE demonstrating their low thermal conductivity (B): PolyHIPE on a hot plate (a, b) and on ice (c) [148].

PolyHIPEs can serve as effective carriers for drug encapsulation, producing bioactive scaffolds for tissue engineering applications. Hu *et al.* loaded Ibuprofen, an anti-inflammatory drug, within Pickering PLGA emulsion templates obtained by solvent evaporation [55]. The scaffold exhibited an initial burst release, with approximately 55% of the drug released within 24 hours, followed by sustained slow release, reaching around 65% of drug release in 196 hours. The fast and slow drug release profiles were attributed to the initial release from the outer surface of the scaffold and the increased diffusion path from the inner side of the scaffold, respectively. Similarly, Artemisia argyi oil (AAO) was loaded into an acrylamide PolyHIPE stabilized by surfactant, Pickering, and dual emulsifiers [71]. Scaffolds stabilized by Pickering particles exhibited slow release of AAO due to closed cellular morphology, while surfactant and dual emulsifier-stabilized HIPE templates exhibited an initial burst followed by slow release. Since the dual-emulsified Pickering HIPE template exhibited an improved modulus, the antibacterial activity of the dual-emulsified Pickering HIPE template was further investigated; the AAO-loaded scaffolds exhibited an inhibition zone of more than 4 mm for 2 weeks. Alternatively, Yang *et al.* produced a drug carrier HIPE template by mixing a solvent (dichloromethane), drug (enrofloxacin), and a polymer blend followed by solvent evaporation. The produced enrofloxacin PolyHIPE exhibited fast and complete drug release, with 80% of the drug released in 2.5 hours, reaching 98% within 10 hours [143].

1.6.4. Other

Rarely reported applications and/or the features of prepared Pickering PolyHIPEs will be reviewed in this section. Zhu *et al.* obtained a superhydrophobic Pickering PolyHIPE when the particle with a single cavity was used as an HIPE stabilizer. The observed high water-contact angle (~152°) was attributed to rough pore surface due to embedded particles and the trapped air in pores as well as in the cavity of

the particles [149]. Guan *et al.* reported superhydrophobic Pickering PolyHIPEs with the WCA 162° [150]. The increased hydrophobicity was due to efficient post-modification of PolyHIPE due to Si groups on the silica decorated pore surface, allowing tetraethyl orthosilicate (TEOS) and 1H,1H,2H,2H-perfluorooctyltrichlorosilane (FDTS) grafting on the pore surface. Another rarely reported application of Pickering PolyHIPE is sound absorption. Liu *et al.* used Pickering PolyHIPE as a sound absorber and reported it as an efficient low-frequency sound absorber due to its hierarchical porous structure, allowing higher surface area to contact air molecules and therefore, dissipate sound energy [151]. Additionally, electrically conducting composite Pickering PolyHIPEs can be prepared by using Ti_3AlC_2 [152] and silver nanoparticles [86] paving the way for high surface electrodes for biosensor applications based on PolyHIPEs

1.7. Conclusion

Pickering PolyHIPEs offer significant advantages in various applications due to their larger pores compared to conventional counterparts and the potential for functionality during synthesis. While the interconnected porous structure of PolyHIPEs is crucial for their potential functionalities, there has been no compilation of reported methods to achieve interconnected Pickering PolyHIPEs until now. This review is the first to specifically focus on Pickering PolyHIPEs, addressing their notorious closed porous structure and categorizing the achieved interconnectivities.

Moreover, the mechanical properties, which are notorious in the context of PolyHIPEs, are examined. However, conflicting reports exist in the literature, particularly regarding Pickering PolyHIPE morphology. Computational studies investigating the effect of particle distribution in PolyHIPEs may shed light on these discrepancies.

On the other hand, while the straightforward preparation of Pickering PolyHIPEs is an attractive feature, it presents challenges in understanding the cause-and-effect relationship, as a single parameter can impact the morphology and physical properties of both HIPEs and PolyHIPEs in a complex manner. The review also compiles and reports various applications of Pickering PolyHIPEs. In conjunction with advancements in nanomaterials like metal-organic frameworks, the interest in Pickering PolyHIPEs as a supporting material is expected to increase proportionally.

CHAPTER 2

Preparation of Interconnected Pickering Polymerised High Internal Phase Emulsions by Arrested Coalescence

*Enes Durgut [a, b], Colin Sherborne [a], Betül Aldemir Dikici [c], Gwendolen C. Reilly [a, b], Frederik Claeyssens [a, b, *]*

[a] *Kroto Research Institute, Department of Materials Science and Engineering, University of Sheffield, Sheffield, United Kingdom*

[b] *Department of Materials Science and Engineering, INSIGNEO Institute for In Silico Medicine, The University of Sheffield, Sheffield, United Kingdom*

[c] *Department of Bioengineering, Izmir Institute of Technology, Urla, Izmir, 35433, Turkey*

Abstract

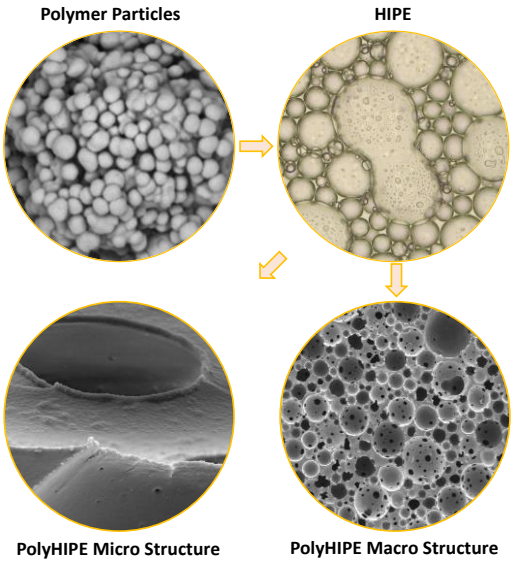

Emulsion templating is a method that enables the production of highly porous and interconnected polymer foams called polymerized high internal phase emulsions (PolyHIPEs). Since emulsions are inherently unstable systems, they can be stabilized either by surfactants or by particles (Pickering HIPEs). Surfactant-stabilized HIPEs form materials with an interconnected porous structure, while Pickering HIPEs typically form closed pore materials. In this study, we describe a system that uses submicrometer polymer particles to stabilize the emulsions. Polymers fabricated from these Pickering emulsions exhibit, unlike traditional Pickering emulsions, highly interconnected large pore structures, and we related these structures to arrested coalescence. We describe in detail the morphological properties of this system and their dependence on different production parameters. This production method might provide an interesting alternative to poly-surfactant-stabilized-HIPEs, in particular where the application necessitates large pore structures.

Keywords: Pickering emulsions, arrested coalescence, microparticles, HIPE, PolyHIPE

2.1. Introduction

Emulsion templating is a manufacturing method for creating porous interconnected polymeric materials. An emulsion is classified as a high internal phase emulsion (HIPE) when the internal droplet volume ratio is greater than 74% of the total volume fraction, which is the theoretical volume limit achievable from monodisperse spheres in a 3D close-packed face-centered cubic (FCC) array [64]. The mixing of a cross-linkable hydrophobic monomeric liquid with water creates a water-in-oil (w/o) emulsion, polymerization of the oil phase (continuous phase) and removal of the water phase (internal phase) leaves behind a porous foam called a polymerised HIPE (PolyHIPE). The mixing of a crosslinkable hydrophobic monomer liquid with water creates a water-in-oil (w/o) emulsion, and polymerization of the oil phase (continuous phase) and removal of the water phase (internal phase) leaves behind a porous foam called a polymerized HIPE (PolyHIPE). The PolyHIPE's internal structure replicates the emulsion at the monomer gel point. The porosity, average pore, and pore throat size are determined by tailoring various parameters such as the amount of the internal phase, surfactant, and stirring speed during the emulsification [3].

Emulsions are thermodynamically unstable systems. When two immiscible liquids are mixed together without the stabilizing surfactant or particles, the droplet phase rapidly coalesces to minimize the contact area, and this causes the emulsion to separate back into its two bulk phases [3]. Surfactants can be used to stabilize the emulsion by locating themselves at the interface between the two liquids to lower the interfacial tension and prevent droplet coalescence. Hypermer B246 [114,122,153–156] and Span 80 [157,158] are two common non-ionic surfactants used to stabilize w/o emulsions. Nevertheless, the surfactant removal from the final product is a laborious and costly process that can require intensive washing with solvents [87]. Additionally, conventional PolyHIPEs possess small pores, typically 1–50 µm in size, which limits their application where the permeability is important [80], or where large pores can be useful, for example, for vascularization in tissue engineering applications [47].

In addition, particles can be used to stabilize the emulsion. These emulsions are termed Pickering emulsions. Here, particles with intermediate wettability localize at the oil/water interface. Silica oxide [143], titania [79], hydroxyapatite [159], and polystyrene [72] are some of the commonly used particles to prepare Pickering HIPEs. Particles to be used in HIPE are generally subjected to a surface modification such as oleic acid [66] or cetyltrimethylammonium bromide (CTAB) [73] modification to tune their wettability. Rather than lowering the interfacial tension, particles form a solid barrier around the dispersed droplets, which inhibits the coalescence of emulsion droplets [160]. The attachment/detachment energy of particles to/from the interface is higher compared to that of surfactants, which leads to superior emulsion stability in Pickering emulsions [161]. Additionally, the

incorporated particles may introduce further functionalities in the final PolyHIPE such as magnetic or light responsiveness [162] or antibacterial properties [163].

While particle stabilization offers several advantages over surfactant stabilization such as cost-effectiveness, higher stability, and lower toxicity (depending on the nature of the particles [4]) and potentially adding functionality [162], Pickering PolyHIPEs exhibit a closed pore structure. The formation of pore throats, which connect pores to each other, in poly-surfactant-stabilized-HIPEs is attributed to rupturing of the thin monomeric film between the neighbouring droplets due to the polymerization-induced volume shrinkage [62] or post-polymerization treatments [28].

Alternatively, the pore throat formation due to the depletion attraction-induced droplet/pore coalescence has been proposed recently [64]. According to the common view, the rigid particle shell around Pickering emulsion droplets increased the viscoelasticity of the continuous film separating two neighbouring droplets, and the consequent thicker monomeric film resists rupturing during polymerization or post-polymerization treatments. The absence of interconnected pores prevents Pickering PolyHIPEs from being used for applications such as filtration or tissue engineering that require the use of substrates exhibiting an open cellular morphology. To overcome this problem, there have been several efforts to create interconnected Pickering PolyHIPEs. Inducing volume contraction during polymerization is achieved either by increasing the crosslinker content or by adding a co-monomer undergoing relatively higher shrinkage during polymerization [89,90]. This approach requires the addition of substances that might not be relevant or applicable to the final application of the PolyHIPE or requires intensive crosslinking. Using a combination of a surfactant with the Pickering particles is a commonly used approach to obtain interconnected PolyHIPEs [66,68,88]. However, while this system enables the fabrication of PolyHIPEs with large interconnected pores, the PolyHIPE will contain leachables, which might need to be removed. Alternatively, particle etching is demonstrated to obtain interconnected PolyHIPEs; however, this necessitates solvent extraction [72].

We aimed to prepare 2-ethylhexyl acrylate–isobornyl acrylate–trimethylolpropane triacrylate (EHA/IBOA/TMPTA) Pickering PolyHIPEs, where the emulsion template was stabilized by polymeric microparticles (IBOA/TMPTA) sharing a similar chemical composition with the continuous phase of the HIPE. The HIPE was successfully synthesized, and the PolyHIPE is observed to exhibit an interconnected porous structure. The obtained PolyHIPE was compared with PolyHIPEs where the HIPE templates were stabilized by Hypermer B246 and hydrophobic silica (HDK H30) morphologically. Furthermore, the effects of the IBOA microparticle size and concentration and the internal phase fraction were also investigated morphologically. We hypothesized that the interconnected porous structure of Poly-IBOA-stabilized HIPE is due to partial but arrested coalescence of emulsion droplets, which is the phenomenon commonly observed in Pickering emulsions.

2.2. Materials

2-Ethylhexyl acrylate (EHA), isobornyl acrylate (IBOA), trimethylolpropane triacrylate (TMPTA), polysorbate 20 (Tween 20), potassium persulfate (KPS) and 2-hydroxy-2-methylpropiophenone (photoinitiator, PI) were purchased from Sigma-Aldrich (Poole, UK). Hypermer B246-SO-M was received as a sample from Croda (Goole, UK). Pyrogenic silica (HDK H30) was purchased from Wacker.

2.3. Methods

2.3.1. The Nomenclature of Samples

Synthesized IBOA microparticles are named according to the IB-X formula where IB stands for IBOA and X defines the size of particles: large(L, 724 nm), medium (M, 199 nm), and small (S, 103 nm). PolyHIPEs are defined using the abbreviation U(W)T ,where U is the internal phase fraction, W is the stabilizer type, either Hypermer B246 (Hyp), IBOA (IB), ot silica (Si), and T is the stabilizer concentration. For example, 80(IB-L)5 defines the PolyHIPE having an 80% wt internal phase and stabilized by 5% wt of large IBOA particles. 80(Hyp)5 defines the PolyHIPE having an 80% wt internal phase and stabilized by 5% wt Hypermer B246.

2.3.2. Preparation of Microparticles

IBOA microparticles were prepared by the formation of oil-in-water (o/w) emulsion, followed by its subsequent polymerization, as listed in Table 2.1. Briefly, the continuous phase was prepared by dissolving respective amounts of Tween 20 (0.09, 0.45 and 0.9 g for IB-L, IB-M and IB-S, respectively) in order to tune the emulsion droplet/particle size and 0.18 g of KPS in 9 g of deionized water (dH2O) in a glass flask at room temperature. Next, 1 g of the internal phase consisting of the 0.75 g IBOA and 0.25 g TMPTA blend was added to 9 g of the continuous phase in a 20 mL glass flask. The ultrasonic processor horn was immersed approximately 2 cm deep into the mixture. The mixture was emulsified through sonication at 100 Watts, 30 kHz (Hielscher UP100H, Hielscher Ultrasound Technology) for a minute. The prepared emulsion was placed in a convection oven at 65 °C for 18 h for polymerization. Particles were washed with 30 mL of methanol for 15 min.

Table 2.1: The IBOA and TMPTA ratio (% wt), Tween 20 concentration in respect to continuous water phase (% wt)[a], KPS concentration in respect to internal organic phase (% wt)[b], average particle size (D_p), and polydispersity index (*PDI*) of IBOA microparticles.

ID	Internal Phase		Continuous Phase		D_p (nm)	*PDI*
	IBOA (%)	TMPTA (%)	Tween 20[a] (%)	KPS[b] (%)		
IB-L	75	25	0.10	2	724	0.04
IB-M	75	25	0.50	2	198	0.03
IB-S	75	25	1.00	2	103	0.03

The mixture was centrifuged at 14,000 RPM for 15 min, then the supernatant was removed. Particles were resuspended in 20 mL of water through sonication for a minute and dried at 65 °C overnight.

2.3.3. Preparation of EHA/IBOA PolyHIPE

The emulsion continuous phase was prepared by mixing a monomer blend consisting of EHA (2.52 g, 63% wt), IBOA(0.84 g, 21% wt), and the crosslinker TMPTA (0.64 g, 16% wt) in a 40 mL glass flask. The respective amount of the stabilizer, either Hypermer B246, IBOA microparticles, or silica nanoparticles, and 0.1 g of PI were added and mixed into 4 g of the monomer blend (Table 2.2). Particles were dispersed in the monomer phase by sonication at 100 Watts, 30 kHz for a minute. The HIPE was prepared by the addition of respective amounts of dH_2O (12, 16 and 22.7 g for the samples of 75, 80 and 85% porosity, respectively) dropwise using a syringe pump at 0.8 mL/min into the continuous phase while the mixture was being stirred using the overhead stirrer at 500 RPM (Pro40, SciQuip). The produced HIPE was mixed for an additional 5 minutes after all the internal phase was added. The produced HIPEs were poured onto a glass Petri dish (the thickness of HIPEs were ~ 1 cm) and polymerized through the belt conveyor UV curing system (GEW Mini Laboratory, GEW Engineering UV). The polymers taken out of the dish were dried in an oven at 60 °C overnight. Additionally, a low internal phase emulsion (LIPE) with a 33% internal phase stabilized by the above-mentioned stabilizers was prepared while keeping the stabilizer to internal phase ratio the same as the HIPE's.

Table 2.2: Density (ρ), porosity ($P_\emptyset$), emulsion droplet size (P_d), polydispersity index of emulsion droplet size ($PDI\ P_d$), pore size (P_p), polydispersity index of pore size ($PDI\ P_p$), pore throat size (P_t), number of pore throats per pore (#) and degree of openness (D_o) of PolyHIPEs.

Sample	ρ (g/cm^3)	$P_\emptyset$	P_d (µm)	$PDI\ P_d$	P_p (µm)	$PDI\ P_p$	P_t (µm)	#	D_o
$80(Hyp)_5$	1.02	78.29	10	0.25	8	0.61	6.14	16.40	0.083
$80(IB\text{-}M)_5$	1.01	76.74	50	0.45	49	0.72	14.99	11.27	0.076
$80(Si)_5$	0.55	57.70	80	0.28	85	0.84	N/A	N/A	N/A
$80(IB\text{-}M)_1$	1.04	77.41	91	0.42	86	2.31	55.83	16.73	0.088
$80(IB\text{-}M)_{10}$	0.98	75.26	34	0.42	21	0.93	7.49	4.46	0.026
$80(IB\text{-}L)_5$	1.05	76.34	65	0.53	74	1.01	34.26	10.87	0.113
$80(IB\text{-}S)_5$	1.00	75.82	39	0.35	27	0.89	11.37	3.66	0.035
$85(IB\text{-}M)_5$	0.97	81.16	49	0.39	56	0.62	21.91	13.47	0.117
$75(IB\text{-}M)_5$	0.96	72.43	49	0.80	54	0.81	12.49	4.73	0.033

2.3.4. Characterization

IBOA microparticles were 8 nm thick and gold-coated and were imaged using a scanning electron microscope (Inspect F, FEI) where the accelerating voltage and the spot size were 5 kV and 3, respectively. The oarticle size of IBOA microparticles was calculated by averaging the diameter of 300 particles measured from scanning electron microscopy (SEM) micrographs using the software ImageJ. The polydispersity index of particles was calculated according to the formula

$$PDI = \left(\frac{\sigma}{D_p}\right)^2 \quad (1)$$

where σ is the standard deviation and D_p is the average particle size. Contact angle was measured by the sessile drop test and analyzed using the integrated software (FTA32, First Ten Angstroms) for IB-M and silica particles, which were placed on a double-sided tape and squeezed with the glass slide to smoothen the surface, as well as EHA/IBOA/TMPTA and IBOA/TMPTA polymer films photo-polymerized between two glass slides.

HIPEs and LIPEs were imaged under the light microscope (CX43, Olympus), and optical micrographs were captured using the integrated camera (DP27, Olympus). The average emulsion droplet size was calculated by averaging 100 emulsion droplets measured from optical micrographs using ImageJ. Viscosity of HIPEs was measured on a rheometer (AR2000, TA Instruments) by using a standard steel cone (40 mm 2°) at 25 °C.

The microarchitecture of PolyHIPE samples was investigated by SEM using a protocol similar to that used for IBOA microparticle imaging. The average pore size was calculated by averaging 250 pore sizes measured from SEM micrographs using ImageJ. The statistical correction factor was applied to reduce the error due to uneven sectioning according to the formula [3,105]:

$$P_p = \frac{2}{\sqrt{3}} P_m \quad (2)$$

Where P_p is the corrected average pore size and P_m is the measured.

Number of pore throat per pore and degree of openness are calculated from SEM micrographs as well; 15 highly interconnected pores, which are 2-2.5 times larger than the average pore size, were chosen; number of pore throat on each chosen pore counted and averaged to deduce number of pore throat per pore. Additionally, degree of openness was calculated according to the formula [3]:

$$D_o = \frac{\sum A_i}{A_p} \quad (3)$$

Where D_o is the degree of openness, A_i is the overall surface area of pore throats on a single pore and A_p is the surface area of the pore. The pore surface is considered as a cap of an hemisphere.

The average pore throat size was measured using a mercury intrusion porosimeter (AutoPore V, Micrometrics), where the contact angle of mercury was 130° and the highest applied pressure was 30.000 psi. The bulk density of cylindrically cut PolyHIPE samples was calculated by dividing the measured mass by calculated volume from a known geometry. The skeletal density of PolyHIPEs were measured using a pycnometer (AccuPyc 1340, Micromeritics). The porosity of PolyHIPEs was calculated according to the formula:

$$P_{\emptyset} = \left(1 - \frac{\rho_{sd}}{\rho_c}\right) 100 \quad (4)$$

Where $P_{\emptyset}$ is the porosity, ρ_{sd} is the skeletal density, ρ_c is the calculated density. Available particle surface is calculated according to the formula:

$$A_{ps} = \frac{N_p \, x \, A_{mc}}{V_{int}} \quad (5)$$

Where A_{ps} is the available particle surface defining the sum of the mid-circular area of particles dispersed in the continuous phase per volume of internal phase, N_p is the number of particles in the continuous phase, A_{mc} is the average mid-circular area of the given particle and V_{int} is the volume of internal phase used to prepare HIPE.

2.4. Results and Discussion

2.4.1. IBOA Microparticles

The particles listed in Table 2.1 were successfully synthesized by the emulsion polymerization method and are represented in Figure 2.1. Increasing emulsifier concentrations (Tween 20) yielded reduced average particle size, as previously reported [164]. The diameters of the particles prepared using 0.1, 0.5, and 1% Tween 20 were measured to be 724, 198, and 103 nm, respectively. The polydispersity indices of all the produced particles were between 0.03 and 0.04. Irregular shaped particles were also observed in IB-L. The reduced amount of the stabilizer in the emulsion system might not have efficiently stabilized the emulsion droplets, leading to irregular shaped particles.

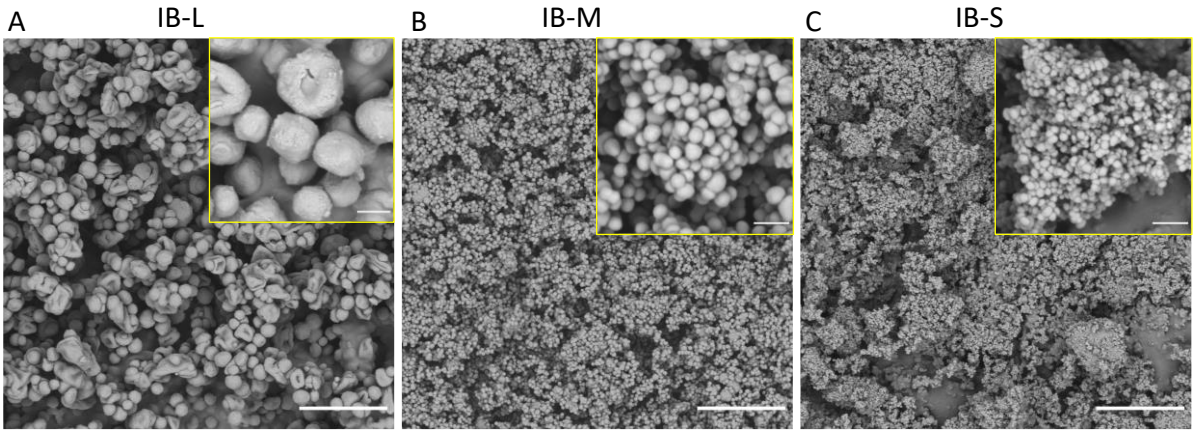

Figure 2.1: SEM images of IBOA microparticles; IB-L (A), IB-M (B) and IB-S (C). Scale bars are 5 µm and 500 nm for main images and insets, respectively.

2.4.2. Emulsion Droplets

80(Hyp)5, 80(IB-M)5, and 80(Si)5 HIPEs and LIPEs were successfully prepared. Microscopic evaluation of emulsion droplets was conducted, and the micrographs are presented in Figure 2.2. The average HIPE emulsion droplets sizes are 10.6, 50.7, and 80.1 µm for 80(Hyp)$_5$, 80(IB-M)$_5$, and 80(Si)$_5$ HIPEs, respectively (Figure 2.2 A–C). Emulsion droplets of Pickering HIPEs exhibit larger pores than that of surfactant-stabilized emulsion droplets, as reported previously [165]. The 80(Si)5 HIPE exhibits a larger pore size than 80(IB-M)$_5$, although the silica particles are smaller, 20 nm [71], than the synthesized IB-M. The silica-stabilized emulsion also exhibits a very high viscosity (see Figure 2.3), which increases with the amount of the internal phase (or water uptake). Indeed, the 80(Si)$_5$ HIPE did not show any significant flow when its vial was turned upside down, in contrast with the two other emulsions. This high viscosity also means that high water incorporation is difficult to obtain due to inefficient mixing. Indeed, approximately 1.2 g (or 7.5%) of water was not incorporated in the 80(Si)$_5$ HIPE. Thus, the high viscosity of the HIPE also has the effect of producing larger emulsion droplets and reduced maximum internal phase uptake because of inefficient mixing and the consequent reduced breakdown of large droplets into smaller ones [160].

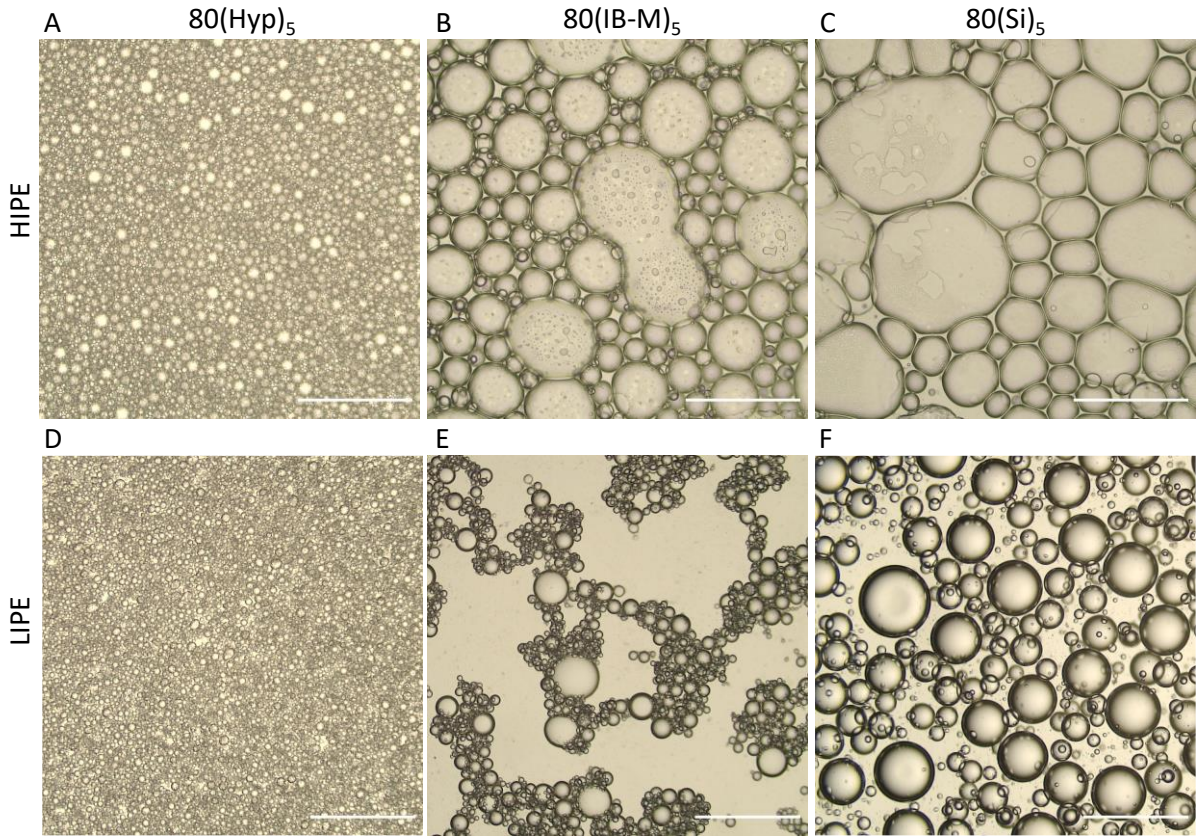

Figure 2.2: Optical micrographs of HIPE (A-C) and LIPE (D-F) stabilized by either Hypermer B246, IB-M and silica nanoparticles. Scale bars are 200 µm.

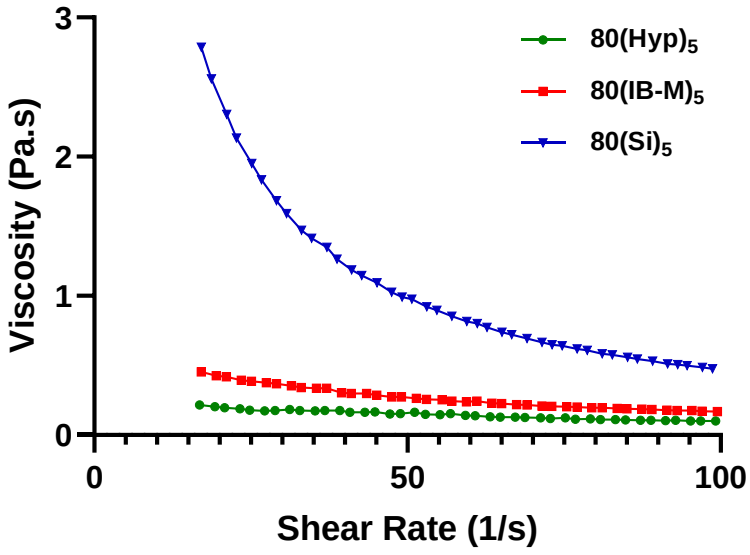

Figure 2.3: The viscosity of HIPE samples as a function of shear rate.

Partially coalesced droplets are observed in 80(IB-M)$_5$ HIPE (Fig. 2.4 B) as observed previously and attributed to arrested coalescence [166,167]. Partial coalescence of multiple 80(IB-M)$_5$ emulsion droplets is also observed and provided in Figure 2.4. To obtain the images of the HIPE, the emulsions were placed in between a glass slide and a coverslip, and this action might have induced coalescence in the HIPE and might not give a reliable overview on the 3D emulsion behavior. In order to image the organization of emulsion droplets, LIPEs were prepared while keeping the particle concentration to internal phase ratio the same as that for HIPEs. It was observed in optical micrographs of LIPEs (without placing them in between a microscope slide and a coverslip) that the IB-M-stabilized droplets form dense aggregates; larger droplets are covered with small droplets, and these small droplets seem to function as a bridging connection between the relatively larger droplets (Figure 2.2 E). A similar droplet aggregation was observed previously and attributed to arrested coalescence [168]. This behaviour is distinct from both 80(Hyp)$_5$ and 80(Si)$_5$ HIPEs, they do not exhibit the level of droplet aggregation shown in the 80(IB-M)$_5$ LIPE.

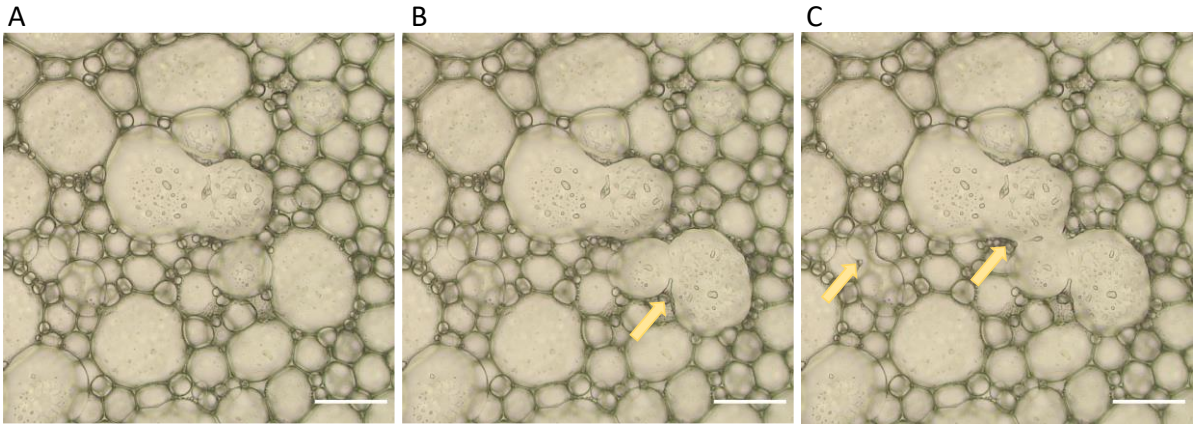

Figure 2.4: Demonstration of partial coalescence of emulsion droplets in 80(IB-M)$_5$.The necking of emulsion droplets is indicated by orange arrows. Images were captured within a minute. Scale bars are 100 µm.

The difference in droplet aggregation between 80(IB-M)$_5$ and 80(Si)$_5$ might be associated with the particle localization at the oil/water interface. However, the contact angles of IB-M and silica nanoparticles are very similar with values of 125.6 and 126.1°, respectively. Given that our measurements are a convolution of hydrophobicity and surface roughness, as induced by the nanoparticles, the inherent hydrophilicity/hydrophobicity of the materials tends to increase when cast on a surface in the nanoparticle form, as highlighted in detail in ref [169]. We measured the contact angle on cast films of EHA/IBOA/TMPTA (the same composition as that of the continuous phase) and IBOA/TMPTA (the same composition as that of IB-M) to be 63.9°. Therefore, the estimation of particle localization at the oil/water interface is difficult in the current experimental design.

Total stability of 80(Si)$_5$ emulsion droplets might be due to the prevention of emulsion droplet contact either by total coverage of emulsion droplets by silica functioning as a mechanical barrier or resistance of the viscoelastic thin monomer film between emulsion droplets. For 80(IB-M)$_5$ emulsion droplets, the insufficient coverage of droplets with particles can lead to initiation of coalescence but being arrested due to migration of the particles to the contact point (or the necking region) and jamming to prevent the interfacial mobility [15]. On the other hand, interparticle attraction forces might be another mechanism resulting in flocculated emulsion droplets. In either case, it is expected to obtain an interconnected porous structure upon polymerization of the 80(IB-M)$_5$ template due to their flocculated state. The pore throat formation might be due to thin film rupture between neighbouring pores or partial but arrested coalescence of emulsion droplets. If the pore throat formation is due to the arrested coalescence of droplets, it is expected that observe dense particle layer surrounding pore throats and in-between pores is observed due to particle jamming at the necking region of these partially coalesced emulsion droplets.

2.4.3. The Effect of Stabilizer Type on PolyHIPE Morphology

PolyHIPEs listed in Table 2.2 were successfully synthesized and morphologically investigated through the acquired SEM images provided in Figure 2.5. The pore sizes of PolyHIPEs are 8, 49, and 85 µm for 80(Hyp)$_5$, 80(IB-M)$_5$, and 80(Si)$_5$, in correlation with the emulsion droplet size observed under the light microscope.

Interestingly, 80(IB-M)$_5$ exhibits an interconnected porous structure which is an uncommon morphology for Pickering PolyHIPEs [160]. However, pore throats of 80(IB-M)$_5$ differ from pore throats of 80(Hyp)$_5$ in two ways. First, 80(Hyp)$_5$ represents a nearly homogeneous distribution of pore throats, regardless of the pore size. On the other hand, 80(IB-M)$_5$ exhibits an interconnected porous structure especially on the relatively larger pores together with submicron-sized pore throats. Second, relatively smaller pores of 80(IB-M)$_5$ are generally closed; however, they contain submicron pore throats (Figure 2.5 E). Additionally, pore throats observed in 80(IB-M)$_5$ are encircled with a dense particle layer. This observation is considered as an indication of pore throat formation due to partial but arrested coalescence of emulsion droplets. While 80(Si)$_5$ does not exhibit pore throats, thinned pore walls are occasionally observed. Thinned regions of the pore walls are considered susceptible regions for pore throat formation during post-processing and commonly observed in Pickering PolyHIPEs [165,170].

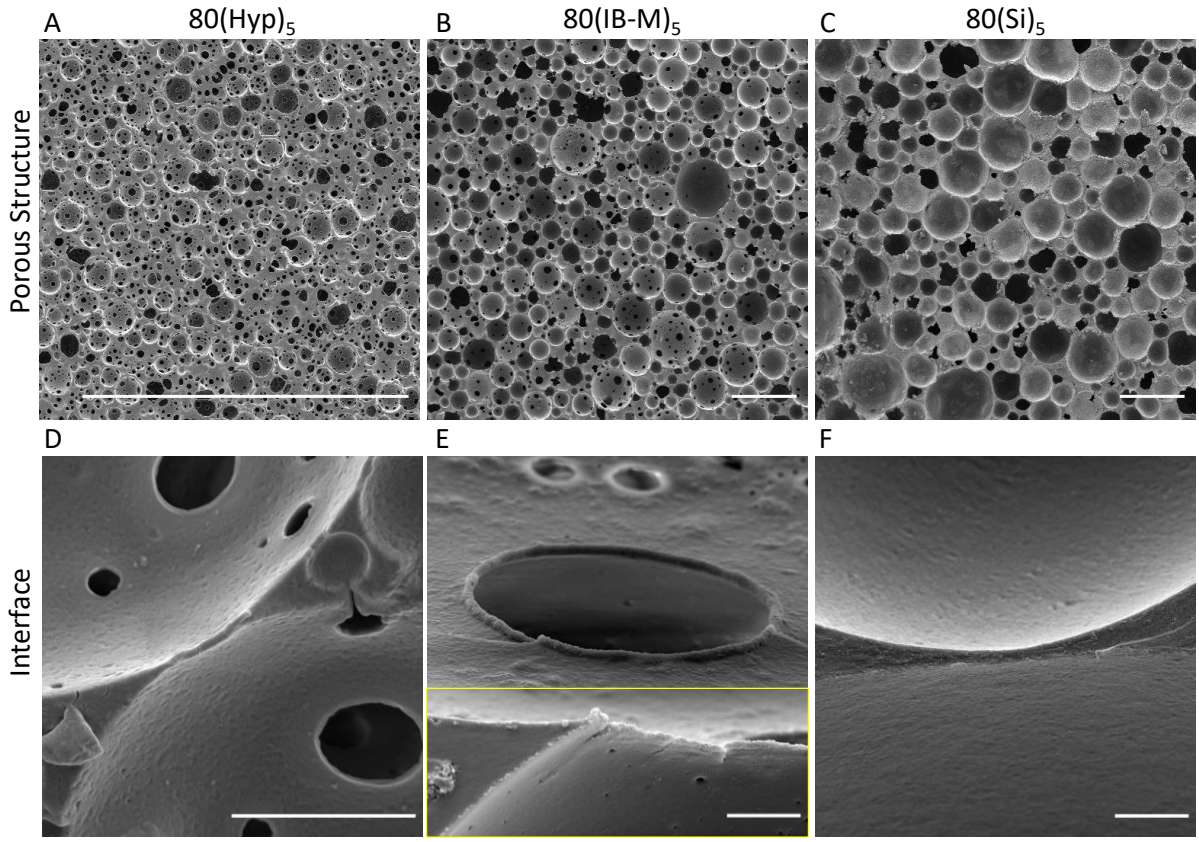

Figure 2.5: SEM images 80(Hyp)$_5$, 80(IB-M)$_5$ and 80(Si)$_5$ focusing on porous structure (A-C) and interface (D-E). Images from same region, one focusing on pore throat and the other focusing on the interface are merged (E). Scale bars are 250 µm (A-C) and 5 µm

Furthermore, a thin polymer film separating two neighbouring pores is observed in 80(Hyp)$_5$ (Figure 2.5 D) and 80(Si)$_5$ (Figure 2.5 F) but is absent between the highly interconnected pores of 80(IB-M)$_5$ (Figure 2.5 E). Instead, there is a curved pore–pore junction, which is delineated by a dense particle layer. The similarity between pore throats and the pore–pore junction leads us to conclude that any pore throat in the SEM results in a pore–pore junction (which is a throat in the transverse view). Additionally, micron-sized pores are observed in close proximity to the larger pores. These micron-sized pores correlate to the bridging emulsion droplets observed in LIPEs. Therefore, it is concluded that the conventional pore throats are due to partial coalescence of emulsion droplets, whose further coalescence was arrested by the dense particles jamming the necking region of droplets, and submicron openings on the pore surface are due to partial coalescence of micron-sized droplets.

2.4.4. IBOA Microparticle Stabilized PolyHIPEs

Assuming that the interconnected porous structure observed in 80(IB-M)$_5$ is due to the partial and arrested coalescence of emulsion droplets, it is expected to observe increased interconnectivity as the available particle surface to stabilize the internal phase decreases; the more particle-free regions on emulsion droplets would be available for droplets to contact. The available particle surface is defined

as the particle mid-circular area in a given weight fraction per volume of the internal phase. Therefore, 80(IB-M)$_5$ is chosen as a control, and the available particle surface is reduced by decreasing the particle concentration [80(IB-M)$_1$, 0.19 cm^{-1}], increasing the particle size [80(IB-L)$_5$, 0.27 cm^{-1}], and increasing the internal phase fraction [85(IB-M)$_5$, 0.66 cm^{-1}]. Samples were compared with their higher available particle surface counterparts; 80(IB-M)$_{10}$ (1.88 cm^{-1}), 80(IB-S)$_5$ (1.88 cm^{-1}), and 75(IB-M)$_5$ (1.25 cm^{-1}).

SEM images demonstrating the porous structure of prepared PolyHIPEs are represented in Figure 2.6. The average pore size of PolyHIPEs increases as the particle concentration reduces (Fig. 6 A, B) [67] or particle size increases (Fig. 2.6 C, D) [171], in accordance with the previous reports. The average pore throat size, number of pore throat per pore and the degree of openness increased in samples with the low particle availability.

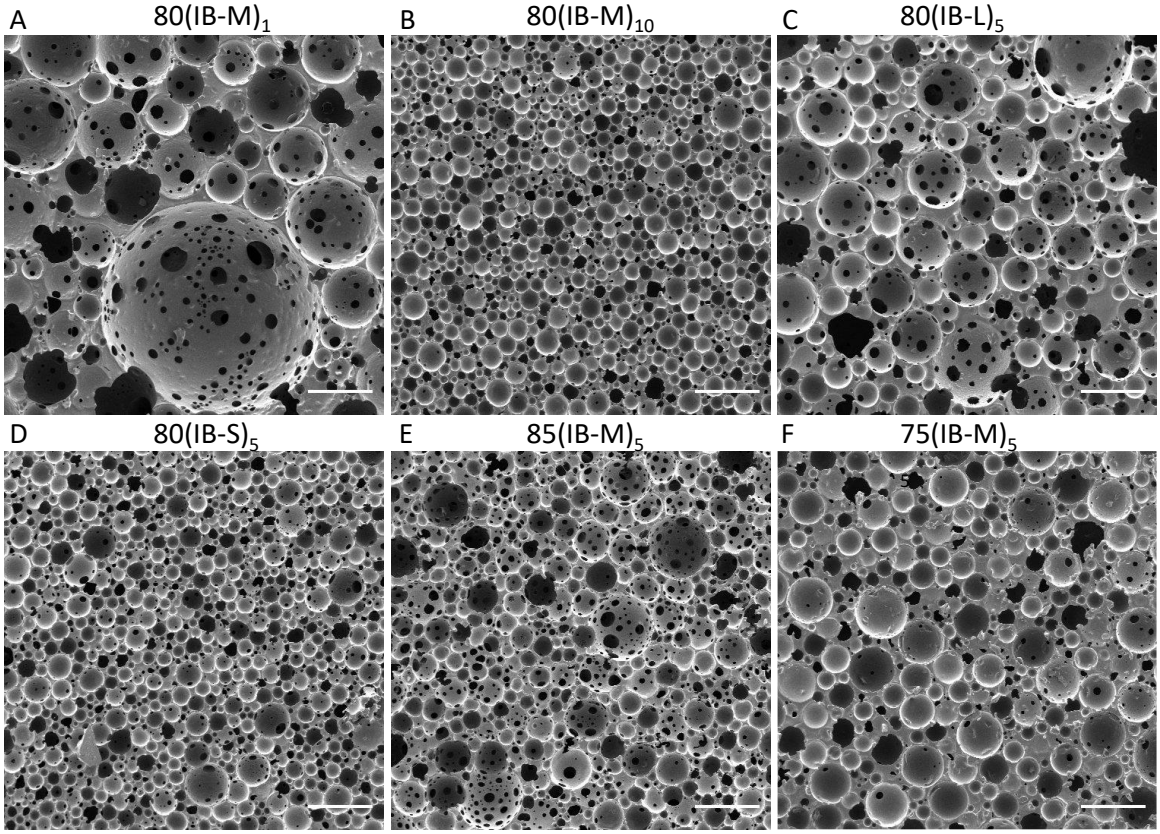

Figure 2.6: SEM images of PolyHIPEs stabilized by IBOA microparticles demonstrating the overall porous structure. Scale bars are 250 µm.

Interestingly, the internal phase fraction did not significantly affect the pore size when the internal phase fraction was increased from 75 to 85% (Fig. 2.6 E, F). This result contradicts with the previous reports, where the increase in internal phase fraction leads to increased pore size due to limited coalescence phenomenon; the complete coalescence of emulsion droplets to reach total surface coverage [91,124].

There can be two arguments to explain the unaffected pore size as the internal phase fraction is increased: (1) there might be a sufficient number of particles to stabilize the increased internal phase fraction. In this case, the reduction in pore size as the particle concentration is increased [80(IB-M)$_5$ vs 80(IB-M)$_{10}$] would not be observed. However, as shown in Table 2.2, an increase in particle concentration from 5% to 10% reduces the average pore size. Alternatively, (2) the HIPE might not take up the increased internal phase fraction. In this case, there should not be a porosity difference between 75(IB-M)$_5$ and 85(IB-M)$_5$. However, the porosity increased from 72.43 to 81.16 as the internal phase fraction is increased from 75 to 85%. Additionally, according to mercury intrusion measurements, the total pore surface areas are 26, 27, and 26 m^2/g, while the total pore volumes are 2.88, 3.61, and 4.98 mL/g for the internal phase fractions 75, 80, and 85%, respectively. On the other hand, the interconnectivity is increased, as deduced from the increase in the average pore throat size, number of pore throats per pore, and degree of openness as the internal phase fraction is increased from 75 to 85% (Table 2.2). This finding is considered as another supporting fact for the formation of interconnected porous structures due to arrested coalescence. Since the weight percentage of particles used are the same, they can stabilize the same amount of interfacial area. Insufficiency of particles as the internal phase fraction is increased allows a higher number of emulsion droplets to partially coalesce. Since the interfacial area of partially coalesced droplets is lower than two separate droplets, the interfacial area is balanced due to partial coalescence without significantly affecting the pore size but increasing interconnectivity.

SEM images focusing on the microarchitecture of PolyHIPEs are provided in Figure 2.7. Similar to 80(IB-M)$_5$; particle covered interconnects (Fig. 2.7 A, E), pore-pore junction similar to pore throat (Fig. 2.7 C), micron sized pores (Fig. 2.7 B-D, F) and submicron pore throats. The continuous polymer film separating two pores is occasionally observed in 80(IB-M)$_{10}$ and 80(IB-S)$_5$ (Fig. 2.7 B, D), in correlation with the reduced interconnectivity compared to other IB PolyHIPEs.

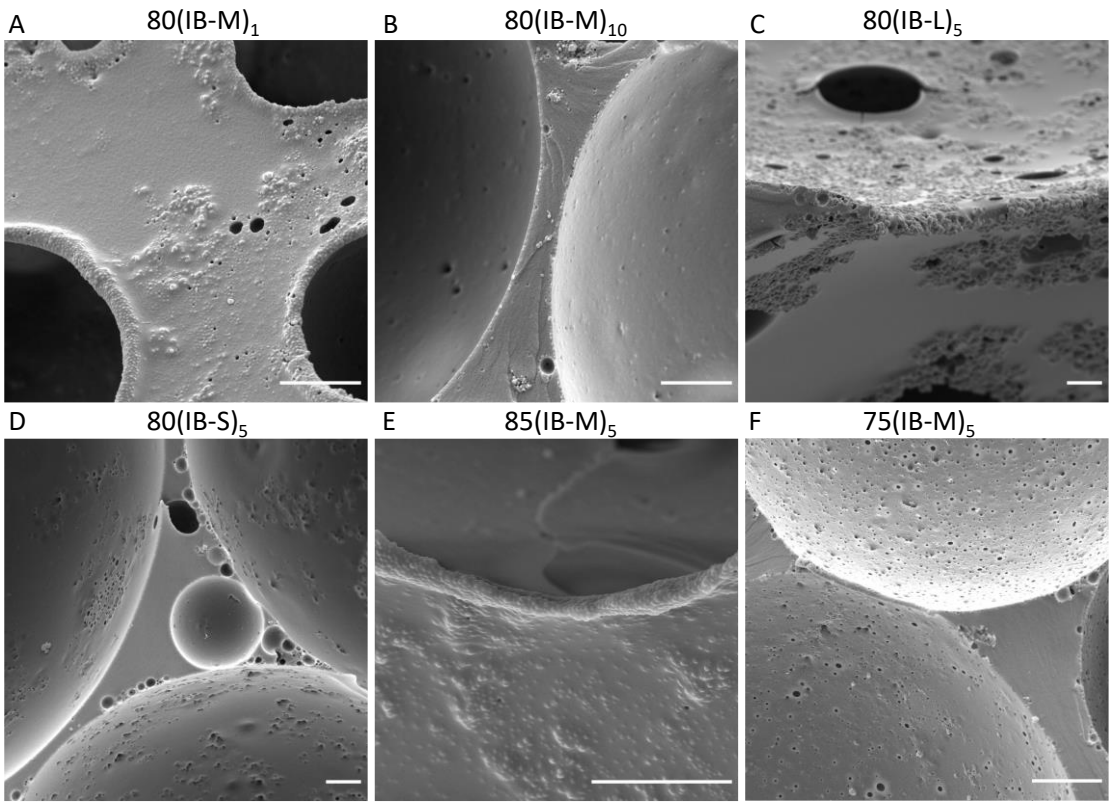

Figure 2.7: SEM images of PolyHIPEs stabilized by IBOA microparticles focusing on pore surface and interfaces. Scale bars are 5 µm.

Micron-sized pores are observed in all samples, but their frequency varies. However, it is hard to evaluate them quantitatively. While the formation of submicron pore throats is also attributed to partial coalescence of micron-sized pores, particle leaching from the pore surface might be another mechanism or a co-mechanism to induce their formation. Mercury intrusion was used to evaluate if submicron pore throats connected pores to each other. It has previously been reported that mercury intrusion provides a pore throat distribution rather than a pore size in PolyHIPEs [105] . The presence of submicron pore throats can be seen in Figure 2.8. A bimodal pore throat size distribution is observed in high particle availability samples; 80(IB-M)$_{10}$, 80(IB-S)$_5$, and 75(IB-M)$_5$.

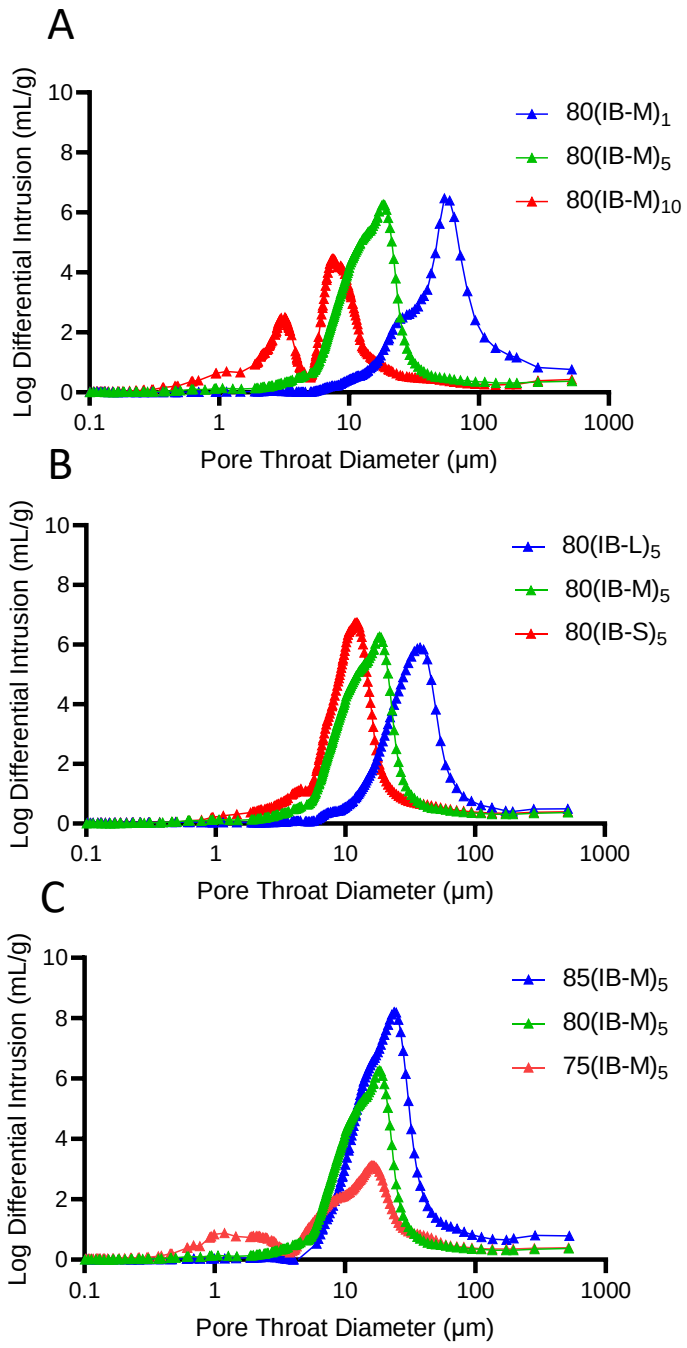

Figure 2.8: Pore throat diameter (µm) as a function of log differential intrusion (ml/g) obtained from mercury intrusion porosimeter for the samples where the particle concentration (A), particle size (B) and internal phase fraction (C) is tuned.

Alternatively, the effect of leftover or adsorbed Tween 20 to the particle surface on the PolyHIPE morphology is also considered. Tween 20 is a surfactant with a high hydrophilic–lyophilic balance (16.7), which preferentially stabilizes oil-in-water emulsions. Indeed, Tween20 does not stabilize EHA/IBOA PolyHIPEs and any high-water-ratio emulsions rapidly experience phase inversion. The

production of polymer spheroids due to subsequent polymerization of double emulsions (oil-in-water type within the water droplets) has been reported previously [124,165]. Thus, as these artifacts were not observed, any effects of potential leftover Tween 20 after washing can be discarded. On the other hand, Tween 20 might be adsorbed onto the particle surface and affect their wettability and associated localization.

In order to evaluate if the Tween 20 adsorbs on the particles and affects the PolyHIPE morphology, emulsifier-free particles were synthesized. This was performed by immediate photopolymerization after emulsification via sonication since the oil droplets have a tendency to coalesce in the absence of a surfactant. These particles were used to prepare PolyHIPEs using the same recipe as that used to prepare the poly-IBOA-stabilized HIPEs. Similar morphological features were observed, as previously discussed, such as pore throats (Fig. 2.9 B), particle layers surrounding the pore throats (Fig. 2.9 C), and no thin polymer film separating the pores but instead a dense layer of particles (Fig. 2.9 D), indicating that the effect of any absorbed Tween20 is minimal on the final PolyHIPE morphology. On the other hand, the submicron pore throats or pore throats at the scale of the stabilizing particles are not observed. This observation eliminates the possibility of their formation due to particle leaching.

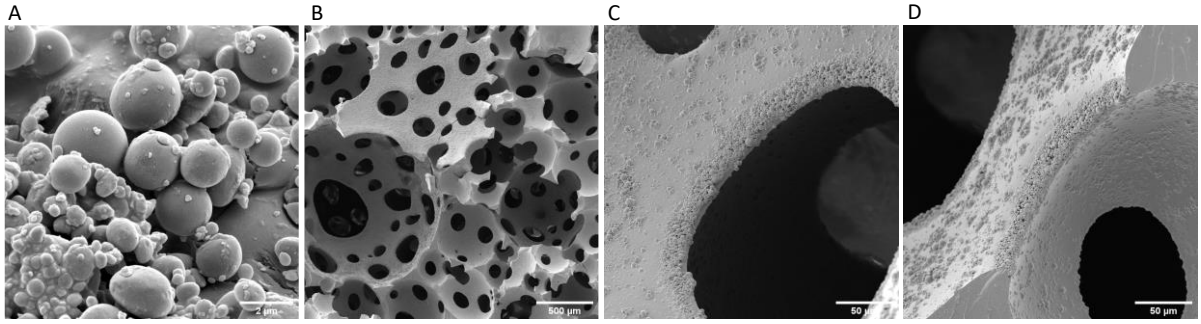

Figure 2.9: SEM images of IBOA particles prepared through photopolymerization without surfactant (A), PolyHIPE synthesized when the emulsifier-free particles were used as a sole stabilizer; overall porous structure (B), the pore throat (C) and pore interface (D).

While the particle size, particle concentration, and internal phase fraction affect the HIPE in a complex manner, the results obtained in these experiments can be simplified and demonstrated in Figure 2.10; when the emulsion is particle-insufficient, the frequency of droplet contact is increased. Particles migrate to the necking region between droplets to arrest further the coalescence of droplets. Due to the scarcity of particles, micron-sized droplets cannot be stabilized; thus, they coalesce. Consequently, PolyHIPEs with a larger pore size, a high number of interconnects, a reduced number of micron-sized pores, and associated submicron interconnects are produced (0.19–0.66 cm^{-1}). An increase in particle availability first manifests itself as a loss of interconnects due to reduced particle free regions on emulsion droplets rather than affecting the emulsion/pore size, as observed upon decreasing the

internal phase fraction from 85 to 75% (0.66–1.25 cm^{-1}). A further increase in the available particle surface leads to efficient stabilization of smaller droplets as well as micron-sized droplets. Efficient coverage of emulsion droplets prevents their partial coalescence; however, particle-covered-micron sized droplets either function as a stabilizer or their partial coalescence leads to the induction of submicron pore throats (1.25–1.88 cm^{-1}).

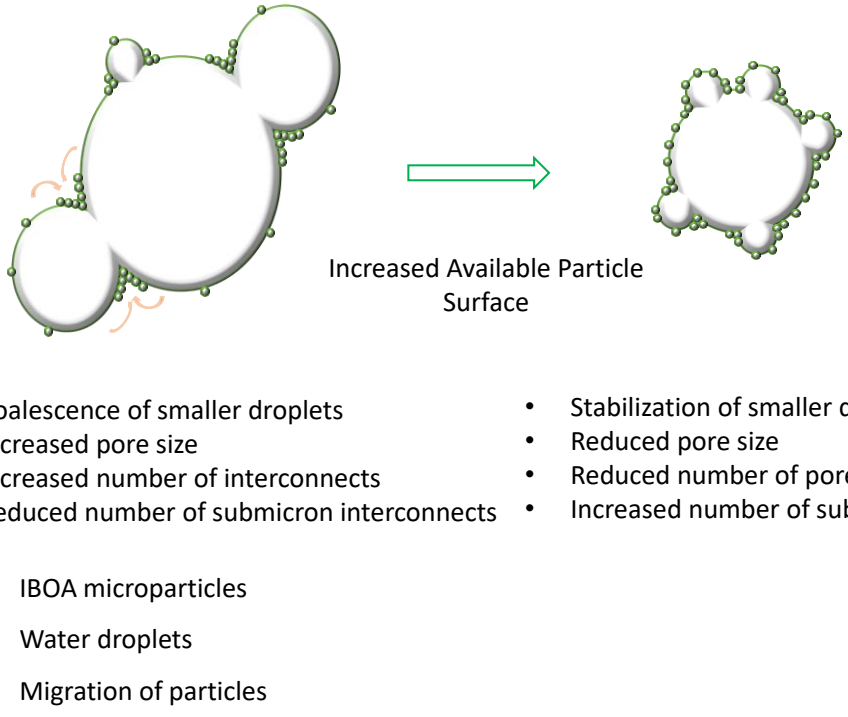

Figure 2.10: The schematic demonstration of proposed pore throat formation due to arrested coalescence.

2.5. Conclusion

In this study, the formation of interconnected porous Pickering PolyHIPEs with a bimodal pore throat size distribution is demonstrated without any surfactant and/or particle surface modification. The interconnected porous structure is attributed to arrested coalescence and supported by morphologic similarities between pore throats and the pore–pore junctions, where both are covered by a dense particle layer. To the best of our knowledge, this is the first time that pore throat formation due to arrested coalescence in PolyHIPEs has been demonstrated. Such PolyHIPEs can be used when the purity of the material is important since the stabilizer has the same composition as that of the material itself. Additionally, due to tunable openness and the larger pore size, as compared to that of poly-surfactant-stabilized-HIPEs, these structures will likely find interesting new applications as tissue engineering scaffolds. Additionally, the existence of a bimodal distribution of pore throats (micron and sub-micron) might have interesting consequences for mass transport in these porous materials and might lead to new filtering devices, insulation materials, or absorbent foams for environmental

applications. On the other hand, the effect of interparticle and monomer–particle interactions, the forces during the polymerization such as volume shrinkage or depletion attraction on partial coalescence of pores, and the applicability of this method to other systems have not been elucidated yet.

CHAPTER 3

Modifying Pickering Polymerized High Internal Phase Emulsion Morphology by Adjusting Particle Hydrophilicity

*Enes Durgut [a,b],Muchu Zhou [c], Betül Aldemir Dikici [d], Reza Foudazi [c] Frederik Claeyssens [a, b, *]*

[a] Kroto Research Institute, Department of Materials Science and Engineering, University of Sheffield, Sheffield, United Kingdom

[b] Department of Materials Science and Engineering, INSIGNEO Institute for In Silico Medicine, The University of Sheffield, Sheffield, United Kingdom

[c] Department of Chemical, Biological and Materials Engineering, University of Oklahoma, Oklahoma, United States

[d] Department of Bioengineering, Izmir Institute of Technology, Urla, Izmir, 35433, Turkey

Abstract

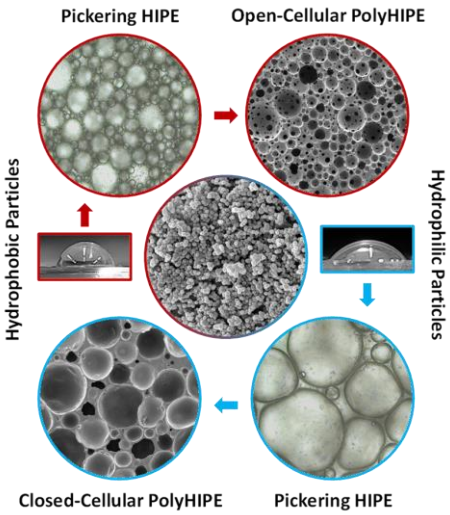

This study investigates the use of submicron polymeric particles with varying crosslinking densities as the sole stabilizer for producing Polymerized High Internal Phase Emulsions (PolyHIPE). We establish a direct correlation between the crosslinking density and the hydrophilicity of the polymer particles. The hydrophilicity of these particles significantly influences the morphology and rheology of HIPEs. These differences manifest as various morphological variations in the resulting PolyHIPE templates. It was discovered that by increasing the crosslinker weight percentage in the particles from 0 to 100%, PolyHIPEs with semi-open, open, and closed porous structures can be obtained. Furthermore, non-crosslinked particles were observed to dissolve in the continuous phase, acting as macromolecular surfactants that generate small pores akin to surfactant-stabilized structures in PolyHIPE. These findings offer fresh insights into the relationship between particle localization at the interface, HIPE rheology, and the formation of pore throats in Pickering PolyHIPEs, leading to the creation of either closed or open porous networks. Additionally, interfacial rheological results demonstrate that particles synthesized with varying monomer-to-crosslinker ratios exhibit different interfacial elasticities, which are linked to PolyHIPE morphology

Keywords: Pickering emulsions, rheology, arrested coalescence, particles, HIPE, PolyHIPE

3.1. Introduction

Polymerized High Internal Phase Emulsions (PolyHIPEs) are highly porous polymeric materials created using the emulsion templating method. This method relies on the production of a stable emulsion and its subsequent polymerization, which requires the use of emulsion stabilizers. Traditionally, surfactants serve as the stabilizers for the emulsion, resulting in templates with small pores (1-50 µm) and interconnected pore throats that connect adjacent pores. [105,172]. Alternatively, colloidal particles can be employed to stabilize emulsions, known as Pickering emulsions. Since the successful production of Pickering PolyHIPEs in 2007 by Menner *et al.* [28], there has been a growing interest in replacing surfactants with colloidal particles due to their efficiency in emulsion stabilization [12,13] and their functional properties [83,125]. Pickering PolyHIPEs are recognized for their larger pore sizes compared to conventional PolyHIPEs but lack pore throats [68,69,74]. Although the formation of pore throats in PolyHIPEs has not been fully elucidated, the closed porous structure of Pickering PolyHIPEs is attributed to a thick interfacial polymer film that separates neighboring pores, unlike conventional PolyHIPEs, which resist rupturing during or after polymerization [66,75]. While a closed cellular morphology is advantageous in applications requiring encapsulation, it limits their use in applications where an interconnected porous structure is necessary. For instance, applications involving diffusion, mass transfer, or cell ingrowth require such interconnected porous structures [173–175].

While Pickering PolyHIPEs are often associated with their closed cellular morphology, there have been a few reports demonstrating an interconnected pore structure. For instance, to achieve a stable Pickering HIPE, colloidal particles are typically subjected to surface modifications to adjust their hydrophilicity. This enables the particles to be situated at the oil/water interface and serve as emulsion stabilizers. Several reports have shown that the degree of surface modification influences the openness of the resulting templates, ranging from closed to interconnected porous structures [73,93,95]. Additionally, Zhang *et al.* reported that the use of sulfonated styrene particles as a HIPE stabilizer results in open and closed cellular morphologies when the continuous phase consists of butyl acrylate and styrene, respectively [96]. Assuming that particle-monomer interactions are minimal in the mentioned studies, both the degree of surface modification of particles and changes in the hydrophilicity of the continuous phase are factors influencing particle localization at the oil/water interface. Therefore, we hypothesize that the localization of particles at the oil/water interface can be a determining factor in the openness of Pickering PolyHIPEs.

The 2-ethylhexyl acrylate/isobornyl acrylate/trimethylolpropane triacrylate (EHA/IBOA/TMPTA) blend is a commonly used monomer blend for PolyHIPE production due to its tunable mechanical properties and ease of manufacture. EHA/IBOA/TMPTA PolyHIPEs have found applications in various fields, such

as protein immobilization [176], serving as scaffolds for bone tissue engineering [114] and in the development of microfluidic devices for osteogenesis-on-a-chip [177]. Recently, two noteworthy developments have further enhanced the utility of EHA/IBOA/TMPTA PolyHIPEs as model porous materials. First, a straightforward method for surface functionalization via orthogonal photo click chemistry has been established [178]. Second, the successful formulation of HIPE-based resin for vat polymerization with commercial 3D printers has been achieved [179] which was further coated with nickel to obtain highly porous metal-based lattice structures [180]. Given the simplicity of manufacturing these PolyHIPEs, they can also serve as model systems for advancing our understanding and testing new hypotheses in emulsion templating.

Recently, we explored the use of IBOA/TMPTA microparticles as the sole HIPE stabilizer to produce an open cellular morphology in EHA/IBOA/TMPTA Pickering PolyHIPEs. This observation led us to propose a new mechanism for pore throat formation in Pickering PolyHIPEs: the partial but arrested coalescence of emulsion droplets. Additionally, we investigated the impact of the internal phase ratio, particle size, and particle concentration on PolyHIPE morphology and openness [65]. However, we did not evaluate the effect of particle hydrophilicity on this proposed mechanism. In this study, we aim to investigate the influence of particle hydrophilicity on HIPE morphology, rheology, interfacial viscoelasticity of the emulsions, and Pickering PolyHIPE morphology. We achieved this by using particles with varying compositions of TMPTA, ranging from 100% IBOA to 100% TMPTA. Tuning the TMPTA concentration in the particles allows us to modulate their hydrophilicity, as TMPTA is inherently hydrophilic. This approach enables us to examine the impact of particle hydrophilicity on the aforementioned parameters without requiring additional surface modifications.

3.2. Materials

EHA, IBOA, TMPTA, polysorbate 20 (Tween 20), potassium persulfate (KPS), and 2-hydroxy-2-methylpropiophenone (photoinitiator, PI) were purchased from Sigma-Aldrich (Poole, UK).

3.3. Methods

3.3.1. Nomenclature of Samples

The particles are designated with codes like IB_xTM_y, where x and y represent the weight percentages of IBOA and TMPTA used in particle synthesis, respectively. The prefix before the particle code, either (h) or (p), indicates whether it's associated with HIPE or PolyHIPE, respectively. For instance, (p)$IB_{75}TM_{25}$ signifies a PolyHIPE templated from an emulsion stabilized by particles containing 75% wt IBOA and 25% wt TMPTA.

3.3.2. IBOA Microparticle Synthesis

The particles were prepared as outlined in section 2.3.3. The continuous phase was created by dissolving 0.5% wt of Tween 20 (0.9 g) and 0.2% wt of KPS (0.36 g) in 18 g of dH_2O, using magnetic stirring at 500 RPM for 5 minutes. Subsequently, 2 g of the internal phase, consisting of an IBOA/TMPTA blend, and 18 grams of the continuous phase were combined in a 40 mL plastic tube. The emulsion was formed by subjecting this mixture to ultrasonication at 100 Watts and 30 kHz using an ultrasonicator (Hielscher UP100H, Hielscher Ultrasound Technology) for 2 minutes. The resulting emulsion droplets were thermally polymerized in a convection oven at 65 °C for 16 hours. The polymer particles obtained were washed with 30 mL of methanol and then centrifuged at 14,000 RPM for 15 minutes. This washing process was repeated twice. After removing the methanol, the particles were suspended in 40 mL of water and dried in a convection oven at 65 °C for 24 hours.

3.3.3. Preparation of PolyHIPE

The continuous phase was prepared by mixing 4 grams of EHA/IBOA/TMPTA (63/21/16% wt) and 0.2 grams of IBOA/TMPTA particles through ultrasonication at 100 Watts and 30 kHz for a minute. Subsequently, 0.1 grams of photoinitiator were added to the monomer/particle mixture. The internal phase, consisting of 16 grams of deionized water, was added to the continuous phase using a syringe pump operating at a rate of 0.8 mL/min, while the system was mixed at 500 RPM (Pro40, SciQuip). During the emulsification process, the rotor blade was continuously adjusted to the top position as the emulsion volume increased. All the HIPEs were prepared within a span of 24 minutes. The resulting HIPEs were transferred to a glass petri dish (the thickness of HIPE was ~ 1 cm) and polymerized using a belt conveyor UV curing system (GEW Mini Laboratory, GEW Engineering UV) within one minute.

3.3.4. Preparation of Thin Films

Thin films were prepared with the same composition of particles for conducting water contact angle measurements. One gram of monomer blends was mixed with 0.025 g of PI. The monomer blend was squeezed between two glass slides and photopolymerized using the UV curing system.

3.3.5. Characterization

The IBOA/TMPTA particles were mounted onto double-sided carbon tape and coated with an 8 nm thick layer of gold. Subsequently, the particles were imaged using a scanning electron microscope (Inspect F, FEI) with a 5 kV accelerating voltage and a 3 µm spot size. The sizes of 200 particles were manually measured from the SEM images using ImageJ software. The polydispersity index of the particles was calculated using the following formula:

$$PDI = \left(\frac{\sigma}{D_p}\right)^2 \quad (1)$$

Where σ is the standard deviation of droplet size and $D_p$is the average droplet size.

A sessile drop test was performed to measure the water contact angle on polymer films with the same particle composition cast onto a glass slide. Glass slides were positioned on a flat surface, and images were captured using a smartphone (RedMI 10, Xiaomi) mounted on a tripod from a distance of approximately 2 cm from the samples. The images were subsequently analyzed using ImageJ software, with the assistance of the LB-ADSA plugin [181]. The average emulsion droplet size was determined by measuring the diameter of 100 droplets using ImageJ software. These measurements were taken from optical micrographs (CX43, Olympus) of freshly prepared HIPEs.

To deduce the molecular weight of the dissolved IBOA, we employed gel permeation chromatography (GPC) (Viscotek GPCmax VE 2001, Malvern Panalytical). The $IB_{100}TM_0$ particles were first dissolved in the continuous phase, and the mixture was then centrifuged at 14,000 RPM for 5 minutes to collect a gel-like IBOA. This collected gel-like IBOA was subsequently mixed with tetrahydrofuran (THF) before conducting the GPC measurement. For the dissolved $IB_{100}TM_0$ particles, 1H nuclear magnetic resonance (NMR) spectra were recorded using an NMR spectrometer (Avance AVIII 400 MHz NMR, Bruker) operating at 400.13 MHz. A 30° pulse for excitation was used, with 64 k acquisition points over a spectral width of 20 ppm, 16 transients, and a relaxation delay of 1 second.

The rheological tests included step flow and frequency sweep tests, which were conducted using a rheometer (AR2000, TA Instruments) with a cross-hatched steel plate (60 mm, 2°) at 25 °C. The applied shear rate ranged from 10 to 0.1 s^{-1} during the step flow test, and the frequency ranged from 10 to 0.1 Hz during the frequency sweep test. The skeletal density of PolyHIPEs was characterized using a pycnometer (AccuPyc 1340, Micromeritics). The porosity ($P_{\emptyset}$) of the samples was determined by subtracting the skeletal density (ρ_{sd}) from the calculated bulk density (ρ_c) using the following formula [182]:

$$P_{\emptyset} = \left(1 - \frac{\rho_{sd}}{\rho_c}\right) 100 \quad (2)$$

The bulk density (ρ_c) was calculated based on a cylindrically molded EHA/IBOA/TMPTA monolith, which had a composition similar to the continuous phase of the HIPEs. This value was then used to determine the porosity according to Equation 2.

To characterize the pore size of the PolyHIPEs, the diameter of 200 pores was measured from SEM images obtained using the same procedure as for the SEM imaging of particles. Since the PolyHIPE samples contain micron-sized pores, they were excluded from the measurement by acquiring images

at lower magnifications (500x for (p)$IB_{100}TM_0$ and 100x for the remaining samples). This was achieved by laser cutting the samples, which caused the polymer to melt and eliminated the smaller features. Additionally, a statistical correction factor was applied to reduce errors introduced during uneven sectioning of pores [3,51]. The median pore diameter, obtained from the mercury intrusion porosimeter (AutoPore V, Micrometrics), was used as the average pore throat size of the samples. This is because the pore size provided by the mercury intrusion porosimeter corresponds to the pore throat size in PolyHIPEs [105].

The dilatational rheology of the particle-adsorbed oil-water interface was characterized using an optical tensiometer (Attension KSV Instruments, Biolin Scientific) at room temperature. The pendant drop of the aqueous phase was oscillated in the continuous phase containing IBOA/TMPTA particles at various frequencies (0.05-0.5 Hz) to obtain measurements of interfacial tension variation. Since 0.2 g of IBOA/TMPTA particles, as used in the emulsion formulation, resulted in the continuous phase turning white and limited the observation of the pendant drop, a reduced quantity of 0.001 g of IBOA/TMPTA particles was used for all cases. Figure 3.1 shows the transparent oil phase both without and with 0.0005 g and 0.001 g of IB_0TM_{100} particles. The amplitude was kept constant for all measurements.

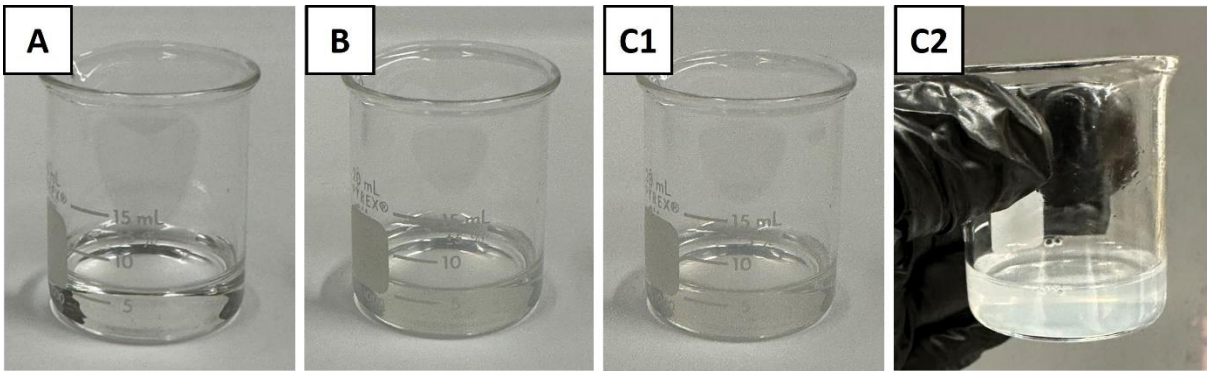

Figure 3.1: Clear and transparent continuous phase without adding IBOA/TMPTA particles(A); continuous phase containing 0.0005 g of particle IB_0TM_{100} (B); and continuous phase containing 0.001 g of particle IB_0TM_{100} (C1-C2).

3.4. Results and Discussion

3.4.1. IBOA Microparticles

SEM images of IBOA microparticles prepared through ultrasound-assisted emulsion polymerization are presented in Figure 3.2. The particle size gradually increased from 199 to 211 nm as the TMPTA content in the particles increased from 0% to 50%. A further increase in TMPTA content resulted in a reduction in the average particle size, reaching 145 nm for $IB_{25}TM_{75}$ and 60 nm for IB_0TM_{100} (Fig. 3.3 A). In contrast, the PDI of the particles gradually increased as the TMPTA content increased, peaking at

$IB_{25}TM_{75}$ and then reducing to 0.12 in IB_0TM_{100}. Additionally, although the particles were predominantly spherical, complex nonspherical particles were occasionally observed, especially in $IB_{50}TM_{50}$ and $IB_{25}TM_{75}$. Similar amorphous-shaped particles were previously observed in a blend of styrene, methyl methacrylate, and acrylic acid and were attributed to the incompatibility between constituents and subsequent phase separation [149]. Given that TMPTA is a water-miscible and relatively hydrophilic component of the organic mixture, a similar mechanism might have contributed to increased PDI, particularly in $IB_{25}TM_{75}$, and the formation of nonspherical shapes.

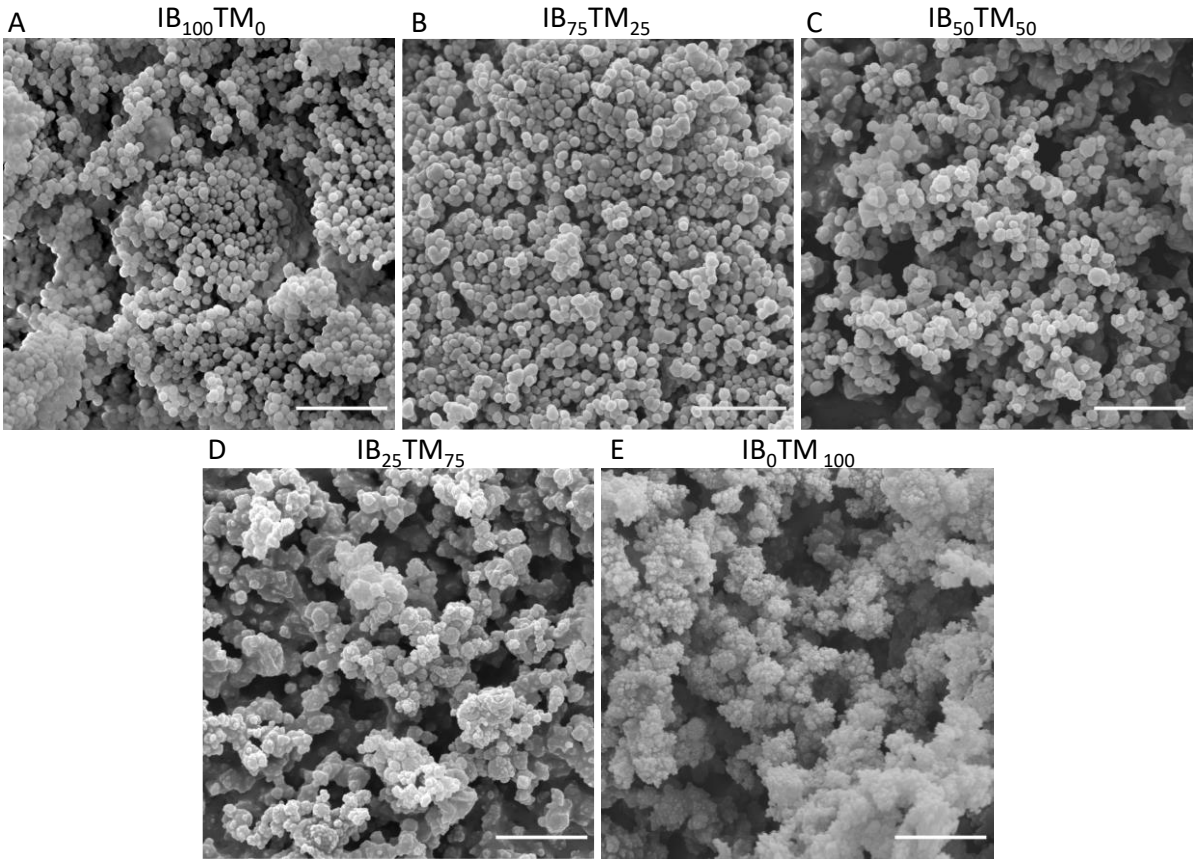

Figure 3.2: SEM images of particles with various IBOA and TMPTA content: $IB_{100}TM_0$ (A), $IB_{75}TM_{25}$ (B), $IB_{50}TM_{50}$ (C), $IB_{25}TM_{75}$ (D) and IB_0TM_{100} (E). Scale bars are 2 µm.

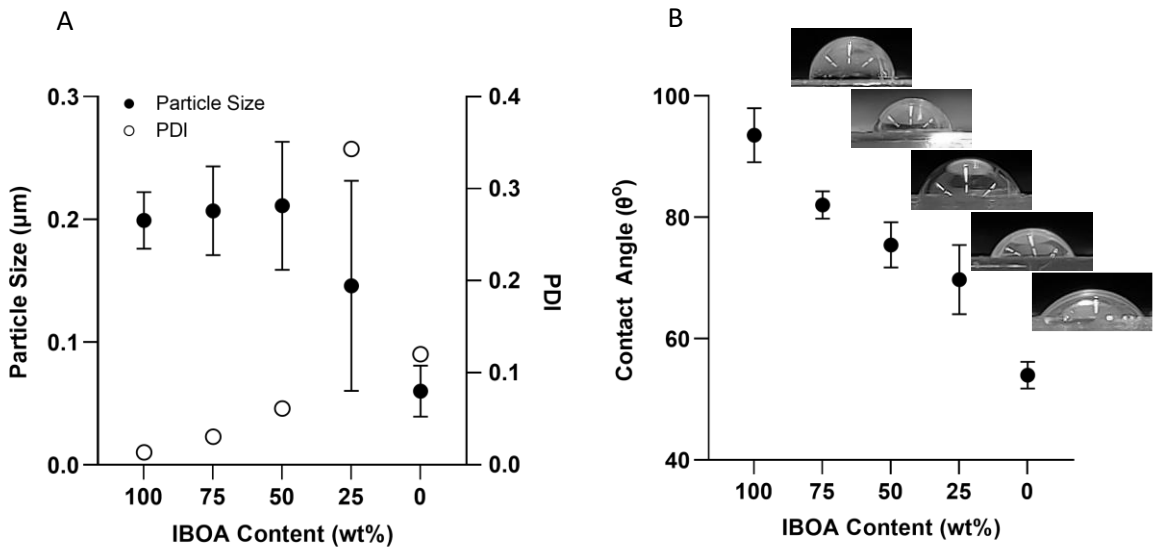

Figure 3.3: The size and polydispersity index of IB-TM particles (A). The contact angle measurement of the thin polymeric film shares a similar composition with the IB-TM particles (B).

Contact angle measurements on a thin polymer film, which shares the same composition as the particles, were conducted and are presented in Figure 3.3 B. These water contact angle measurements were performed on a polymer film instead of on the particles themselves to eliminate the influence of surface roughness on the water contact angle. The increase in TMPTA content in the polymer composition led to a reduction in the contact angle, decreasing from 93.5° ($IB_{100}TM_0$) to 54.0° (IB_0TM_{100}). The ability to adjust the water contact angle of the particles by varying the IBOA/TMPTA content allows for the investigation of particle hydrophilicity's impact on HIPE/PolyHIPE morphology without the need for surface modifications.

3.4.2. HIPE

3.4.2.1. The Continuous Phase

After the particles were dispersed in the continuous organic phase through sonication, the continuous phase transformed into an opaque whitish liquid, indicating the formation of a suspension. However, the dispersion of $IB_{100}TM_0$ resulted in a transparent liquid with an observed increase in the viscosity of the continuous phase compared to other particle-dispersed continuous phases (Fig. 3.4 A). It is known that the viscosity of particle dispersions increases with particle concentration due to heightened interparticle interactions [29,165] However, in this case, only the $IB_{100}TM_0$ dispersion exhibited a noticeable increase in viscosity, even though the particle concentration and average particle size were similar to $IB_{75}TM_{25}$ and $IB_{50}TM_{50}$. This phenomenon aligns with the observations made by *Tu et al.*, where a transparent-colored continuous phase with increased viscosity was previously noted when non-crosslinked styrene particles were dispersed in a styrene solution. This effect was attributed to the

swelling of particles within the continuous phase [72]. However, since $IB_{100}TM_0$ is not crosslinked, there is also the possibility that it might dissolve in the organic phase. To assess the dissolution of non-crosslinked IBOA, two cylindrical polymer monoliths were synthesized through free-radical polymerization (similar to PolyHIPE synthesis) with a composition similar to that of $IB_{100}TM_0$ and $IB_{75}TM_{25}$. These monoliths were kept in the EHA/IBOA/TMPTA mixture. The $IB_{100}TM_0$ polymer cylinder completely dissolved within the organic mixture within 2 days (Fig. 3.4 B).

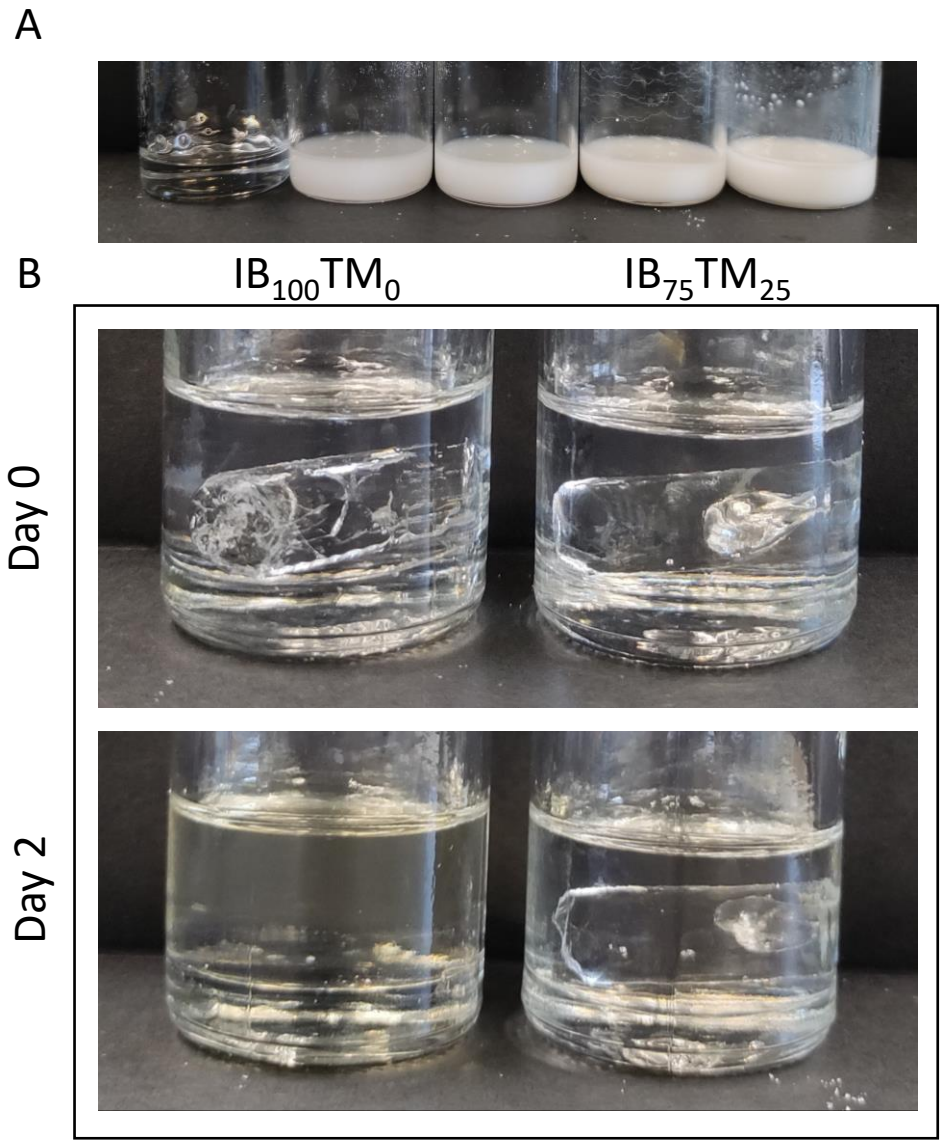

Figure 3.4: The particle dispersion in the continuous phase after being sonicated for a minute; $IB_{100}TM_0$, $IB_{75}TM_{25}$, $IB_{50}TM_{50}$, $IB_{25}TM_{75}$, and IB_0TM_{100} from left to right (A). Polymeric cylinders with the exact composition of $IB_{100}TM_0$ and $IB_{75}TM_{25}$ in the continuous phase demonstrate the dissolution of non-crosslinked cylinders within 2 days (B).

3.4.2.2. HIPE Stability and Droplets

The HIPEs were successfully prepared, and digital micrographs are presented in Figure 3.5. A portion of the HIPEs was photopolymerized, while the remainder was kept at room temperature to observe

emulsion stability. Within 15 minutes after preparation, visible large emulsion droplets were observed in (h)$IB_{25}TM_{75}$. Furthermore, (h)$IB_{25}TM_{75}$ experienced sedimentation and emulsion droplet coalescence within a week. This was an intriguing observation, as emulsions stabilized by particles with lower TMPTA content ($IB_{50}TM_{50}$) and higher TMPTA content (IB_0TM_{100}) did not exhibit observable emulsion instability for a week. Additionally, (h)$IB_{100}TM_0$ and (h)$IB_{50}TM_{50}$ only began to show sedimentation after 5 weeks.

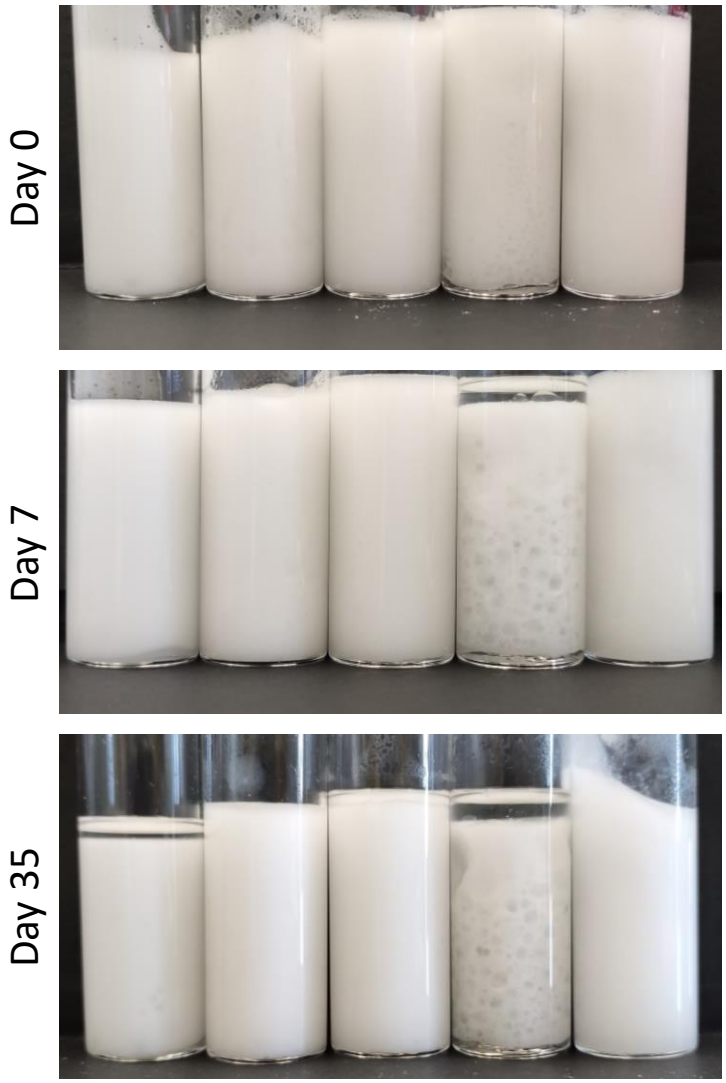

Figure 3.5: Digital images of (h)$IB_{100}TM_0$, (h)$IB_{75}TM_{25}$, (h)$IB_{50}TM_{50}$, (h)$IB_{25}TM_{75}$, and (h)IB_0TM_{100} from left to right at Day 0, 7, and 35.

HIPEs were imaged under a light microscope, and the optical micrographs are presented in Figure 3.6. The average emulsion droplet sizes are provided in Table 3.1. It has been previously reported that emulsion droplet size correlates with particle size [171]. However, the emulsions in this experimental setup do not conform to this rule. (h)$IB_{100}TM_0$ exhibited significantly smaller emulsion droplets with an average size of ~14 μm, despite the particle size of $IB_{100}TM_0$ being similar to $IB_{75}TM_{25}$ and $IB_{50}TM_{50}$. Such small emulsion droplets are typically observed in surfactant-stabilized HIPE emulsions.

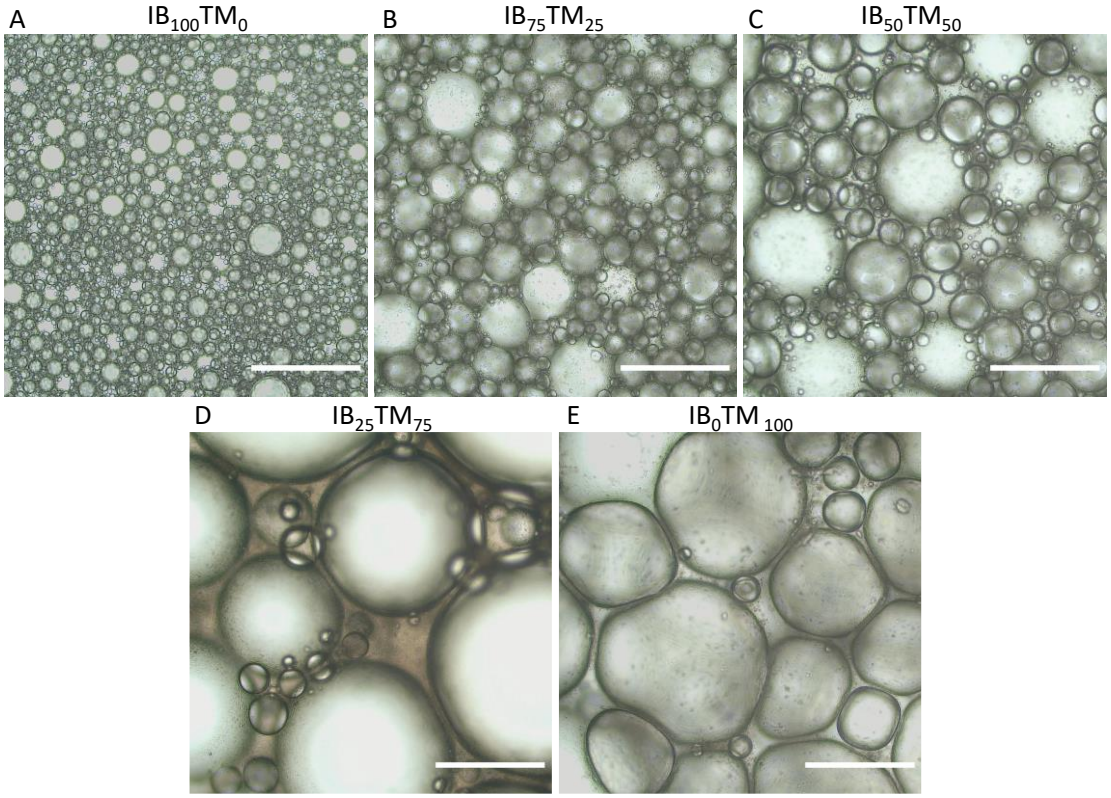

Figure 3.6: Optical micrographs of HIPEs stabilized by IB-TM particles demonstrating the emulsion droplet size and the droplet shape. Scale bars are 200 µm.

Table 3.1: Skeletal density (ρ_{sd}), porosity ($P_{\emptyset}$), emulsion droplet size (*d*), polydispersity index of emulsion droplet size (*PDI d*), pore size (P_p), polydispersity index of pore size (*PDI* P_p), pore throat size (P_t), and relative pore throat size (P_t/P_p) of PolyHIPEs.

Sample	ρ_{sd} (g/cm3)	$P_{\emptyset}$	*d* (µm)	*PDI d*	P_p (µm)	*PDI* P_p	P_t (µm)	P_t / P_p
(p)$IB_{100}TM_0$	0.94	75.04	14.32	0.40	23.68	0.34	3.31	0.14
(p)$IB_{75}TM_{25}$	1.03	77.49	44.82	0.39	72.12	0.40	17.37	0.24
(p)$IB_{50}TM_{50}$	1.03	77.72	58.12	0.58	79.21	0.44	23.29	0.29
(p)$IB_{25}TM_{75}$	1.02	78.58	114.09	1.02	148.36	1.22	58.27	0.39
(p)IB_0TM_{100}	0.33	28.64	146.57	0.40	205.46	0.42	N/A	N/A

This discrepancy may be attributed to the dissolution of $IB_{100}TM_0$ particles within the continuous phase, where they function as a macro-molecular surfactant rather than a typical Pickering stabilizer. Consequently, (h)$IB_{100}TM_0$ should be evaluated separately from the rest of the samples. Additionally, the smallest particle, IB_0TM_{100}, produced emulsions with the largest average droplet size of 146 µm. This is intriguing since previous reports have shown that emulsion droplet size correlates well with various sizes of $IB_{75}TM_{25}$ particles (ranging from 100 to 700 µm) [65]. The highest PDI of emulsion droplets was observed in (h)$IB_{25}TM_{75}$, approximately equal to 1. The reduced uniformity of emulsion

droplets in (h)IB25TM75 might be due to a combination of the high PDI of $IB_{25}TM_{75}$ particles and the reduced stability of the HIPE. Furthermore, emulsion droplets in all samples appear spherical, except for (h)IB_0TM_{100}, which exhibits deformed spherical emulsion droplets, typically observed in Pickering HIPEs (Fig. 3.6 E).

3.4.2.3. Rheology of HIPE

The rheological properties of the samples were measured, and the analyzed results are presented in Figure 3.7. The frequency sweep results (Fig. 3.8) clearly indicate that all samples exhibit G' > G" at all frequencies, confirming solid-like behaviour, as expected for HIPEs with a unimodal droplet size distribution [183]. The viscosity of HIPE samples as a function of shear rate is provided in Figure 3.4 A. An increase in TMPTA content from 25% to 75% in the particles results in a reduction in viscosity. This trend is expected since the increase in emulsion droplet size leads to a decrease in viscosity when the internal phase volume of the HIPEs remains the same [3,29]. However, IB_0TM_{100} exhibits the highest viscosity despite having the largest emulsion droplets (Fig. 3.7 A). The observed increase in viscosity for (h)$IB_{25}IB_{75}$ between 1-10 s^{-1} is attributed to phase separation of the sample during the measurement. This is because this particular sample is less stable compared to the other HIPE samples.

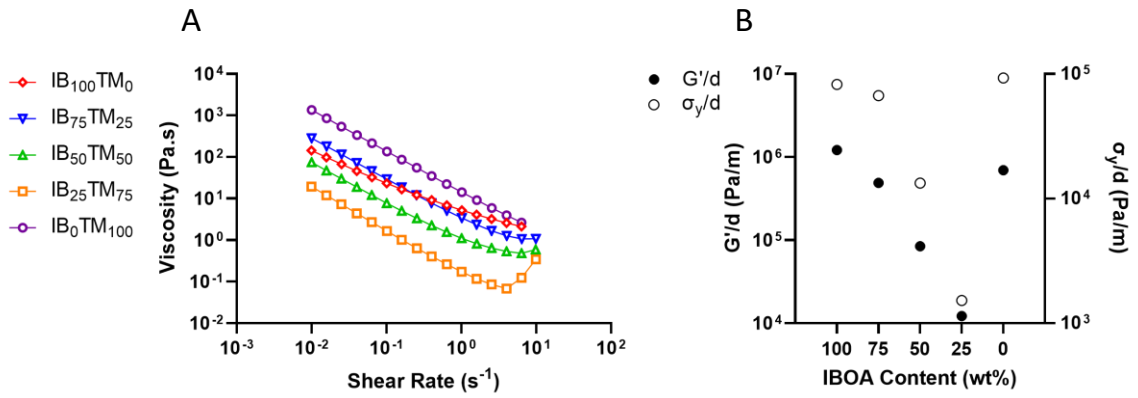

Figure 3.7: The viscosity of HIPE samples as a function of shear rate obtained from step flow test (A) and, scaled elastic modulus (G') and yield stress (σ) of HIPE samples obtained from frequency sweep test (B).

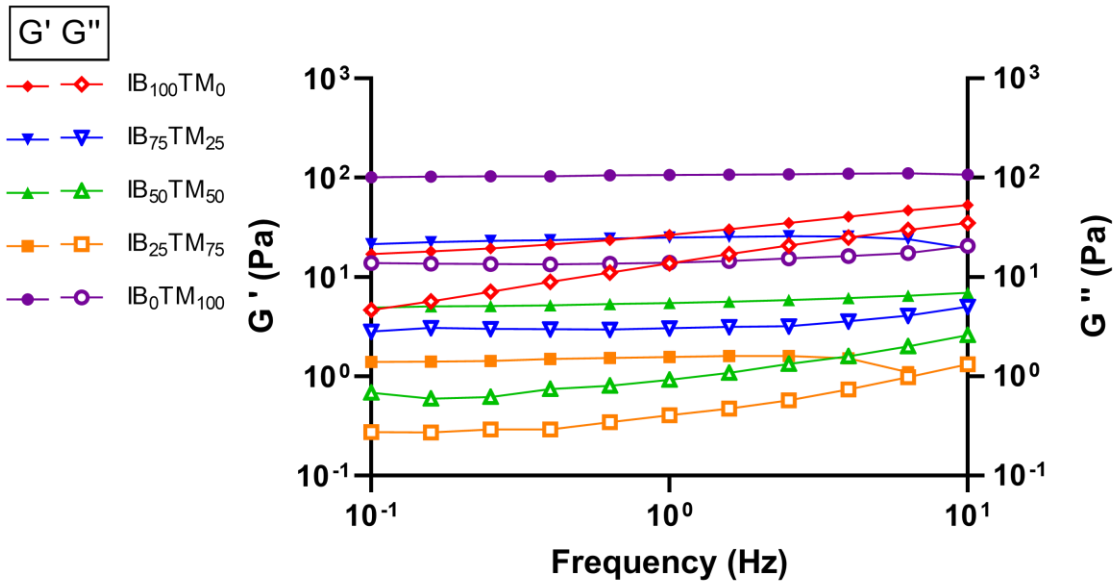

Figure 3.8: The frequency sweep test conducted on HIPE samples and the dependence of G' and G'' on oscillation frequency is plotted.

The elastic properties of HIPEs scale with Laplace pressure, which is calculated as the interfacial tension divided by the droplet size. This holds true when the contribution of interdroplet interaction and interfacial rheology to bulk elasticity is negligible [41]. The prepared HIPEs have relatively large droplet sizes, on the order of tens of micrometers, where the effect of interdroplet interaction is very negligible. Determining the effective interfacial tension when particles are at the interface is not straightforward. Therefore, we compare the elastic properties by scaling them with droplet size, as shown in Figure 3.4 B. In other words, we divide the shear modulus (obtained from the G' plateau in frequency sweep data) and yield stress (obtained by fitting the Herschel-Bulkley model) by droplet size to better illustrate the effect of interfacial phenomena. To draw a meaningful conclusion, (h)$IB_{100}TM_0$ should be excluded from the comparison due to the dissolution of particles in the continuous phase. For samples with stable particles, the trend is not monotonic. (h)IB_0TM_{100} exhibits the highest scaled shear modulus and yield stress among the Pickering HIPE samples, indicating that the effective interfacial tension in this sample is the highest and/or the interfacial rheology is responsible for the observed trend. This observation is further discussed in Section 3.4.4. and attributed to the effective interfacial tension.

It is well-established that under similar experimental conditions, Pickering HIPEs exhibit higher viscosity compared to surfactant-stabilized HIPEs due to attractive interparticle interactions, excluded volume effects, and attractive lateral capillary interactions [43]. Additionally, previous reports have shown that Pickering HIPEs have elastic moduli that are several orders of magnitude higher than surfactant-stabilized HIPEs [43,184]. In our previous work, we examined the rheological behavior of

HIPEs stabilized by Hypermer B246 (a surfactant), $IB_{75}TM_{25}$, and silica (a commonly used colloidal stabilizer). We found that Hypermer B246 and $IB_{75}TM_{25}$ stabilized HIPEs exhibited comparable viscosity, while silica-stabilized HIPEs had higher viscosity despite having significantly larger droplet sizes than both Hypermer B246 and $IB_{75}TM_{25}$-stabilized HIPEs. The distinctive properties of (h)$IB_{75}TM_{25}$ and its atypical morphology (interconnected porous) were attributed to the localization of particles at the interface. $IB_{75}TM_{25}$ particles were predominantly observed around the pore throats in the PolyHIPE, rather than being distributed on the pore surface. Therefore, we concluded that the prevention of coalescence of emulsion droplets was not due to the typical particle shielding of droplets but rather the jamming of particles at the necking region of initially coalesced emulsion droplets. This phenomenon provided intermediate viscosity and droplet size compared to Hypermer B246 and silica-stabilized HIPEs [65].

In the case of (h)$IB_{75}TM_{25}$, (h)$IB_{50}TM_{50}$, and (h)$IB_{25}TM_{75}$ samples, their behavior aligns with our previous report. Within these three samples, as the TMPTA content in the particles increases, the droplet size also increases, leading to a decrease in viscosity and emulsion stability. However, this observed trend is not followed in the case of (h)IB_0TM_{100}. In (h)IB_0TM_{100}, we observe typical Pickering HIPE properties, including large and deformed-spherical emulsion droplets. Despite being stabilized by smaller particles, this sample exhibits increased viscosity as well as improved emulsion stability. The transition from atypical properties ((h)$IB_{75}TM_{25}$, (h)$IB_{50}TM_{50}$, and (h)$IB_{25}TM_{75}$) to typical properties ((h)IB0TM100) can be attributed to the particle hydrophilicity in the given experimental setup.

3.4.3. PolyHIPE

3.4.3.1. The Porous Structure

PolyHIPEs from IB/TM particle-stabilized HIPEs were successfully prepared, and the properties of PolyHIPEs are listed in Table 3.1. Both the skeletal density and the porosity of the samples are nearly the same, with no significant differences, except for (p)IB_0TM_{100}. Since the skeletal density is the density of the material composing the PolyHIPE skeleton, it should be the same within all the samples. Additionally, since the internal phase volume was equal in all the HIPE samples, the porosity of the samples should also be the same. Therefore, the reduced skeletal density obtained by the pycnometer and the accordingly calculated reduced porosity of (p)IB_0TM_{100} indicate a closed porous structure. This suggests that gas could not penetrate into the closed porous structure of (p)IB_0TM_{100}, thus, the skeletal density was underestimated. Additionally, the bulk densities of all the samples were measured as approximately 0.22 g/cm³.

Particle hydrophilicity had a major impact on the porous structure as well as on the number-averaged pore size distribution of the Pickering PolyHIPEs, as shown in Figure 3.9. The pore sizes and their uniformity in the PolyHIPEs correlate with the emulsion droplets observed in optical micrographs. (p)$IB_{100}TM_0$ has the smallest average pore size at 23.7 µm. As discussed in the previous section, the stabilization of the HIPE is likely due to dissolved IBOA particles functioning as a macromolecular surfactant. The dissolution of non-crosslinked particles in the continuous phase and its effect on maximum internal phase uptake have been previously observed [170]. This was confirmed by Hua *et al.*, who reported that yet-to-be-dissolved particles were functioning as a stabilizer, while the dissolved particles were forming the skeleton of the porous material [97]. However, to our knowledge, this is the first time that surfactant-stabilized-grade small pore sizes in Pickering PolyHIPEs have been obtained by utilizing the dissolution of colloidal particles as an emulsion stabilizer. While (p)$IB_{100}TM_0$ exhibits pores with a few pore throats (Fig. 3.9 A), there are occasionally observed but extremely large and interconnected pores as well (Fig. 3.10). These atypical pores might be due to being stabilized by yet-to-be-dissolved $IB_{100}TM_0$ particles, and their existence might depend on both the standing time of the HIPE or the sonication duration during the particle dispersion within the continuous phase. (p)IB_0TM_{100} is the only Pickering PolyHIPE exhibiting conventional Pickering PolyHIPE morphology: closed and large pores compared to conventional surfactant-stabilized PolyHIPEs. The pores in (p)IB_0TM_{100} samples exhibit a deformed spherical morphology, which correlates well with the corresponding HIPE optical micrographs (Fig. 3.9 E).

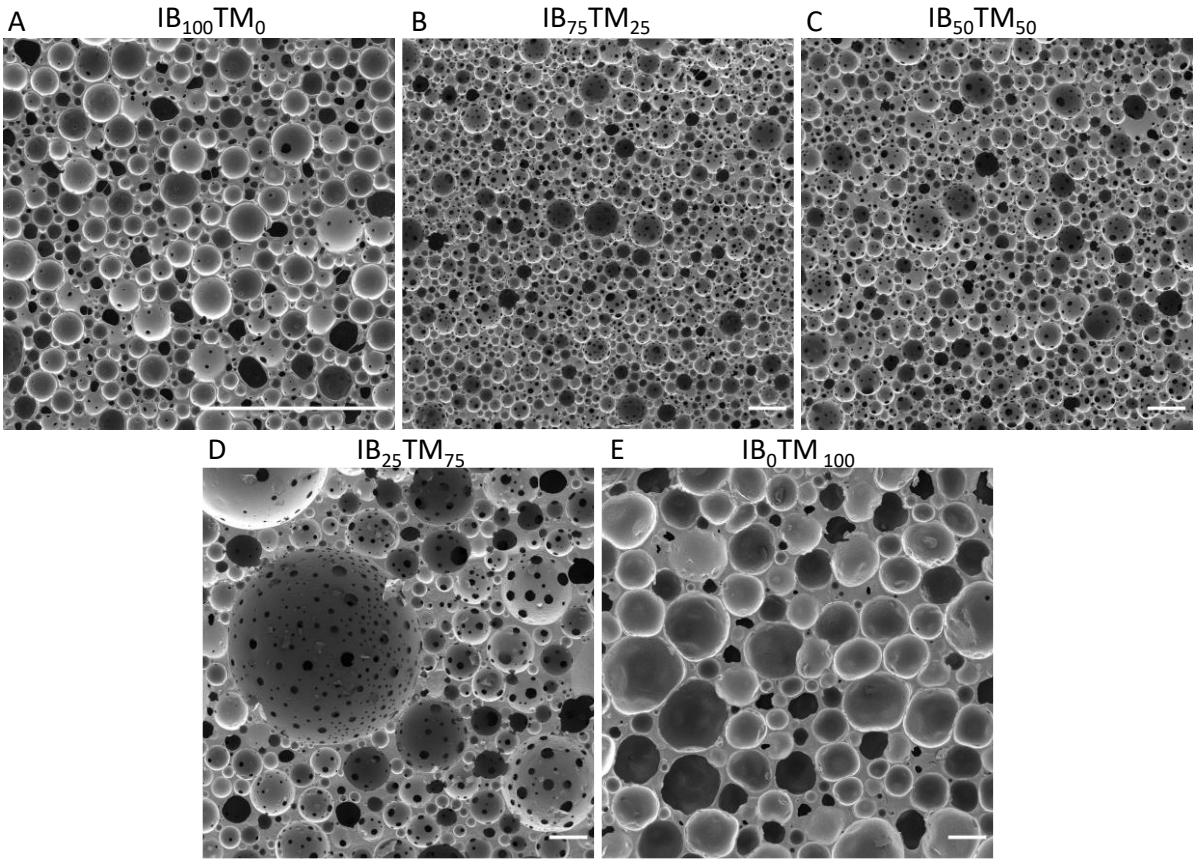

Figure 3.9: SEM images of laser-cut PolyHIPEs, templated from IB-TM-stabilized HIPEs demonstrating the overall porous structure (A-E). Scale bars are 250 µm.

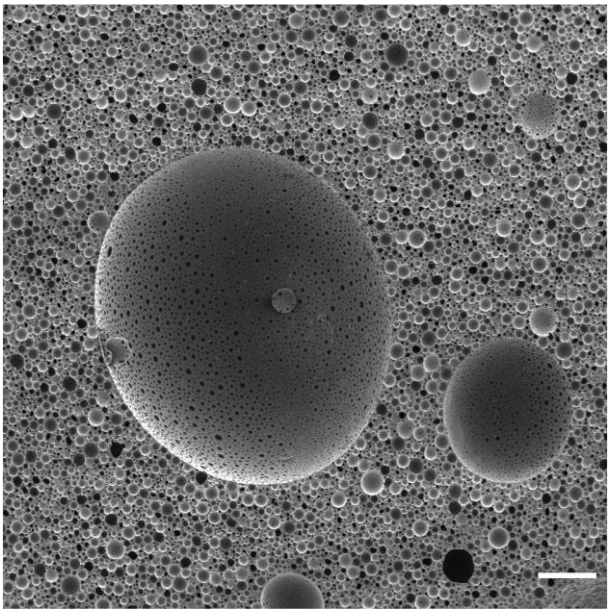

Figure 3.10: SEM image of (p)$IB_{100}TM_0$ demonstrating the occasionally observed large (up to 1 mm) and highly interconnected pores. The scale bar is 250 µm.

3.4.3.2. The Microstructure

All the IBOA-TMPTA blend particle-stabilized HIPE templates exhibit an interconnected porous structure (Fig. 3.9 B-D). In our previous study [65], we attributed pore throat formation under the current experimental conditions to arrested coalescence. Similarly, both pore throats and pore-pore junctions were densely covered with particles, providing evidence of pore throat formation due to the partial coalescence of emulsion droplets that were subsequently arrested by particle jamming. The interconnected porous structure of Pickering PolyHIPEs, except for (p)IB_0TM_{100}, has been confirmed, and the average pore throat size and distribution have been obtained through mercury intrusion porosimeter (Fig. 3.11). The pore throat size of the samples correlates with the pore size. (p)$IB_{100}TM_0$ exhibits a bimodal pore throat size distribution with peaks at approximately 1 and 6 µm. The second peak at around 6 µm might be attributed to the occasionally observed extremely large and interconnected pores of (p)$IB_{100}TM_0$. (p)$IB_{25}TM_{75}$ is another sample exhibiting a bimodal pore throat size distribution, which is expected since (p)$IB_{25}TM_{75}$ also exhibits a bimodal pore size distribution.

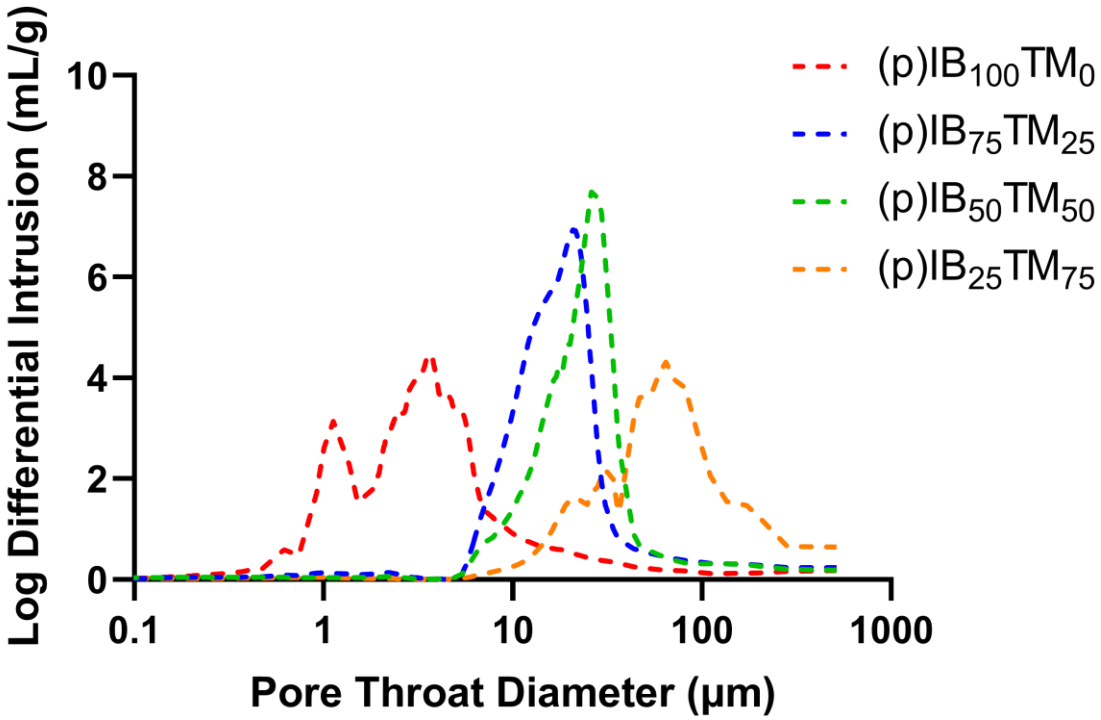

Figure 3.11: The obtained pore throat diameter (µm) from mercury intrusion porosimeter as a function of log differential intrusion (mL/g).

SEM images of PolyHIPEs focusing on the pore surface and interface are presented in Figure 3.12. In (p)$IB_{100}TM_0$, a smooth pore surface is observed, with particles sporadically observed on the polymer wall but not on the pore surface itself (Fig. 3.12 A). Both (p)$IB_{75}TM_{25}$ and (p)$IB_{50}TM_{50}$ exhibit similar

micromorphology, with submicron pore throats especially noticeable on the relatively smaller pores. These submicron pore throats are hypothesized to result from the arrested coalescence of nearby micron-sized pores (Fig. 3.12 B-C). The micron-sized pores are also found at the pore-pore interface. Pores in these samples have both smooth and rough patches on their surfaces due to embedded particles. Pore throats and pore-pore junctions exhibit a similar morphology, densely covered with particles. In contrast, (p)$IB_{25}TM_{75}$ shares the micromorphology seen in other IBOA/TMPTA blends, except for the pore surface. In (p)$IB_{25}TM_{75}$, relatively large interconnected pores exhibit roughness, while relatively smaller pores have smooth surfaces (Fig. 3.12 D). Finally, (p)IB_0TM_{100} exhibits a solid polymer film that separates neighbouring pores (Fig. 3.12 E). In this case, regardless of pore size, the pores have rough surfaces similar to the large pore surfaces of (p)$IB_{25}TM_{75}$

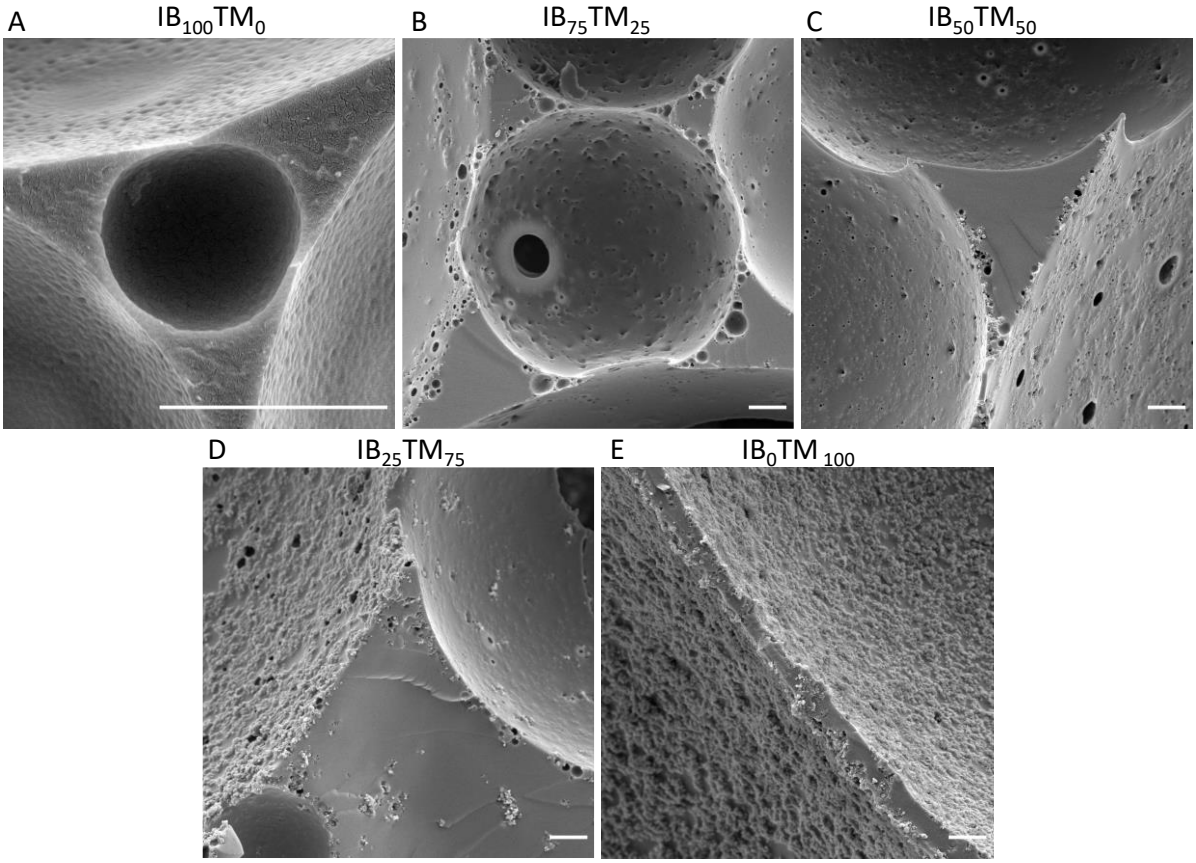

Figure 3.12: The microstructure of PolyHIPE samples. The smooth pore surface and the polymer interface separate pores from each other (A). Pore surface with smooth and rough regions, submicron pore throats, and micron-sized pores at the close vicinity of larger pores (B and C). The rough and the smooth pore surface of large and small pores, respectively (D). Polymeric film separates two pores and the rough surface of pores (E). Scale bars are 2.5 μm.

Considering that IB_0TM_{100} particles are the most hydrophilic among the particles, making them expected to be wetted more by the internal water phase, it's not surprising to observe these particles

located towards the void (pore surface). However, the similar localization of $IB_{25}TM_{75}$ particles on the large, interconnected pores of (p)$IB_{25}TM_{75}$ remains unexplained.

Additionally, the effect of leftover Tween 20 on particles is also considered. $IB_{100}TM_0$ particles were dissolved in deprotonated chloroform, and NMR analysis was conducted to evaluate whether Tween 20 was adsorbed onto the particles. The NMR results showed Tween 20 remnants on the $IB1_{00}TM_0$ particles, with a molar ratio of 1 to 0.15. However, the impact of Tween 20 remnants should be minimal for several reasons. First, Tween 20 is a hydrophilic surfactant that preferentially stabilizes oil-in-water emulsions. Second, even if all Tween 20 were absorbed onto the particle surface during particle synthesis, the overall weight percentage of Tween 20 in the continuous phase would be 0.25%. Experiments showed that neither 0.25% nor 5% wt of Tween 20 in the continuous phase is able to stabilize the given HIPE. Finally, all the particles were prepared with the same amount of Tween 20; however, both HIPE and PolyHIPE samples exhibit significant rheological and morphological differences.

3.4.4. Interfacial Rheology

The dilatational interfacial rheology was performed to investigate the effect of interfacial rheology in the presence of different particles on the morphology of PolyHIPEs. The dilatational modulus (E) is defined as follows [185,186]:

$$E = A_0 \frac{\Delta\gamma}{\Delta A} \tag{3}$$

where A_0 is the pendant drop interface area, ΔA is the interface area difference, and $\Delta\gamma$ is the interfacial tension difference because of the volume oscillation. The dilatational elastic modulus (E') and viscous modulus (E'') are defined as follows [186]:

$$E = |E|\cos(\phi) + i|E|\sin(\phi) = E' + iE'' \tag{4}$$

where ϕ is the phase angle, $E' = |E|\cos(\phi)$, and $E'' = |E|\sin(\phi)$. The interfacial tension and interface area oscillation are fitted with a sinusoidal function to obtain the interfacial moduli. Figure 3.13 shows the typical normalized pendant drop interface area and interfacial tension oscillation curves at 0.5 Hz and 0.1 Hz for the blank interface (i.e., in the absence of particles), respectively. As seen, the blank interface also shows dilatational rheological properties, which can be attributed to the surface activity of monomers and crosslinkers. Figure 3.13 A shows the aqueous phase drop immersed in the clear continuous phase containing 0.001 g of $IB_{100}TM_0$, whereas Figure 3.14 is the aqueous phase drop immersed in the translucent continuous phase containing 0.001 g of IB_0TM_{100}. The typical normalized oscillation curves for 0.001 g $IB_{100}TM_0$-adsorbed interface, to which different waiting times

were applied, are provided in Figure 3.15. Figure 3.16 shows the typical normalized oscillation curves for the 0.001 g IB_0TM_{100}-adsorbed interface. Without applying the waiting time, the $IB_{100}TM_0$-stabilized interface is already viscoelastic (Figure 3.15 A), indicating quick adsorption of $IB_{100}TM_0$ at the interface. Nevertheless, for IB_0TM_{100} particle with 0 h waiting time, the shape of the pendant drop almost remains the same during oscillation, and the interfacial tension does not show any oscillation (Figure 3.16 A), demonstrating the adsorption of particles at the interface in Pickering HIPEs has a slower kinetics compared to soluble polymers.

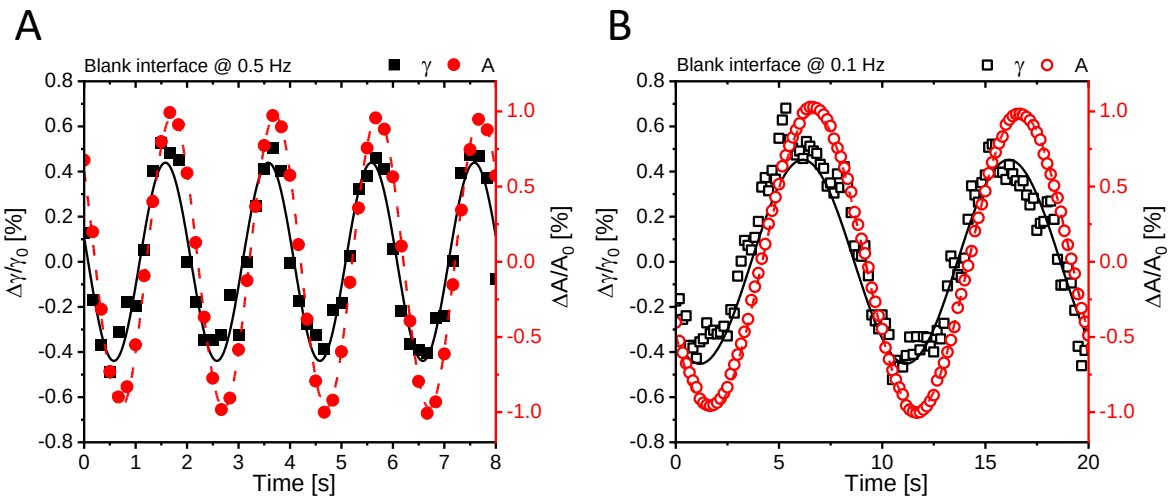

Figure 3.13: The typical normalized pendant drop oscillation curves at 0.5 Hz (A) and 0.1 Hz (B) for the blank interface are shown above. The solid and dashed lines in the above curves are the sinusoidal fitting for interfacial tension and interface area oscillation.

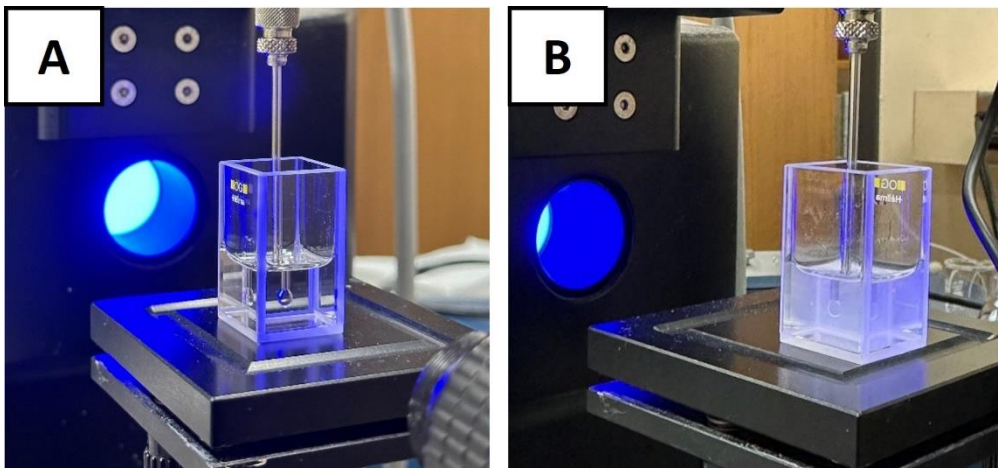

Figure 3.14: The pendant drop of the aqueous phase immersed in the continuous phase containing 0.001 g particle $IB_{100}TM_0$ (A) and 0.001 g particle IB_0TM_{100} (B).

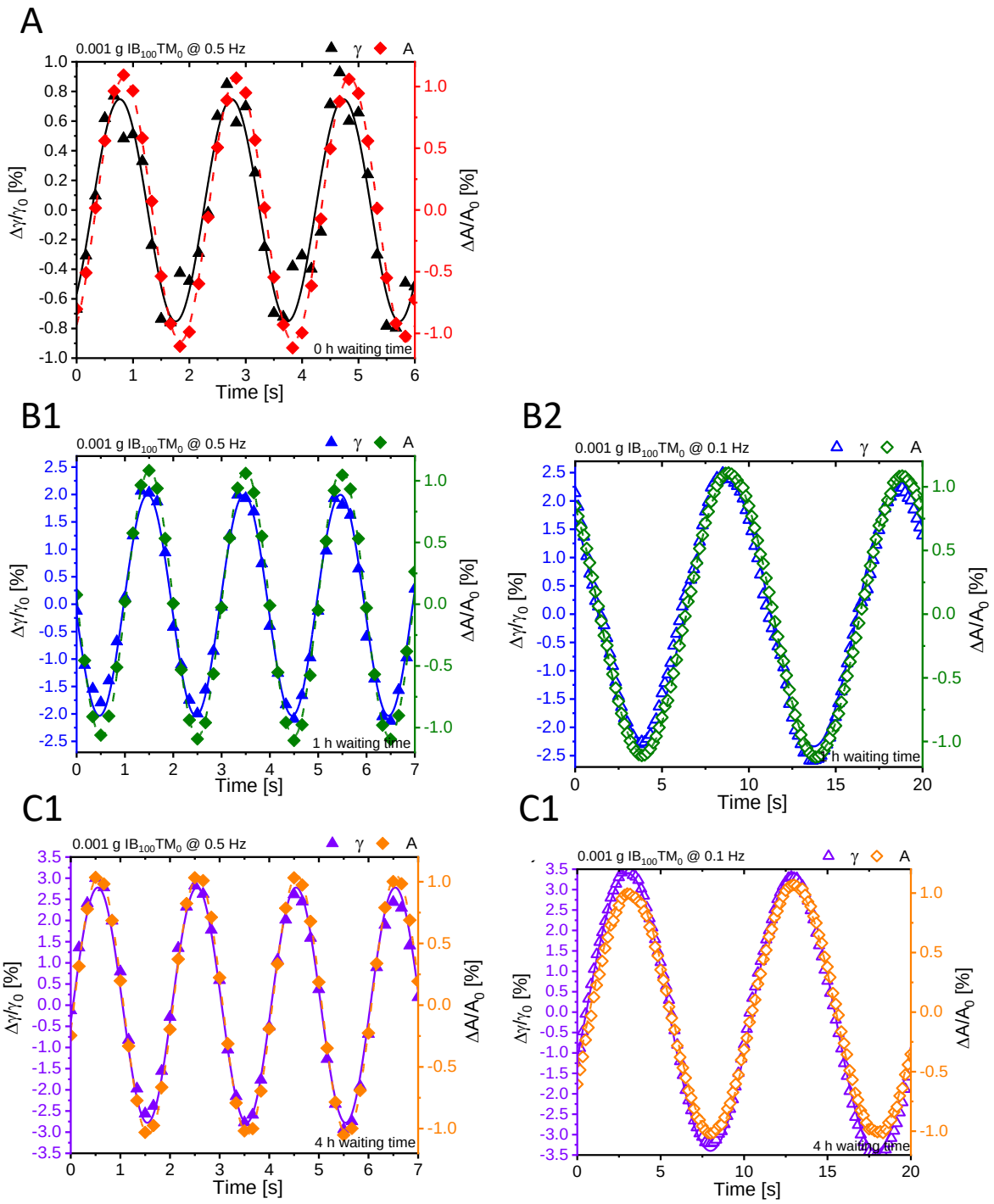

Figure 3.15: 0 h, 1 h, 2 h, and 4 h prior to the volume oscillation were applied, respectively, for particle $IB_{100}TM_0$. The typical normalized pendant drop oscillation curve for particle $IB_{100}TM_0$ interface at 0.5 Hz without waiting (A). The typical normalized pendant drop oscillation curve for particle $IB_{100}TM_0$ interface after 1 h waiting at 0.5 Hz (B1), and 0.1 Hz (B2). The typical normalized pendant drop oscillation curve for particle $IB_{100}TM_0$ interface after 4 h waiting at 0.5 Hz (C1) and 0.1 Hz (C2).

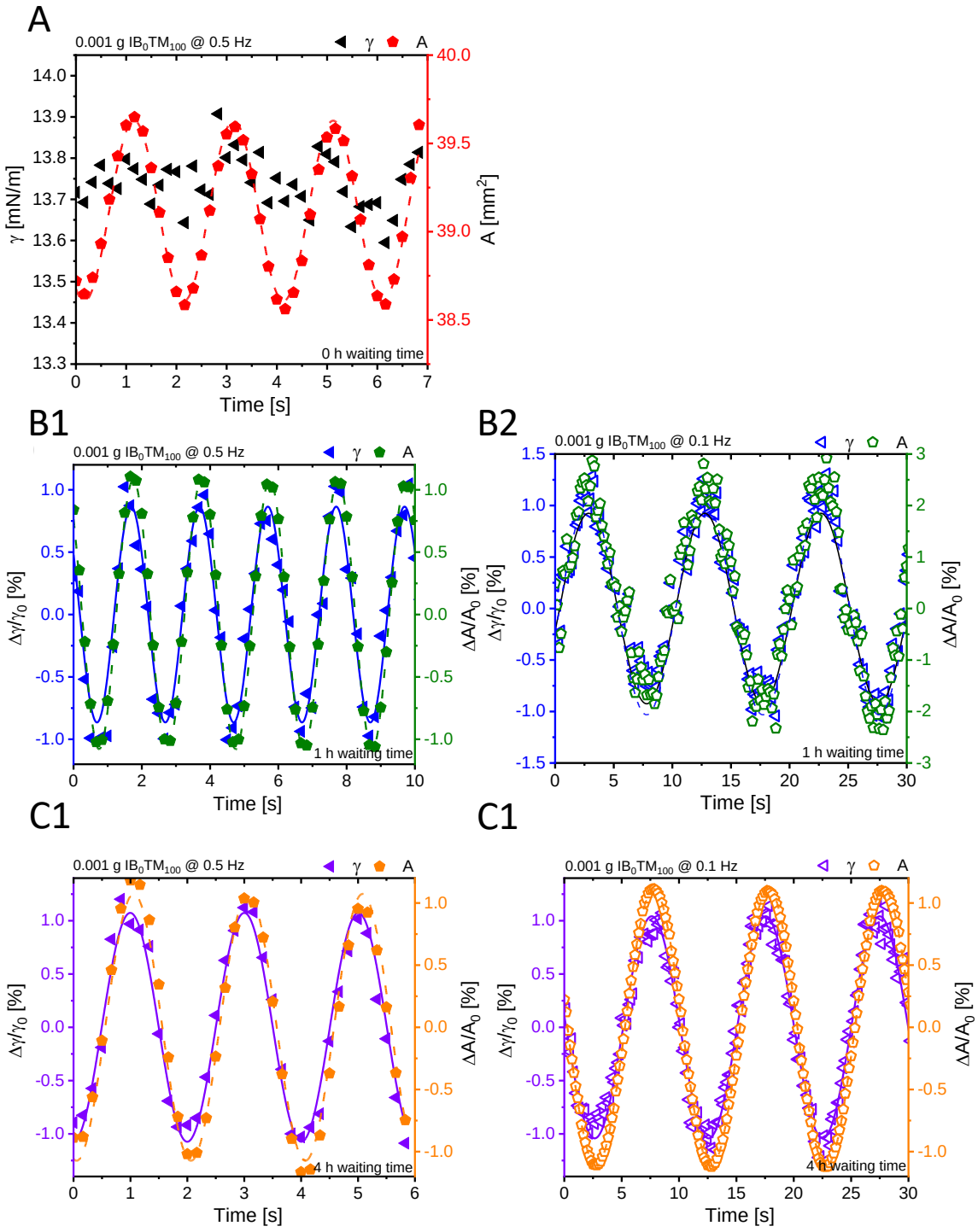

Figure 3.16: 0 h, 1 h, 2 h, 4 h, and over 12 h prior to the volume oscillation were applied, respectively, for particle IB_0TM_{100}. The pendant drop surface area oscillation curve for particle IB_0TM_{100} interface at 0.5 Hz without waiting (A). The surface tension does not show the oscillation. The typical normalized pendant drop oscillation curve for particle IB_0TM_{100} interface after 1 h waiting at 0.5 Hz (B1), and 0.1 Hz (B2). The typical normalized pendant drop oscillation curve for particle IB_0TM_{100} interface after 4 h waiting at 0.5 Hz (C1), and 0.1 Hz (C2).

The measurements were performed after different waiting times, as mentioned earlier, from the drop formation moment to evaluate the interfacial rheological properties in the equilibrium state (i.e., minimizing transient effects). Figure 3.14 typically shows the E' and E'' of $IB_{100}TM_0$-stabilized interface with different waiting times of 0, 1, 2, and 4 h at varied frequencies, indicating that the E' increases as the age of the interface increases. However, the E'' remains almost the same regardless of the waiting time. As mentioned earlier, different waiting times, including 0, 1, 2, 4, and over 12 h are applied before oscillation for particle IB_0TM_{100}, as seen in Figure 3.17. The E' increases over time also for the IB_0TM_{100} interface (see Figure 3.17 inset), although the increase is smaller compared to that of the $IB_{100}TM_0$ interface. The results suggest that a 4 h waiting time is a good approximation of equilibrium interfacial rheology.

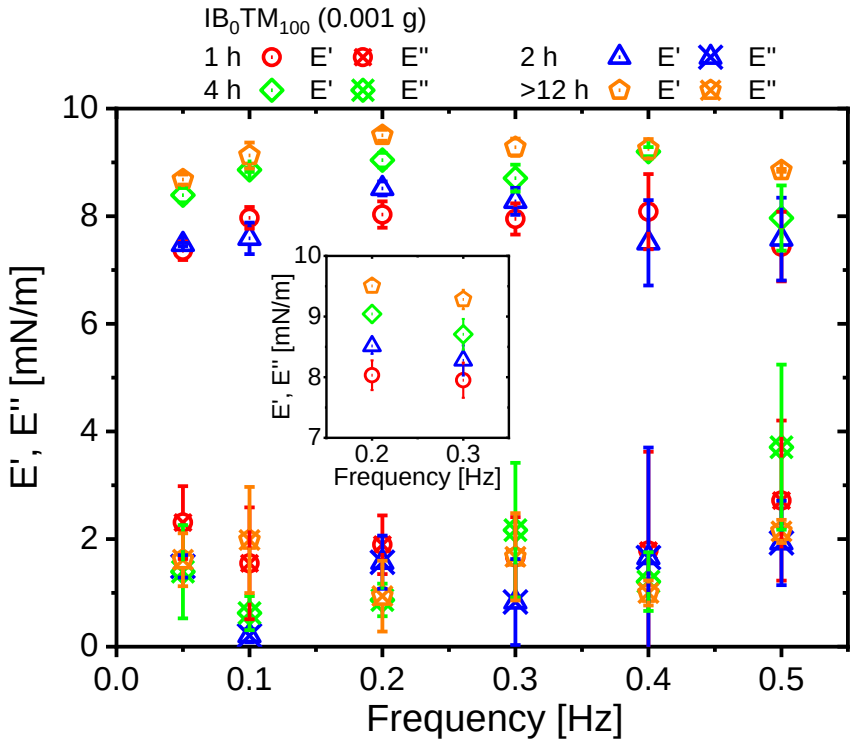

Figure 3.17: E' and E'' of 0.001 g IB_0TM_{100} particle-adsorbed oil-water interface when applying different waiting times of 1 h, 2 h, 4 h, and over 12 h.

Figure 3.18 B shows the E' and E'' of the oil-water interface in the presence of 0.001 g IBOA/TMPTA particles after applying 4 h of waiting at varied frequencies. The interfacial moduli of all samples are independent of the frequency. For blank interface, E' is higher than E'', and the introduction of IBOA/TMPTA particles further increases the elasticity of the interface while the viscous contribution remains unchanged. For particles synthesized with less amount of IBOA, the interfacial elastic modulus of the oil-water interface is lower, while no change in the viscous contribution is observed. The interfacial rheological properties are a function of the particle's hydrophilicity, shape, size, and aggregates [187–191]. Since all of these characteristics change among $IB_{75}TM_{25}$, $IB_{50}TM_{50}$, $IB_{25}TM_{75}$,

and IB_0TM_{100} particles ($IB_{100}TM_0$ was excluded as it dissolves in the continuous phase), it is impossible to attribute the observed changes in interfacial rheology to the characteristics of the particles.

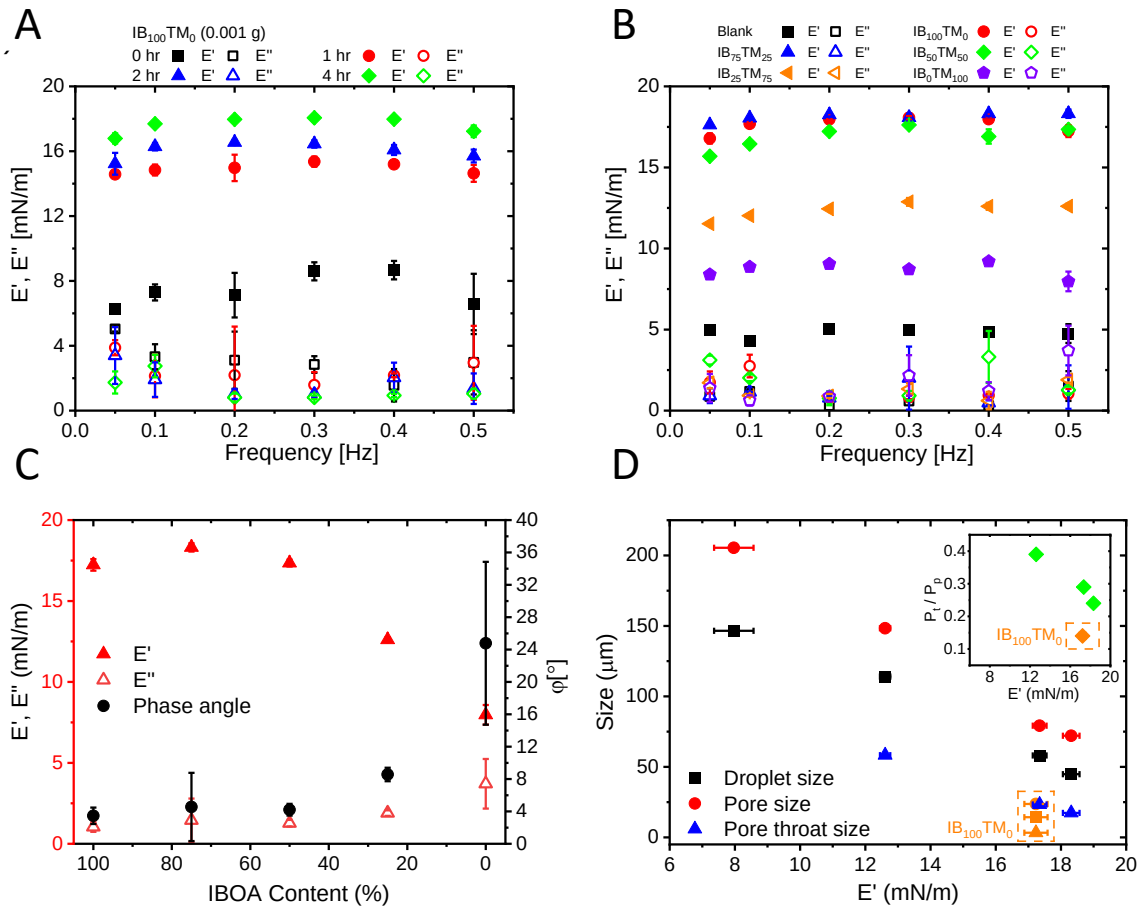

Figure 3.18: E' and E'' of 0.001 g $IB_{100}TM_0$ particle-adsorbed oil-water interface when applying different waiting times of 0, 1, 2, and 4 h (A). Dilatational elastic and viscous moduli of 0.001 g IBOA/TMPTA particles-adsorbed oil-water interface after 4 h waiting (B). The black points are the moduli of the blank interface. The interfacial elastic modulus decreases as decreasing the amount of monomer IBOA in particle synthesis, whereas the interfacial viscous modulus remains unchanged as varying the ratio of IBOA and TEMPTA. Additionally, both interfacial elastic and viscous moduli of IBOA/TMPTA particles-adsorbed oil-water interface are independent of frequency. Dilatational rheological properties of 0.001 g IBOA/TMPTA particles-adsorbed oil-water interface at 0.5 Hz frequency after 4 h waiting (C). The black solid points show the phase angle, which is dependent on IBOA content. The red solid points are the elastic modulus, which decreases with lowering IBOA except for the case of 100 % of IBOA (soluble polymer). The red hollow points are the viscous modulus, which is independent of the IBOA content. HIPE droplet size, PolyHIPE pore size, and PolyHIPE pore throat size as a function of dilatational elasticity (D). The inset shows the P_t / P_p versus interfacial elasticity. The orange points are for $IB_{100}TM_0$ particles, which do not follow the trend due to their solubility in the continuous phase.

Figure 3.18 C shows the E' and E'' of the interface with 0.001 g of different IBOA/TMPTA particles at 0.5 Hz after waiting for 4 h. As supporting information, the interfacial moduli at 0.05 Hz are provided in Figure 3.19. The IBOA/TMPTA particles-adsorbed interface is an elastic-dominated interface with E' higher than E'' at both 0.5 Hz and 0.05 Hz, and the E'' is almost independent of the IBOA content. It

should be mentioned that E' is lower for particles synthesized with less amount of IBOA. However, $IB_{100}TM_0$ is an exception because these particles are dissolved in the continuous phase and act similarly to macromolecular emulsifiers rather than Pickering stabilizers. Additionally, the phase angle increases with a decrease in IBOA content, as seen in Figure 3.18 B, indicating that the interface becomes more viscous for particles synthesized with less IBOA concentration [186]. According to Figure 3.3 B, lower IBOA content increases the hydrophilicity of IBOA/TMPTA particles. However, since the particle positioning at the interface depends on the surface properties of both aqueous and oil phases, it is unclear how this phenomenon increases interfacial viscoelasticity shown in Figure 3.18 C. Nevertheless, the formation of closed-cell structure, as seen in Figure 3.12 E, may be attributed to the increase of interfacial viscoelasticity [192]. We hypothesized that the non-monotonic trend observed in Figure 3.7 for Pickering HIPEs is due to the changes in interfacial tension and/or interfacial rheology. However, Figure 3.18 C shows that the interfacial rheology data has a monotonic trend when the IBOA content of particle decreases from 75 to 0% (Pickering HIPEs). Therefore, the highest scaled modulus and yield stress for IB_0TM_{100} sample in Figure 3.7 can be attributed to changes in effective interfacial tension rather than interfacial rheology.

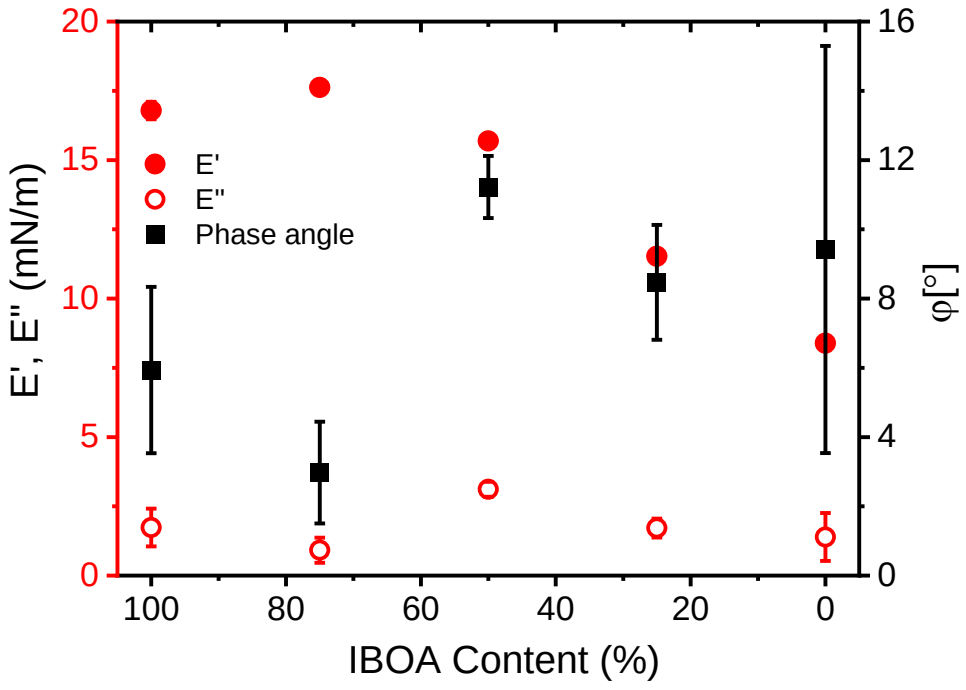

Figure 3.19: Dilatational rheological properties of 0.001 g IBOA/TMPTA particles-adsorbed oil-water interface at lower frequency of 0.05 Hz.

Figure 3.18 D shows the HIPE droplet size, PolyHIPE pore size, and PolyHIPE pore throat size against interfacial elasticity. As seen, droplet, pore, and pore throat sizes decrease for higher interfacial elasticity. To cancel out the effect of pore size on the pore throat size, as discussed in the work of Zhou *et al.* [192], the P_t / P_p versus interfacial elasticity should be studied, as shown in the inset of Figure 3.18 D. Similar to surfactant stabilized HIPEs studied by Zhou *et al.* [192], the P_t / P_p ratio decreases when the interface elasticity decreases. It should be noted that the particle $IB_{100}TM_0$ is highlighted as the orange data points in Figure 3.18D since they are dissolved in the continuous phase and are different from the rest of the IBOA/TMPTA particles.

3.5. Conclusion

We demonstrated the effect of particle hydrophilicity by tuning the crosslinker concentration in particles on Pickering PolyHIPE morphology. It was observed that particle hydrophilicity has a significant impact on emulsion stability, droplet size and shape, and rheology. HIPEs stabilized by particles with a water contact angle of 54° exhibit traditional Pickering HIPE behavior ((h)IB0TM100). On the other hand, HIPEs stabilized by particles with a water contact angle of 82-69° exhibit reduced droplet size, spherical droplets, and reduced viscosity, similar to traditional surfactant-stabilized HIPEs ((h)$IB_{75}TM_{25}$, (h)$IB_{50}TM_{50}$, and (h)$IB_{25}TM_{75}$). The difference in HIPE behavior is also reflected in the morphological differences in PolyHIPEs. It is concluded that it is possible to tune the openness of the PolyHIPE by adjusting the particle hydrophilicity from interconnected to closed porous structure. Additionally, IBOA/TMPTA particle-stabilized oil-water interfaces exhibit viscoelasticity, which is affected by the adsorption time, with the elastic modulus higher than the viscous modulus. Furthermore, lower IBOA content during particle synthesis results in a decrease in interfacial elasticity. Additionally, the dissolution of particles within the continuous phase, functioning as a macromolecular surfactant, is demonstrated, providing conventional PolyHIPE-grade small pores with a semi-open porous structure. These results support the previously proposed mechanism for pore throat formation in Pickering PolyHIPEs by arrested coalescence and provide new insights into the relationship between the mechanism and particle hydrophilicity. Since the rheology of the HIPEs is affected by particle hydrophilicity, and these changes are correlated with PolyHIPE openness, rheological measurements can be conducted to determine if the HIPE template would be interconnected or not.

The demonstrated surfactant-free Pickering PolyHIPEs can be used in applications such as tissue engineering and as catalyst supports due to their tunable pore and pore throat size. The research suggests an innovative approach that involves utilizing both hydrophilic and hydrophobic particles as emulsion stabilizers to achieve a tailored porous structure in PolyHIPE materials. When hydrophilic particles are employed, they tend to result in a closed porous structure while decorating the pore

surfaces with particles. Conversely, the use of hydrophobic particles typically leads to an open-cellular morphology. By combining both types of particles as emulsion stabilizers, it becomes possible to potentially create a hybrid structure that features open-cellular pores while also being adorned with hydrophilic particles. This approach holds promise for offering unique advantages, especially in incorporating functional particles such as metal-organic frameworks. It enables a streamlined, one-pot synthesis method for crafting PolyHIPE materials with precisely engineered pore structures and surface decorations, opening up new possibilities for diverse applications

CHAPTER 4

Surfactant-Free ZIF-8 Decorated and Open Porous Pickering Polymerized High Internal Phase Emulsion

E. Durgut[a,b], J. Foster[c], F. Claeyssens[a,b]

[a] *Kroto Research Institute, Department of Materials Science and Engineering, University of Sheffield, Sheffield, United Kingdom*

[b] *Department of Materials Science and Engineering, INSIGNEO Institute for In Silico Medicine, The University of Sheffield, Sheffield, United Kingdom*

[c] *Department of Chemistry, University of Sheffield, Sheffield, United Kingdom*

Abstract

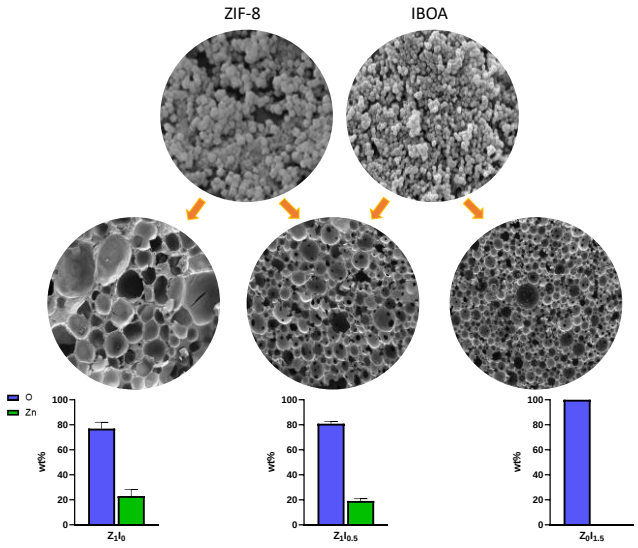

Metal-organic frameworks (MOFs) represent an emerging class of porous materials with significant potential for various applications. However, their utilization in powder form poses challenges for industrial-scale applications. Consequently, there is active research in developing supporting materials for MOFs. This research article explores the effectiveness of loading MOFs, specifically ZIF-8, onto polymerized high internal phase emulsions (PolyHIPEs). ZIF-8 was used as a sole emulsion stabilizer, as well as in combination with polymeric colloidal particles and surfactant as co-stabilizers in the emulsion.The findings indicate that when ZIF-8 is used as the sole emulsion stabilizer, it leads to well-surface-decorated but closed porous PolyHIPEs. Conversely, combining ZIF-8 with IBOA microparticles as emulsion stabilizers results in similarly well-decorated but interconnected porous structures. The common practice of using ZIF-8 with a surfactant produces an interconnected porous structure, but with a poorly decorated porous structure. This is attributed to an antagonistic effect between Hypermer B246 (a surfactant) and ZIF-8. The study employed morphological investigations, SEM micrographs, thermogravimetric analysis, and energy-dispersive X-ray analysis to evaluate the ZIF-8 loading efficacy in PolyHIPEs.

Keywords: Metal-organic frameworks, ZIF-8, PolyHIPE, Pickering emulsion

4.1. Introduction

Metal-organic frameworks (MOFs) represent a class of porous crystalline materials formed through the self-assembly of metal ions and organic linkers. The unique characteristics of MOFs, including high specific area and porosity, enable interactions between the active sites of MOFs and guest molecules. As a result, MOFs have shown significant potential in diverse applications such as gas storage and separation, chemical sensing, and catalysis [193,194]. One well-known subclass of MOFs is the zeolitic imidazole framework, specifically ZIF-8 (Zn(Hmim)2), composed of zinc as the metal center and 2-methylimidazole (Hmim) as the organic linker [193]. ZIF-8 stands out due to its high thermal and chemical stability, a notable advantage as stability is often a drawback in many other MOFs[195]. The popularity of ZIF-8 is mainly due to its high thermal and chemical stability [195] since thermal and chemical stability is a well-known drawback of MOFs [196]. Despite their promise, the industrial-scale application of MOFs is hindered by their polycrystalline powder form. Challenges such as handling difficulties, recycling issues, and the potential for clogging pipes and reactors are associated with the powder form of MOFs [197].

The utilization of polymerized high internal phase emulsions (PolyHIPE) is a commonly employed approach to overcome the limitations associated with the powder forms of MOFs. The preparation of PolyHIPE involves creating a high internal phase emulsion where the internal phase volume constitutes more than 74% of the emulsion. Polymerization of the continuous phase and the removal of the internal phase leave behind a highly porous material (theoretically equivalent to the amount of internal phase) that is interconnected. The highly porous and interconnected nature of PolyHIPEs offers excellent support for MOFs, allowing them to function while embedded in accessible pores.

There are two common ways of using PolyHIPEs as MOF support: (1) synthesizing MOFs within the pores of PolyHIPEs [198–200] or (2) using MOFs as an emulsion stabilizer, as colloidal particles with appropriate wettability can function as emulsion stabilizers (Pickering emulsions) [132,201–203]. Both methods necessitate the usage of surfactant to prepare PolyHIPE since, unlike PolyHIPEs obtained from surfactant-stabilized HIPEs, PolyHIPEs obtained from Pickering HIPE exhibit a closed cellular morphology, meaning pores with no interconnecting pore throats. Since the first method requires interconnected pores for the synthesis of MOFs within the pores, and both methods necessitate accessible pores for MOFs to interact with guest molecules, both methods require the utilization of surfactants.

However, the utilization of surfactants has its drawbacks, requiring intensive washing steps that may adversely react with MOFs, increasing production costs, and raising environmental concerns. For the second method, surfactants and MOFs are used as dual emulsifiers to obtain interconnected PolyHIPEs

[201,202]. However, surfactants and colloidal particles together work antagonistically [88,204]; surfactant molecules might adsorb on the colloidal particles and lead them to be dispersed in either of the emulsion phases, preventing or reducing their function as an emulsion stabilizer, thus affecting the efficacy of pore surface decoration with MOFs.

In our previous reports, we demonstrated that isobornyl acrylate (IBOA) particles (hydrophobic) as HIPE stabilizers result in 2-ethylhexyl acrylate (EHA)/IBOA-based PolyHIPEs exhibiting an open porous structure [65], whereas trimethylolpropane triacrylate (TMPTA) particles (hydrophilic) as emulsion stabilizers result in closed cellular PolyHIPEs with particle-decorated pore surfaces. In this research, we hypothesized that combining IBOA particles and hydrophilic ZIF-8 particles as HIPE stabilizers can provide open porous PolyHIPEs with ZIF-8 decorated pore walls. HIPEs with various concentrations of IBOA and ZIF-8 particles were used as emulsion stabilizers, and their efficacy as emulsion stabilizers as well as in pore wall decoration were investigated. Additionally, Hypermer B246 (surfactant) and ZIF-8 as dual emulsifiers were also utilized and compared.

4.2. Materials

$ZnNO_3.6H_2O$, 2-methylimidazole (Hmim), 2-ethlyhexyl acrylate (EHA), isobornyl acrylate (IBOA), trimethlyolpropane triacrylate (TMPTA) and 2-hydroxy-2-methylpropiophenone were purchased from Sigma Aldrich. Hypermer B246 was provided by Croda.

4.3. Methods

4.3.1. The Synthesis of ZIF-8 and IBOA particles

ZIF-8 is synthesized in accordance with the recipe explained elsewhere with minor modifications [205]. Briefly; $ZnNO_3.6H_2O$ (1.19 g, 4 mmol) and Hmim (1.31 g, 16 mmol) are dissolved separately in 40 mL of methanol by magnetic stirring for an hour. After the dissolution, the $ZnNO_3.6H_2O$ solution is poured into the Hmim solution where the final ratio of $ZnNO_3.6H_2O$:Hmim:Methanol was 1:4:20 (mmol/mmol/mL). The combined solution is not mixed and incubated at 50°C for 6 hours. The prepared ZIF-8 particles were recovered by centrifugation at 5.000 RPM for 20 minutes. Afterward, samples were washed with methanol followed by centrifugation at 10.00 RPM for 10 minutes thrice and dried at 50°C in a convection oven overnight. Polymeric microparticles (3:1 IBOA:TMPTA ratio) were synthesized with exactly the same method explained elsewhere.

4.3.2. Nomenclature of PolyHIPEs

PolyHIPE samples were named according to the weight percentage of the stabilizer used to prepare HIPE and, thus, PolyHIPE. ZIF-8, isobornylacrylate particles, and Hypermer B246 are referenced with

their initials; Z, I and H, respectively. $Z_1I_{1.5}$ refers to PolyHIPE prepared from a HIPE where the emulsion stabilizers were ZIF-8 (1 wt%) and IBOA (1.5 wt%).

4.3.3. The Synthesis of PolyHIPEs

The monomers EHA/IBOA/TMPTA are mixed with a ratio of 63/21/16 wt%. The intended amount of stabilizer, either ZIF-8 or IBOA particles was dispersed within 1 g of the monomer mixture by sonication (Hielscher UP100H, Hielscher Ultrasound Technology) for 30 s. In the case of Hypermer B246, the surfactant was dissolved in the oil mixture first by heating the oil mixture, then the ZIF-8 particles were added and dispersed with sonication. After the stabilizers were dispersed in the oil mixture, 2-hydroxy-2-methylpropiophenone (2%) was added to the monomer-particle mixture, thus, the continuous phase was prepared. 4 g of water was added to the continuous phase and vortexed for 30 s, followed by handshaking for 15 s to prepare HIPE. HIPE was poured onto the glass petri dish and the HIPE was photopolymerized by exposing HIPE to ultraviolet light (UV) for 5 minutes via a UV curing system (Omnicure Series 1000, Lumen Dynamics).

4.3.4. Characterization

Crystallinity of ZIF-8 was evaluated from the record obtained from PXRD, powder diffractometer (Bruker D8 Advance, Bruker) equipped with a copper Kα source (λ=1.5418 Å) operating at 40 kV and 40 mA. The instrument was fitted with an energy-dispersive LYNXEYE detector. Elemental analysis of ZIF-8 was evaluated by CHNSO elemental analyzer (Micro Cube, Vario).

The particle size of ZIF-8 and the average pore size of the PolyHIPEs were measured from the images obtained by scanning electron microscope (SEM) (Inspect FEI, FEI) by using ImageJ. All the samples were 8 nm thick gold coated prior to imaging. Prior to gold coating, PolyHIPE samples were cut into thin pieces by a scalpel and washed with methanol to remove the unattached ZIF-8 particles from the PolyHIPE surfaces. All the samples were imaged at 5 kV accelerating voltage and 3 µm spot size. Elemental analysis of PolyHIPE samples were conducted on carbon coated samples and the EDX (FEI Nova Nano SEM 450, FEI) spectra was collected at 20 kV.

Thermogravimetric analysis (TGA) was conducted on PolyHIPE samples and ZIF-8 to evaluate both the thermal properties and verify the amount of ZIF-8 in PolyHIPE samples by thermo-gravometric analyzer (Pyris 1, PerkinElmer) under N_2 supply with the rate of 20 mL/min. Samples were heated from 30 to 800^{o}C with the rate of 10^{o}C/min.

4.4. Results and Discussion

4.4.1. ZIF-8 Nanoparticles

SEM images and P-XRD pattern of the synthesized ZIF-8 particles are represented in Figure 4.1. As can be observed from the SEM image, fairly monodisperse (0.02 PDI) and cuboidal-shaped particles with an average size of ~200 nm were synthesized (Fig. 4.1 A). Crystallinity of the ZIF-8 nanoparticles are evaluated by P-XRD. Sharp and clear peaks indicating the good crystallinity of ZIF-8 nanoparticles are observed in the XRD pattern, similar to a previous report (Fig. 4.1 B) [205]. Crystallinity and the crystal size of the synthesized ZIF-8 are found to be 85% and 38 nm, respectively.

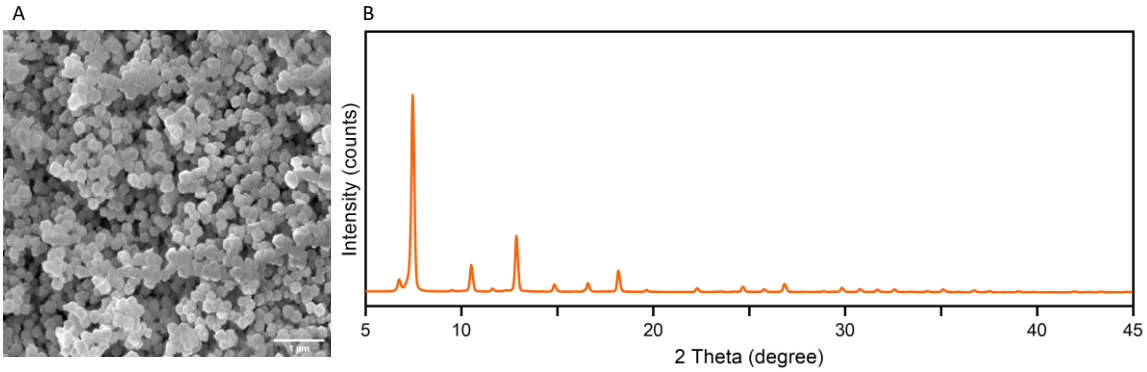

Figure 4.1: SEM micrographs (A) and P-XRD (B) pattern of the synthesized ZIF-8.

4.4.2. HIPEs

HIPEs are generally prepared by the dropwise addition of the internal phase to the continuous phase while the mixture is being stirred. The preparation of HIPEs with similar ingredients using the dropwise addition of the internal phase was previously reported by our research group. However, the method reported required the continuous phase to be as low as ~ 4 mL for efficient mixing. Since the yield of ZIF-8 is known to be low, the continuous phase volume was reduced to ~ 1 mL. There are few reports demonstrating the preparation of HIPE by combining all the ingredients in a single pot and simple handshaking [138,206]. In this research, both the continuous and the internal phases were combined in a glass vial and vortexed/handshaken. HIPEs were successfully prepared within seconds. The digital images of HIPEs and resultant PolyHIPEs for each sample are provided in Figure 4.2. While ZIF-8 as a sole stabilizer successfully stabilized HIPE even at low concentrations (0.5 wt%) with slight creaming, IBOA particles could not stabilize HIPE at the concentrations of 0.5 and 1 wt%, solely. Both Z0I0.5 and Z0I1 samples experienced significant creaming. However, successful HIPE was obtained when the IBOA concentration was increased to 1.5 wt%.

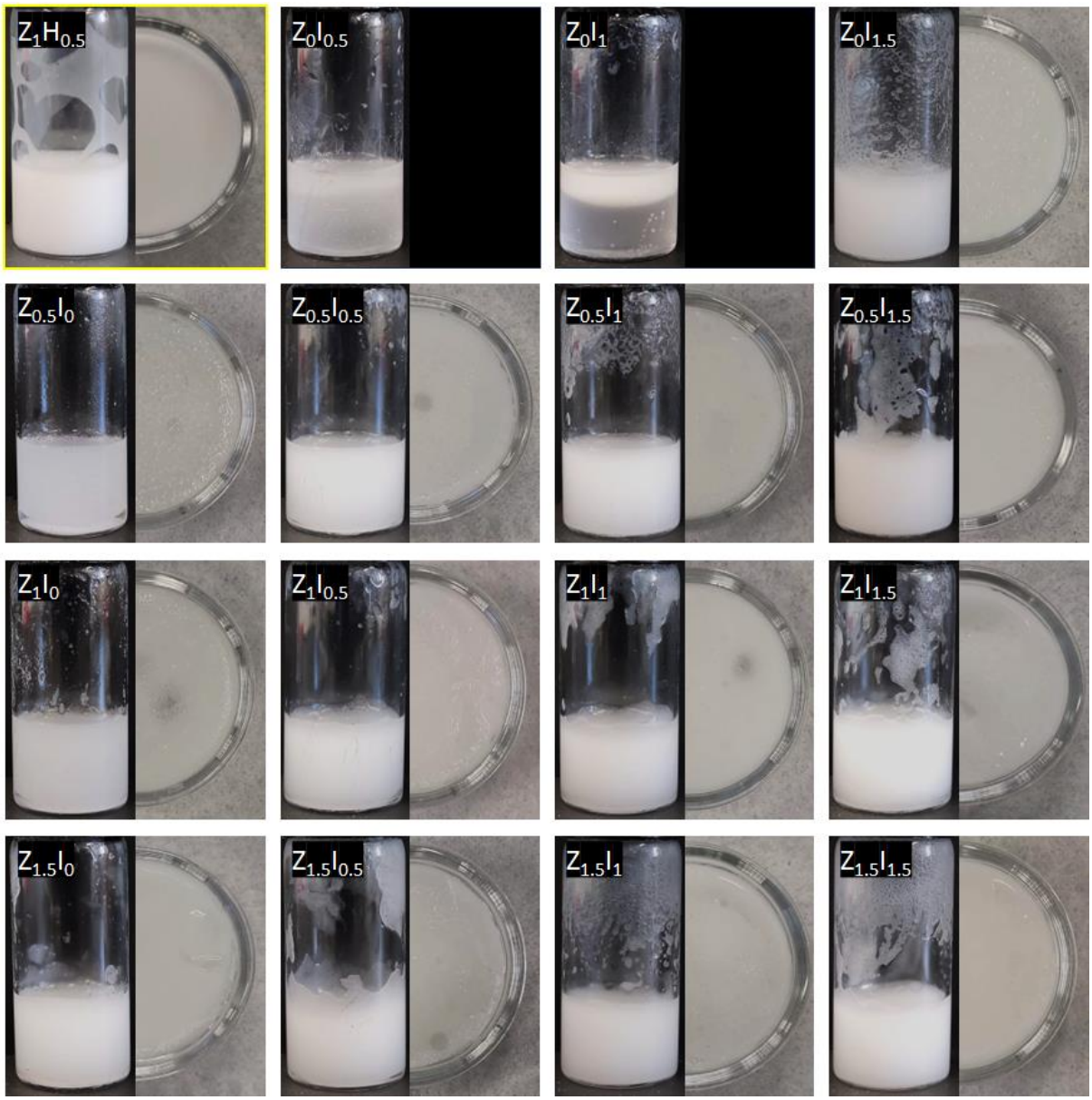

Figure 4.2: Digital images of HIPEs and PolyHIPEs. HIPEs are imaged 5 minutes after being prepared, while the PolyHIPEs are imaged immediately. Images are organized left to right with increasing IBOA content and top to bottom with increasing ZIF-8 content. Hypermer B246 is an exception and therefore framed yellow.

4.4.3. PolyHIPEs

The SEM images demonstrating the overall porous structure of each PolyHIPE sample are provided in Figure 4.3. ZIF-8 as a sole stabilizer provided a closed cellular porous morphology. The rare pore throats observed in the images are non-spherical, and they most probably formed during the post-processing-induced rupturing of the thinner regions of pores. The incorporation of IBOA particles as a co-stabilizer introduced spherical pore throats, due to the previously explained pore throat formation mechanism involving the arrested coalescence of emulsion droplets [65].

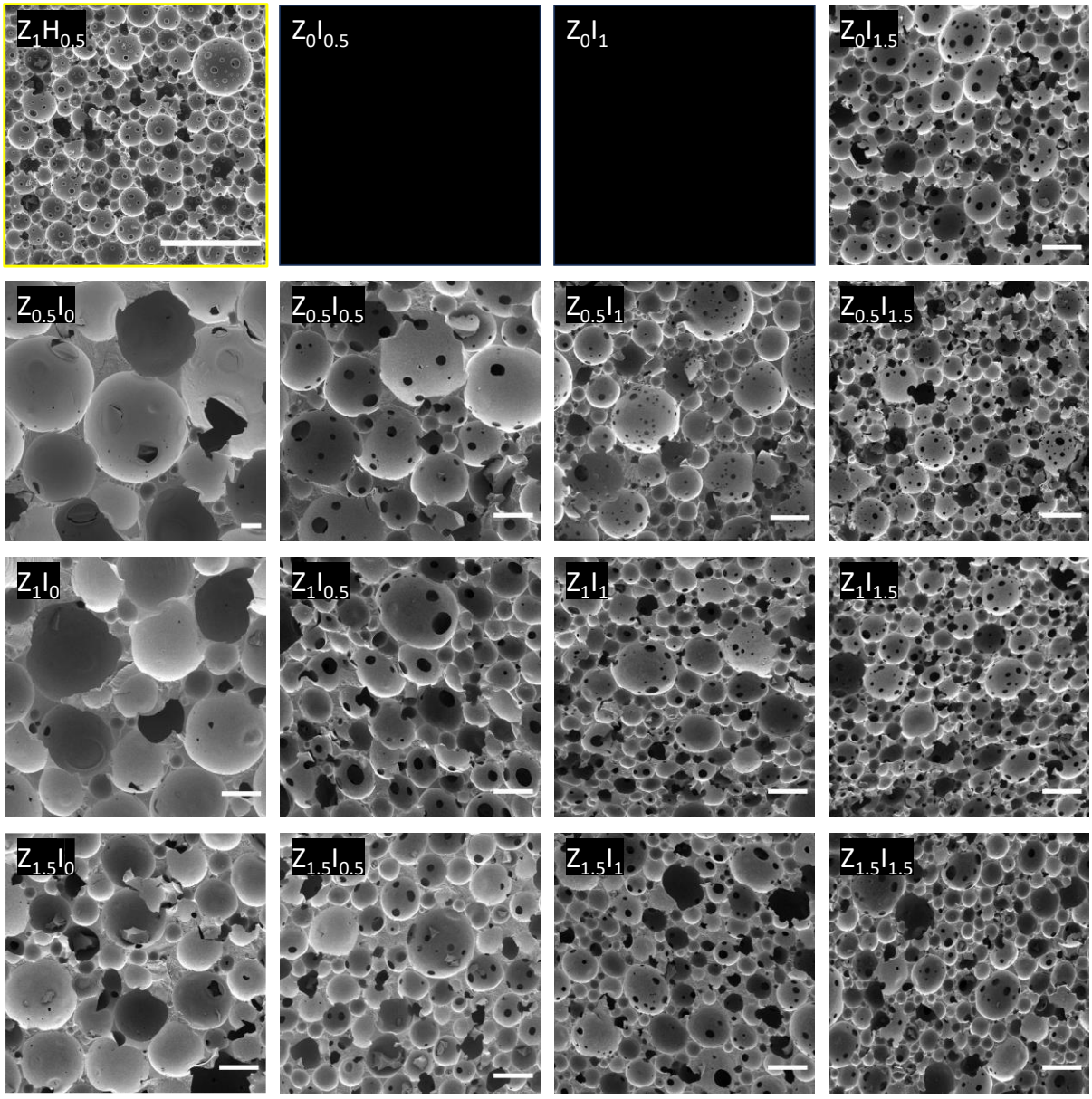

Figure 4.3: SEM images of PolyHIPEs demonstrating the overall porous structure. Scale bars are 200 µm.

The pore size of the samples as a function of stabilizer concentrations is provided in Figure 4.4. When the HIPE is stabilized solely by ZIF-8, the increase in stabilizer concentration resulted in a decrease in the pore size in PolyHIPEs. When both particles are used as dual stabilizers, the increase in ZIF-8 concentration results in a decrease in pore size when the IBOA particle concentration was as low as 0.5 wt%. However, the ZIF-8 concentration did not significantly affect the pore size, especially when the IBOA concentration was 1.5 wt%, where the average pore size of $I_{1.5}$ samples ranged from 109 to 96 µm. In contrast, the addition of IBOA particles significantly affected the pore size of PolyHIPEs, even in $Z_{1.5}$ samples, where the pore size was reduced from 183 to 96 µm as the IBOA concentration increased from 0 to 1.5 wt%. Therefore, it can be concluded that IBOA functions as the main stabilizer in the given dual stabilizer system. On the other hand, it is important to note that there is a density

difference between the particles, where ZIF-8 and IBOA particles have densities of ~1.25 and ~1 g/cm³, respectively, meaning that the same wt% changes in stabilizer concentration result in the presence of a higher number of IBOA particles than that of ZIF-8.

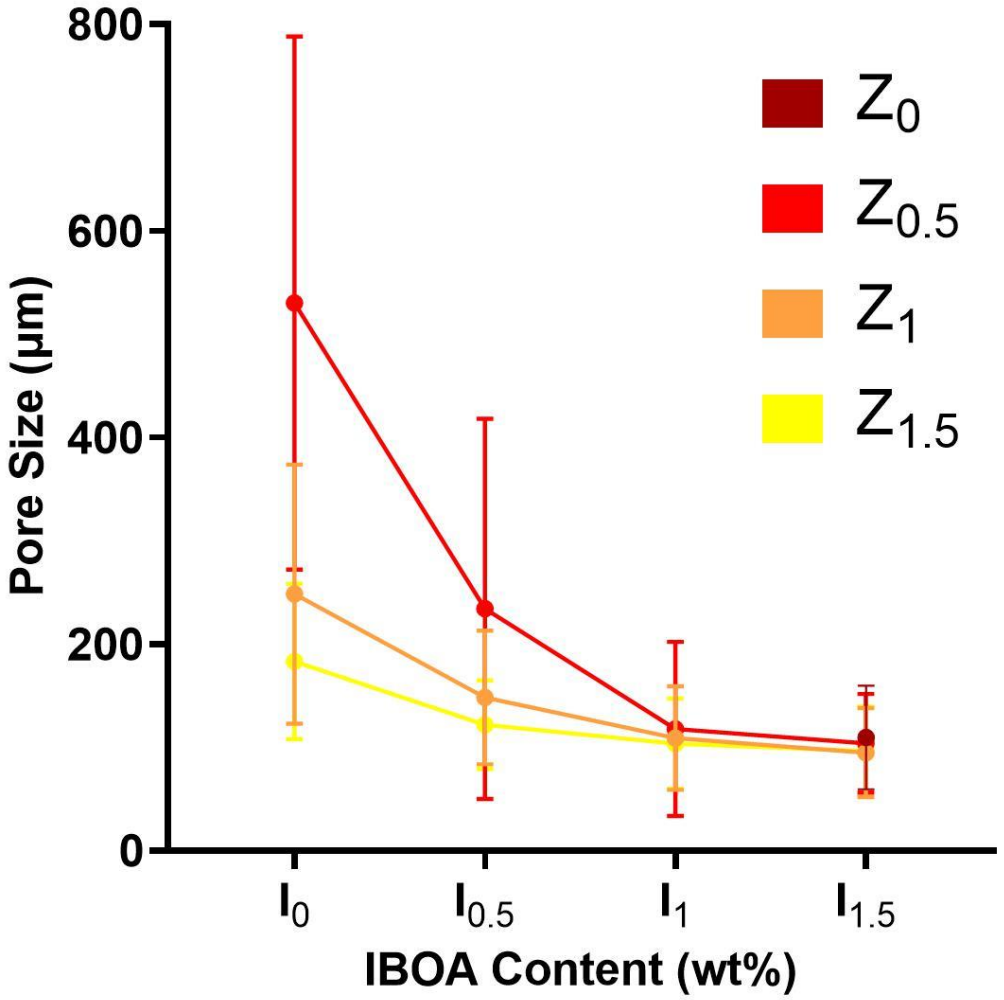

Figure 4.4: Pore size changes in PolyHIPEs as a function of IBOA particle content in the continuous phase for each ZIF-8 content.

The evaluation of pore decoration with ZIF-8 is initially assed by SEM micrographs (Fig. 4.5). The pore surface of $Z_0I_{1.5}$ is smooth; there are rarely observed IBOA particles on the surface. As previously reported, they are generally found around the pore throats since the particle migrate to the necking region of semi-coalesced emulsion droplets, and this necking region represent itself as a pore throat when polymerized. Since the sample does not have any ZIF-8, it was expected to observe smooth pore surface in $Z_0I_{1.5}$.

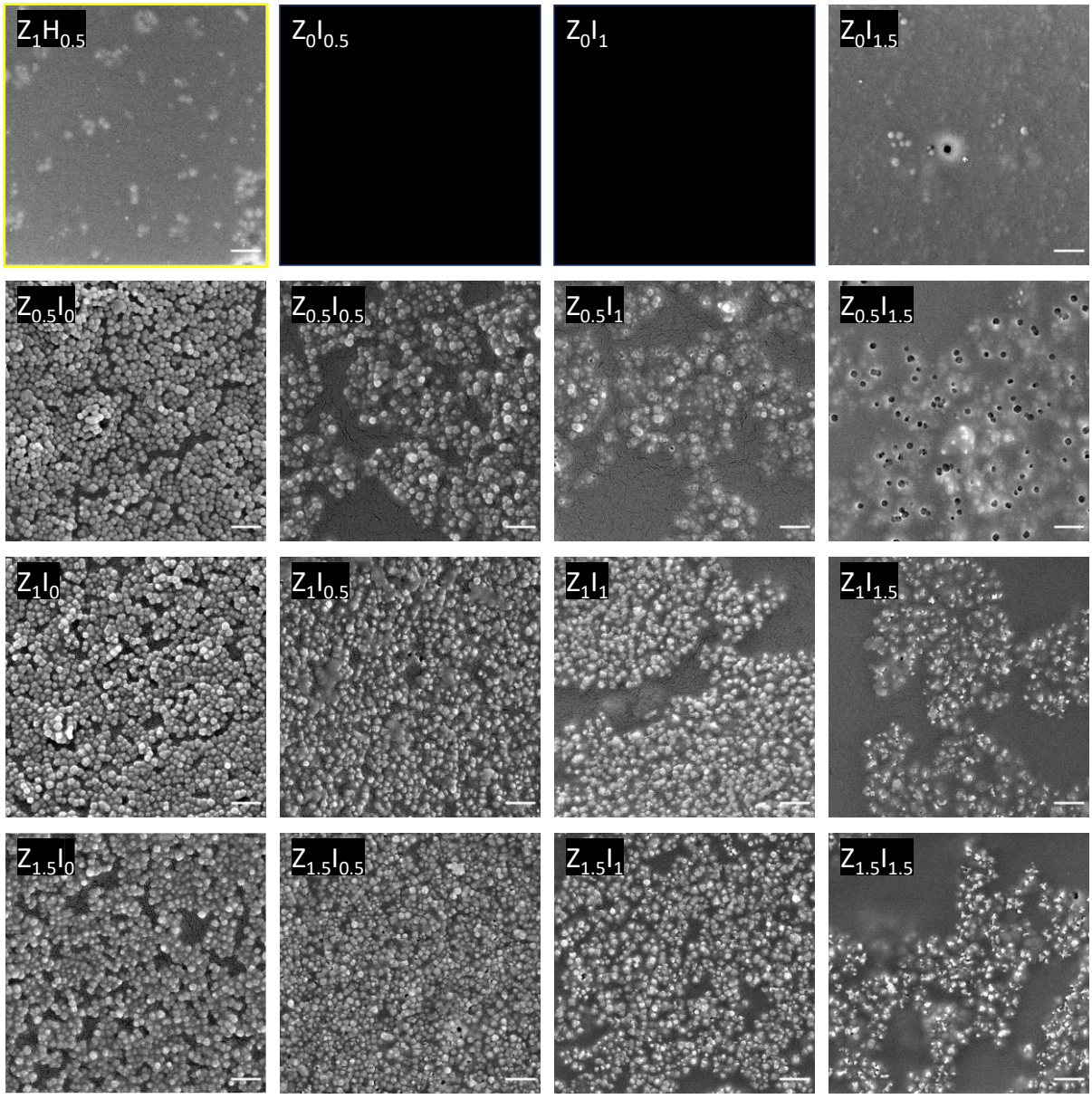

Figure 4.5: The SEM images of the PolyHIPEs focusing on the pore surface. Scale bars are 1 µm.

The incorporation of ZIF-8 as a stabilizer provided ZIF-8 decorated pores in all ZIF-IBOA dual stabilized HIPE templates. It was observed that the increase in IBOA wt% in PolyHIPE, the pore surfaces become scarcely decorated with ZIF-8. Interestingly, in Z0.5I1.5 samples, holes with ~200 nm diameter were frequently observed. This might be due to exhibiting smaller average pore size (104 µm) compared to samples with less IBOA wt% (I0, I0.5 and I1 samples) and containing less amount of ZIF-8 compared the other I1.5 samples. Highly concentrated IBOA particles might have functioned faster to stabilize emulsion and therefore, ZIF-8 particles might have poorly localized at the interface. Therefore, ZIF-8 particles poorly embedded on the pore surface might have washed out during washing steps of the samples, and the removed ZIF-8 might have left behind holes on the pore surface with the same size of ZIF-8 particles. In the case of ZIF-8-Hypermer B246 sample (Z1H0.5) the pore surface exhibit roughness, but it is hard to evaluate if it is deeply embedded ZIF-8 particles on the pore surface or the

leftover surfactant. Since, PolyHIPE obtained from HIPE solely stabilized with Hypermer B246 exhibit similar pore surface as well (Figure 4.6).

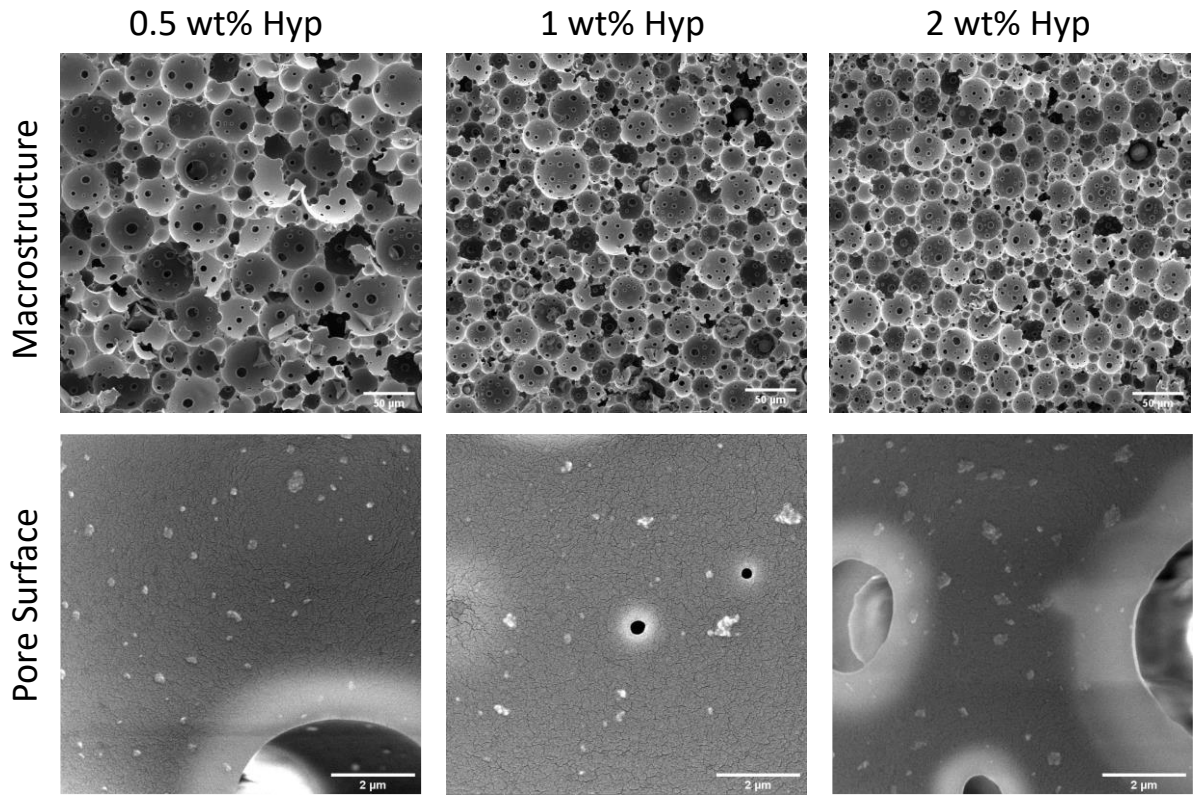

Figure 4.6: PolyHIPEs obtained from HIPEs solely stabilized by 0.5, 1 and 2 wt% Hypermer B246, focusing on both macrostructure and the pore surface. The remnants can be seen on pore surface, which is similar to $Z_1H_{0.5}$.

4.4.4. Validation of Pore Decoration with ZIF-8

The rest of the experiments were conducted on four chosen samples. Samples with only ZIF-8 (Z_1I_0), ZIF-8/IBOA dual emulsified ($Z_1I_{0.5}$), ZIF-8/Hypermer B246 dual emulsified ($Z_1H_{0.5}$) and with only IBOA ($Z_0I_{1.5}$). All the chosen samples were prepared with the same amount of ZIF-8, except $Z_0I_{1.5}$, which was used as a negative control. Hypermer B246 was also added into this experimental setup to compare the efficacy of stabilizers (surfactant vs particle) on ZIF-8 decoration of PolyHIPE pores.

TGA analysis was conducted on the chosen PolyHIPE samples as well as ZIF-8. ZIF-8 exhibited thermal stability up to 500°C (Fig. 4.7), which corresponds well with the previous reports [195]. Similarly, TGA profile of PolyHIPEs composed of EHA/IBOA/TMPTA corresponds well with the previous report [180]. ZIF-8 free PolyHIPE sample ($Z_0I_{1.5}$) left approximately ~2 wt% ash while the ZIF-8 included samples left ~4 wt%. However, the difference in remnant wt% between ZIF-8 free and ZIF-8 loaded samples is higher than the amount of loaded ZIF-8 during synthesis (~1 wt%). Considering that only 35 wt% ZIF-8 is left at the end of 800°C, the leftover of ZIF-8 including PolyHIPE samples should be 2.35 wt%.

Although the leftover wt% do not exaclty match, it can be used as an indication as a presence of ZIF-8 in ZIF-8 loaded PolyHIPE samples.

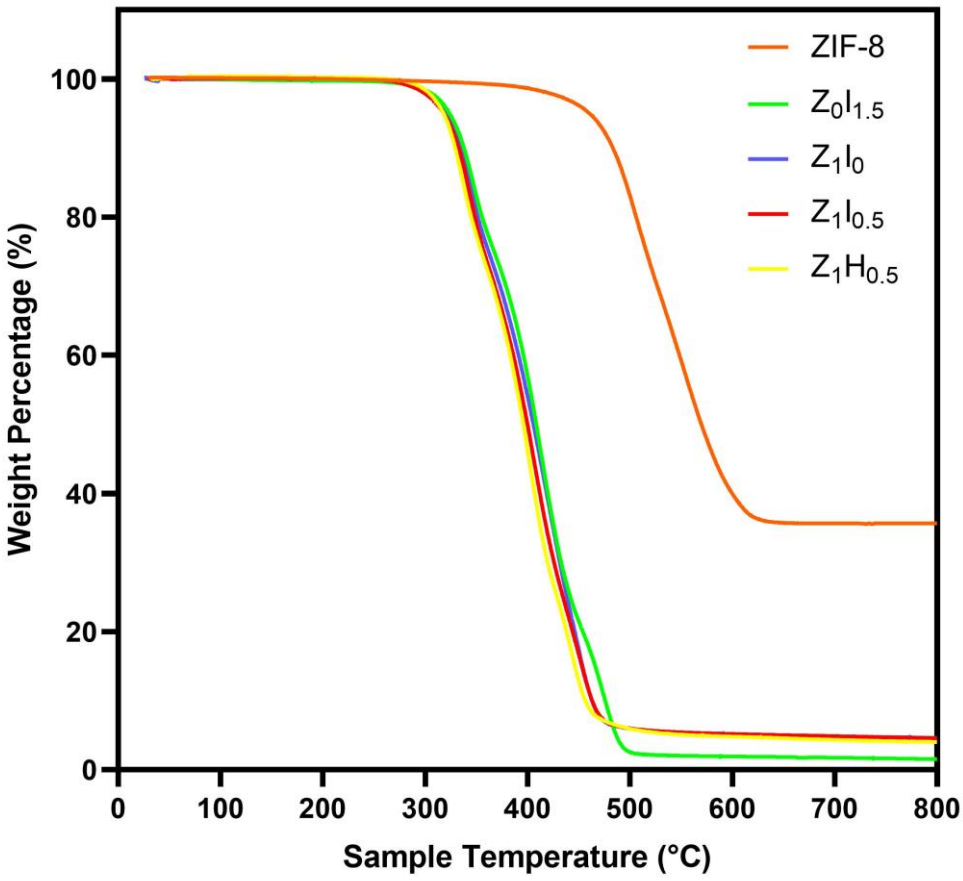

Figure 4.7: TGA curves of ZIF-8 and the chosen PolyHIPE samples provided as weight percentage as a function of sample temperature.

Additionally, EDX was conducted to verify and quantify the presence of ZIF-8. The elemental (O and Zn) map of PolyHIPEs as well as the comparison of O and Zn wt% obtained from the EDX analysis are provided Figure 4.8. Since there was no ZIF-8 in the formulation of $Z_0I_{1.5}$, it was not expected to any Zn signal to be observed in elemental map. For the rest of the samples, it can be seen that the ZIF-8 is mainly located on the pore walls, verifying that the observed particles in SEM images was indeed ZIF-8. Since the samples were coated with carbon, C was omitted during the comparison of elemental wt%. Therefore, the amount of Zn was compared with O. Both Z_1I_0 and $Z_1I_{0.5}$ exhibit the same ratio of Zn compared to oxygen, 20/80 wt%. On the other hand, $Z_1H_{0.5}$ exhibit 10/90 wt% (Fig. 4.8). The reduced zinc content in $Z_1H_{0.5}$ also verifies the hardly identified ZIF-8 particles through SEM micrographs on $Z_1H_{0.5}$ pore surface.

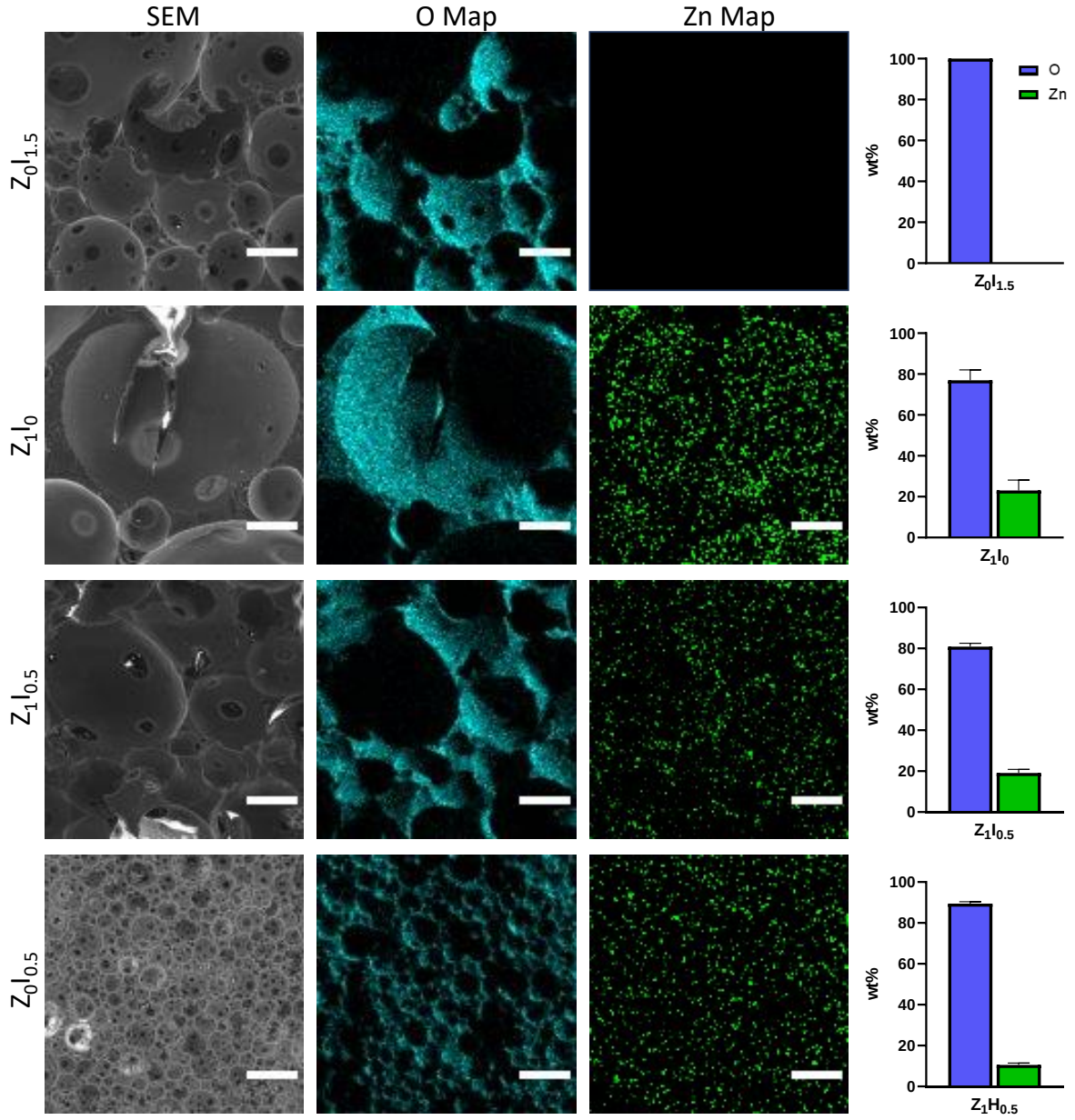

Figure 4.8: SEM micrographs of the chosen samples and both oxygen and zinc mapping on the corresponding SEM image. The comparison of O and Zn wt% for each samples, obtained from EDX measurement.

4.5. Conclusion

In this study, the efficacy of ZIF-8 pore decoration of PolyHIPE with sole ZIF-8 and ZIF-8 together with IBOA particles and the surfactant Hypermer B246 was investigated through SEM, TGA, and EDX analysis. It was observed that a low amount of IBOA particles as a co-stabilizer was sufficient to obtain an interconnected and ZIF-8 decorated porous structure. On the other hand, the ZIF-8/Hypermer B246 system resulted in a reduced loading of ZIF-8 onto the pore surface. This is attributed to the

antagonistic effect between ZIF-8 and Hypermer as a dual emulsifier. The obtained ZIF-8/IBOA Pickering HIPE template might be used as a CO_2 adsorbent and is expected to perform better than only ZIF-8 stabilized Pickering HIPE template thanks to its interconnected porous structure. Additionally, the obtained system can be used further to prepare ZIF-8@CarboHIPE, since the polymeric skeleton of PolyHIPE is degraded at 500 ^{o}C while the ZIF-8 is still thermally stable.

CHAPTER 5

Conclusion

A novel mechanism for pore throat formation in Pickering PolyHIPEs is presented in this study, and key parameters affecting pore openness are explored. The mechanism is subsequently employed to create interconnected Pickering PolyHIPEs decorated with functional ZIF-8 particles.

Originally, the aim was to prepare Pickering PolyHIPEs derived from HIPE, stabilized by synthetically produced polymeric particles with a chemical composition similar to the PolyHIPE skeleton. However, interconnected pores were unexpectedly obtained, prompting a new research question: why are these Pickering PolyHIPEs interconnected? Consequently, the focus of the thesis shifted towards investigating the mechanism behind pore throat formation.

First, the IBOA-stabilized HIPE exhibited rheological properties between conventional surfactant-stabilized HIPE and silica-stabilized HIPE. Microscopic analysis revealed larger pores than conventional HIPE and smaller pores than conventional Pickering HIPE, with occasional semi-coalesced emulsion droplets observed in IBOA-stabilized Pickering HIPE. In the PolyHIPE structure, IBOA particles were primarily found around the pore throats, indicating that the observed particle layers between pores indeed constituted pore throats from a transverse perspective. These observations aligned with the previously reported arrested coalescence mechanism in Pickering emulsion droplets, leading to the hypothesis that pore throat formation results from the arrested coalescence of emulsion droplets due to IBOA particle jamming at the necking region of semi-coalesced emulsion droplets. Parameters known to affect arrested coalescence, such as particle size, concentration, and the internal phase volume of HIPE, were then tested, and the results corroborated the literature, supporting arrested coalescence as a possible pore throat formation mechanism in Pickering PolyHIPEs.

Furthermore, the impact of particle hydrophilicity on Pickering PolyHIPE morphology was investigated. By tuning the cross-linker content in the particles, the effect of hydrophilicity was explored. Non-crosslinked IBOA particles dissolved in the continuous phase of the emulsion and acted as macro-molecular surfactants instead of Pickering stabilizers. Conversely, using solely TMPTA, a water-dispersible particle, yielded the classical Pickering PolyHIPE morphology with large, closed cells. This highlighted the influence of particle hydrophilicity on Pickering PolyHIPE openness.

Based on the previous findings, the hypothesis was formulated that interconnected and hydrophilic particle-decorated pores could be achieved by using both hydrophobic IBOA and water-dispersible ZIF-8 particles as dual stabilizers. Particles with various concentrations were tested to stabilize HIPE and

evaluate their morphology and surface decoration efficacy. Indeed, interconnected and ZIF-8-decorated pores in Pickering PolyHIPEs were obtained. A comparative experiment using surfactant-ZIF-8 dual stabilization, a common method for obtaining interconnected and particle-decorated Pickering PolyHIPEs, was also conducted. However, when surfactant was used, ZIF-8 loading on the surface of PolyHIPE pores was reduced, in line with the previously reported antagonistic effect between surfactants and colloidal particles.

While this study aimed to characterize the surface area of the obtained PolyHIPEs and their CO2 capture performance, these aspects remain to be finalized in the near future.

In summary, a new understanding of pore throat formation in Pickering PolyHIPEs is contributed by this thesis, an area that had been debated in conventional PolyHIPEs. However, there are still important parameters requiring investigation to further elucidate the proposed mechanisms, such as the chemical similarity between particles and the continuous emulsion phase, polymerization-induced forces, and particle mechanical properties. With recent advances in metal-organic frameworks (MOFs), increased attention on Pickering PolyHIPEs as excellent candidates for MOF support in various applications is anticipated.

APPENDIX

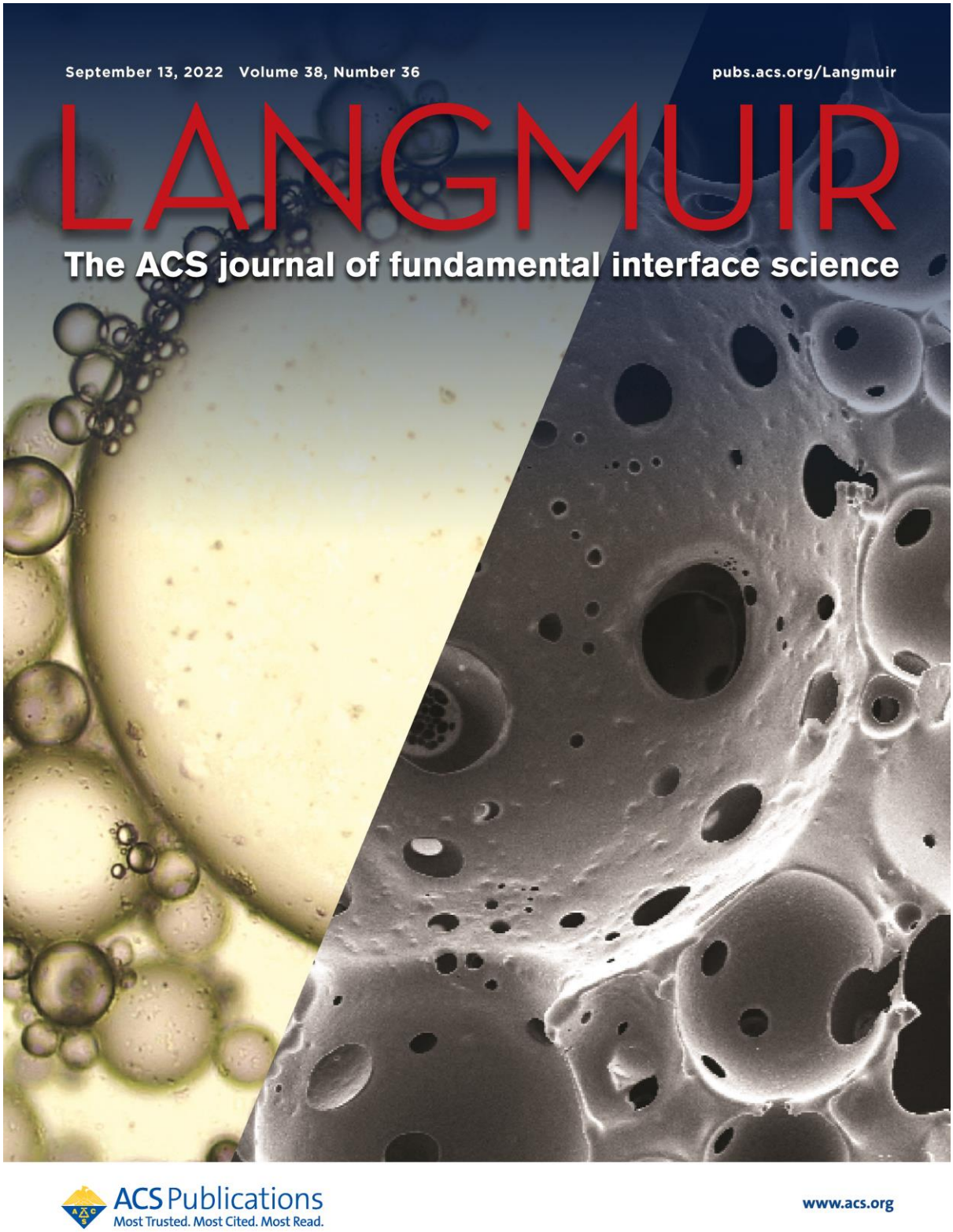
September 13, 2022 Volume 38, Number 36
pubs.acs.org/Langmuir
LANGMUIR
The ACS journal of fundamental interface science
ACS Publications
Most Trusted. Most Cited. Most Read.
www.acs.org

REFERENCES

[1] M.S. Silverstein, PolyHIPEs: Recent advances in emulsion-templated porous polymers, Prog. Polym. Sci. 39 (2014) 199–234. https://doi.org/10.1016/j.progpolymsci.2013.07.003.

[2] N.R. Cameron, High internal phase emulsion templating as a route to well-defined porous polymers, Polymer (Guildf). 46 (2005) 1439–1449. https://doi.org/10.1016/j.polymer.2004.11.097.

[3] B. Aldemir Dikici, F. Claeyssens, Basic Principles of Emulsion Templating and Its Use as an Emerging Manufacturing Method of Tissue Engineering Scaffolds, Front. Bioeng. Biotechnol. 8 (2020). https://doi.org/10.3389/fbioe.2020.00875.

[4] L.E. Low, S.P. Siva, Y.K. Ho, E.S. Chan, B.T. Tey, Recent advances of characterization techniques for the formation, physical properties and stability of Pickering emulsion, Adv. Colloid Interface Sci. 277 (2020) 102117. https://doi.org/10.1016/j.cis.2020.102117.

[5] C. Albert, M. Beladjine, N. Tsapis, E. Fattal, F. Agnely, N. Huang, Pickering emulsions: Preparation processes, key parameters governing their properties and potential for pharmaceutical applications, J. Control. Release. 309 (2019) 302–332. https://doi.org/10.1016/j.jconrel.2019.07.003.

[6] A.M. Bago Rodriguez, B.P. Binks, High internal phase Pickering emulsions, Curr. Opin. Colloid Interface Sci. 57 (2022). https://doi.org/10.1016/j.cocis.2021.101556.

[7] J. Boyd, C. Parkinson, P. Sherman, Factors affecting emulsion stability, and the HLB concept, J. Colloid Interface Sci. 41 (1972) 359–370. https://doi.org/10.1016/0021-9797(72)90122-1.

[8] P. Walstra, Principles of emulsion formation, Chem. Eng. Sci. 48 (1993) 333–349. https://doi.org/https://doi.org/10.1016/0009-2509(93)80021-H.

[9] W. Ramsden, F. Gotch, Separation of solids in the surface-layers of solutions and 'suspensions' (observations on surface-membranes, bubbles, emulsions, and mechanical coagulation).—Preliminary account, Proc. R. Soc. London. 72 (1904) 156–164. https://doi.org/10.1098/rspl.1903.0034.

[10] S.U. Pickering, Cxcvi.—emulsions, J. Chem. Soc. Trans. 91 (1907) 2001–2021.

[11] P.J. Colver, S.A.F. Bon, Cellular Polymer Monoliths Made via Pickering High Internal Phase Emulsions, (2007) 1537–1539.

[12] B.R. Midmore, COLLOIDS AND A SURFACES Preparation of a novel silica-stabilized oil/water emulsion, Colloids Surfaces A Physicochem. Eng. Asp. 132 (1998) 257–265.

[13] N. Bizmark, M.A. Ioannidis, Nanoparticle-stabilised emulsions: Droplet armouring: Vs. droplet bridging, Soft Matter. 14 (2018) 6404–6408. https://doi.org/10.1039/c8sm00938d.

[14] S. Arditty, C.P. Whitby, B.P. Binks, V. Schmitt, P HYSICAL J OURNAL E Some general features of limited coalescence in solid-stabilized, 281 (2003) 273–281. https://doi.org/10.1140/epje/i2003-10018-6.

[15] A.B. Pawar, M. Caggioni, R. Ergun, W. Hartel, P.T. Spicer, Arrested coalescence in Pickering emulsions †, (2011) 7710–7716. https://doi.org/10.1039/c1sm05457k.

[16] F. Matter, A.L. Luna, M. Niederberger, From colloidal dispersions to aerogels: How to master nanoparticle gelation, Nano Today. 30 (2020) 100827. https://doi.org/10.1016/j.nantod.2019.100827.

[17] K. Kim, S. Kim, J. Ryu, J. Jeon, S.G. Jang, H. Kim, D.G. Gweon, W. Bin Im, Y. Han, H. Kim, S.Q. Choi, Processable high internal phase Pickering emulsions using depletion attraction, Nat. Commun. 8 (2017) 1–8. https://doi.org/10.1038/ncomms14305.

[18] D.J. McClements, Critical review of techniques and methodologies for characterization of emulsion stability, Crit. Rev. Food Sci. Nutr. 47 (2007) 611–649. https://doi.org/10.1080/10408390701289292.

[19] I.B. Ivanov, K.D. Danov, P.A. Kralchevsky, Flocculation and coalescence of micron-size emulsion droplets, 152 (1999) 161–182.

[20] M.B.J. Meinders, T. Van Vliet, The role of interfacial rheological properties on, 109 (2004) 119–126. https://doi.org/10.1016/j.cis.2003.10.005.

[21] N. Aubry, Destabilization of Pickering emulsions using external electric fields, (2010) 850–859. https://doi.org/10.1002/elps.200900574.

[22] C. Griffith, H. Daigle, Journal of Colloid and Interface Science Destabilizing Pickering emulsions using fumed silica particles with different wettabilities, J. Colloid Interface Sci. 547 (2019) 117–126. https://doi.org/10.1016/j.jcis.2019.03.048.

[23] H. Kumar, S. Upendar, E. Mani, M.G. Basavaraj, Journal of Colloid and Interface Science Destabilization of Pickering emulsions by interfacial transport of mutually soluble solute, J. Colloid Interface Sci. 633 (2023) 166–176. https://doi.org/10.1016/j.jcis.2022.10.133.

[24] P. Rajinder, Yield stress and viscoelastic properties of high internal phase ratio emulsions, Colloid Polym. Sci. 277 (1999) 583–588. https://doi.org/10.1007/s003960050429.

[25] X. Li, X. Xu, L. Song, A. Bi, C. Wu, Y. Ma, M. Du, B. Zhu, High Internal Phase Emulsion for Food-Grade 3D Printing Materials, ACS Appl. Mater. Interfaces. 12 (2020) 45493–45503. https://doi.org/10.1021/acsami.0c11434.

[26] H. Gao, L. Ma, C. Cheng, J. Liu, R. Liang, L. Zou, W. Liu, D.J. McClements, Review of recent advances in the preparation, properties, and applications of high internal phase emulsions, Trends Food Sci. Technol. 112 (2021) 36–49. https://doi.org/10.1016/j.tifs.2021.03.041.

[27] K.J. Lissant, The geometry of high-internal-phase-ratio emulsions, J. Colloid Interface Sci. 22 (1966) 462–468. https://doi.org/https://doi.org/10.1016/0021-9797(66)90091-9.

[28] A. Menner, V. Ikem, M. Salgueiro, M.S.P. Shaffer, A. Bismarck, High internal phase emulsion templates solely stabilised by functionalised titania nanoparticles, Chem. Commun. c (2007) 4274–4276. https://doi.org/10.1039/b708935j.

[29] B.P. Binks, S.O. Lumsdon, Catastrophic phase inversion of water-in-oil emulsions stabilized by hydrophobie silica, Langmuir. 16 (2000) 2539–2547. https://doi.org/10.1021/la991081j.

[30] P.A. Kralchevsky, I.B. Ivanov, K.P. Ananthapadmanabhan, A. Lips, On the thermodynamics of particle-stabilized emulsions: Curvature effects and catastrophic phase inversion, Langmuir. 21 (2005) 50–63. https://doi.org/10.1021/la047793d.

[31] T.S. Dunstan, P.D.I. Fletcher, S. Mashinchi, High internal phase emulsions: Catastrophic phase inversion, stability, and triggered destabilization, Langmuir. 28 (2012) 339–349. https://doi.org/10.1021/la204104m.

[32] G. Sun, Z. Li, T. Ngai, Inversion of Particle-Stabilized Emulsions to Form High-Internal-Phase Emulsions, Angew. Chemie. 122 (2010) 2209–2212. https://doi.org/10.1002/ange.200907175.

[33] T. Zhang, Z. Xu, Z. Cai, Q. Guo, Phase inversion of ionomer-stabilized emulsions to form high internal phase emulsions (HIPEs), Phys. Chem. Chem. Phys. 17 (2015) 16033–16039. https://doi.org/10.1039/c5cp01157d.

[34] Y. Chen, Z. Wang, D. Wang, N. Ma, C. Li, Y. Wang, Surfactant-Free Emulsions with Erasable Triggered Phase Inversions, Langmuir. 32 (2016) 11039–11042. https://doi.org/10.1021/acs.langmuir.6b03189.

[35] Y. Zou, X. Yang, E. Scholten, Tuning particle properties to control rheological behavior of high internal phase emulsion gels stabilized by zein/tannic acid complex particles, Food Hydrocoll. 89 (2019) 163–170. https://doi.org/10.1016/j.foodhyd.2018.10.037.

[36] J. Song, Y. Sun, H. Wang, M. Tan, Preparation of high internal phase Pickering emulsion by centrifugation for 3D printing and astaxanthin delivery, Food Hydrocoll. 142 (2023) 108840. https://doi.org/10.1016/j.foodhyd.2023.108840.

[37] M. Huang, J. Wang, C. Tan, Tunable high internal phase emulsions stabilized by cross-linking/ electrostatic deposition of polysaccharides for delivery of hydrophobic bioactives, Food Hydrocoll. 118 (2021) 106742. https://doi.org/10.1016/j.foodhyd.2021.106742.

[38] A.Y. Malkin, I. Masalova, P. Slatter, K. Wilson, Effect of droplet size on the rheological properties of highly-concentrated w/o emulsions, Rheol. Acta. 43 (2004) 584–591. https://doi.org/10.1007/s00397-003-0347-2.

[39] R. Pal, Rheology of high internal phase ratio emulsions, Food Hydrocoll. 20 (2006) 997–1005. https://doi.org/10.1016/j.foodhyd.2005.12.001.

[40] C.F. Welch, G.D. Rose, D. Malotky, S.T. Eckersley, Rheology of High Internal Phase Emulsions, Langmuir. 22 (2006) 1544–1550. https://doi.org/10.1021/la052207h.

[41] R. Foudazi, S. Qavi, I. Masalova, A.Y. Malkin, Physical chemistry of highly concentrated emulsions, Adv. Colloid Interface Sci. 220 (2015) 78–91. https://doi.org/10.1016/j.cis.2015.03.002.

[42] S. Arditty, V. Schmitt, J. Giermanska-Kahn, F. Leal-Calderon, Materials based on solid-stabilized emulsions, J. Colloid Interface Sci. 275 (2004) 659–664. https://doi.org/10.1016/j.jcis.2004.03.001.

[43] M. Kaganyuk, A. Mohraz, Role of particles in the rheology of solid-stabilized high internal phase emulsions, J. Colloid Interface Sci. 540 (2019) 197–206. https://doi.org/10.1016/j.jcis.2018.12.098.

[44] A. Langenfeld, V. Schmitt, M.J. Stébé, Rheological behavior of fluorinated highly concentrated reverse emulsions with temperature, J. Colloid Interface Sci. 218 (1999) 522–528. https://doi.org/10.1006/jcis.1999.6427.

[45] S. Zou, Y. Yang, H. Liu, C. Wang, Colloids and Surfaces A : Physicochemical and Engineering Aspects Synergistic stabilization and tunable structures of Pickering high internal phase emulsions by nanoparticles and surfactants, Colloids Surfaces A Physicochem. Eng. Asp. 436

(2013) 1–9. https://doi.org/10.1016/j.colsurfa.2013.06.013.

[46] S. Levine, B.D. Bowen, S.J. Partridge, Stabilization of emulsions by fine particles I. Partitioning of particles between continuous phase and oil/water interface, Colloids and Surfaces. 38 (1989) 325–343. https://doi.org/10.1016/0166-6622(89)80271-9.

[47] J. Rouwkema, N.C. Rivron, C.A. van Blitterswijk, Vascularization in tissue engineering, Trends Biotechnol. 26 (2008) 434–441. https://doi.org/10.1016/j.tibtech.2008.04.009.

[48] A. Barbetta, N.R. Cameron, Morphology and surface area of emulsion-derived (PolyHIPE) solid foams prepared with oil-phase soluble porogenic solvents: Three-component surfactant system, Macromolecules. 37 (2004) 3202–3213. https://doi.org/10.1021/ma035944y.

[49] N.R. Cameron, D.C. Sherrington, Preparation and glass transition temperatures of elastomeric PolyHIPE materials, J. Mater. Chem. 7 (1997) 2209–2212. https://doi.org/10.1039/a702030i.

[50] P. Hainey, I.M. Huxham, B. Rowatt, D.C. Sherrington, L. Tetley, Synthesis and Ultrastructural Studies, of Styrene-Divinylbenzene Polyhipe Polymers, Macromolecules. 24 (1991) 117–121. https://doi.org/10.1021/ma00001a019.

[51] B. Aldemir Dikici, A. Malayeri, C. Sherborne, S. Dikici, T. Paterson, L. Dew, P. Hatton, I. Ortega Asencio, S. MacNeil, C. Langford, N.R. Cameron, F. Claeyssens, Thiolene-and Polycaprolactone Methacrylate-Based Polymerized High Internal Phase Emulsion (PolyHIPE) Scaffolds for Tissue Engineering, Biomacromolecules. 23 (2022) 720–730. https://doi.org/10.1021/acs.biomac.1c01129.

[52] E. Lovelady, S.D. Kimmins, J. Wu, N.R. Cameron, Preparation of emulsion-templated porous polymers using thiol-ene and thiol-yne chemistry, Polym. Chem. 2 (2011) 559–562. https://doi.org/10.1039/c0py00374c.

[53] S. Kramer, P. Krajnc, I. Pulko, Influence of Monomer Structure, Initiation, and Porosity on Mechanical and Morphological Characteristics of Thiol-ene PolyHIPEs, Macromol. Mater. Eng. 2300010 (2023) 1–7. https://doi.org/10.1002/mame.202300010.

[54] P. Dhavalikar, J. Shenoi, K. Salhadar, M. Chwatko, G. Rodriguez-Rivera, J. Cheshire, R. Foudazi, E. Cosgriff-Hernandez, Engineering toolbox for systematic design of polyhipe architecture, Polymers (Basel). 13 (2021). https://doi.org/10.3390/polym13091479.

[55] Y. Hu, X. Gu, Y. Yang, J. Huang, M. Hu, W. Chen, Z. Tong, C. Wang, Facile fabrication of poly(l -Lactic Acid)-Grafted hydroxyapatite/poly(lactic- co -glycolic Acid) scaffolds by pickering high internal phase emulsion templates, ACS Appl. Mater. Interfaces. 6 (2014) 17166–17175.

https://doi.org/10.1021/am504877h.

[56] A. Quell, T. Sottmann, C. Stubenrauch, Diving into the finestructure of macroporous polymer foams synthesized via emulsion templating: A phase diagram study, Langmuir. 33 (2017) 537–542. https://doi.org/10.1021/acs.langmuir.6b03762.

[57] A. Quell, B. De Bergolis, W. Drenckhan, C. Stubenrauch, How the Locus of Initiation Influences the Morphology and the Pore Connectivity of a Monodisperse Polymer Foam, Macromolecules. 49 (2016) 5059–5067. https://doi.org/10.1021/acs.macromol.6b00494.

[58] L. Koch, W. Drenckhan, C. Stubenrauch, Porous polymers via emulsion templating: pore deformation during solidification cannot be explained by an osmotic transport!, Colloid Polym. Sci. 299 (2021) 233–242. https://doi.org/10.1007/s00396-020-04678-5.

[59] L. Koch, S. Botsch, C. Stubenrauch, Emulsion templating: Unexpected morphology of monodisperse macroporous polymers, J. Colloid Interface Sci. 582 (2021) 834–841. https://doi.org/10.1016/j.jcis.2020.08.106.

[60] I. Gurevitch, M.S. Silverstein, Nanoparticle-based and organic-phase-based AGET ATRP polyHIPE synthesis within pickering HIPEs and surfactant-stabilized HIPEs, Macromolecules. 44 (2011) 3398–3409. https://doi.org/10.1021/ma200362u.

[61] S. Kim, J.Q. Kim, S.Q. Choi, K. Kim, Interconnectivity and morphology control of poly-high internal phase emulsions under photo-polymerization, Polym. Chem. 13 (2022) 492–500. https://doi.org/10.1039/d1py01175h.

[62] N.R. Cameron, D.C. Sherrington, L. Albiston, D.P. Gregory, Study of the formation of the open-cellular morphology of poly(styrene/divinylbenzene) polyHIPE materials by cryo-SEM, Colloid Polym. Sci. 274 (1996) 592–595. https://doi.org/10.1007/BF00655236.

[63] A. Menner, A. Bismarck, New evidence for the mechanism of the pore formation in polymerising high internal phase emulsions or why polyHIPEs have an interconnected pore network structure, Macromol. Symp. 242 (2006) 19–24. https://doi.org/10.1002/masy.200651004.

[64] R. Foudazi, HIPEs to PolyHIPEs, React. Funct. Polym. 164 (2021) 104917. https://doi.org/10.1016/j.reactfunctpolym.2021.104917.

[65] E. Durgut, C. Sherborne, B. Aldemir Dikici, G.C. Reilly, F. Claeyssens, Preparation of Interconnected Pickering Polymerized High Internal Phase Emulsions by Arrested Coalescence, Langmuir. (2022). https://doi.org/10.1021/acs.langmuir.2c01243.

[66] V.O. Ikem, A. Menner, T.S. Horozov, A. Bismarck, Highly permeable macroporous polymers synthesized from pickering medium and high internal phase emulsion templates, Adv. Mater. 22 (2010) 3588–3592. https://doi.org/10.1002/adma.201000729.

[67] V.O. Ikem, A. Menner, A. Bismarck, High-porosity macroporous polymers sythesized from titania-particle- stabilized medium and high internal phase emulsions, Langmuir. 26 (2010) 8836–8841. https://doi.org/10.1021/la9046066.

[68] L.L.C. Wong, V.O. Ikem, A. Menner, A. Bismarck, Macroporous polymers with hierarchical pore structure from emulsion templates stabilised by both particles and surfactants, Macromol. Rapid Commun. 32 (2011) 1563–1568. https://doi.org/10.1002/marc.201100382.

[69] Y. Yang, Z. Wei, C. Wang, Z. Tonga, Lignin-based Pickering HIPEs for macroporous foams and their enhanced adsorption of copper(II) ions, Chem. Commun. 49 (2013) 7144–7146. https://doi.org/10.1039/c3cc42270d.

[70] J. Pan, H. Gao, Y. Zhang, J. Zeng, W. Shi, C. Song, Y. Yan, L. Yu, D. Chang, Porous solid acid with high Surface area derived from emulsion templating and hypercrosslinking for efficient one-pot conversion of cellulose to 5-hydroxymethylfurfural, RSC Adv. 4 (2014) 59175–59184. https://doi.org/10.1039/c4ra10383a.

[71] S. Zou, Z. Wei, Y. Hu, Y. Deng, Z. Tong, C. Wang, Macroporous antibacterial hydrogels with tunable pore structures fabricated by using Pickering high internal phase emulsions as templates, Polym. Chem. 5 (2014) 4227–4234. https://doi.org/10.1039/c4py00436a.

[72] S. Tu, C. Zhu, L. Zhang, H. Wang, Q. Du, Pore Structure of Macroporous Polymers Using Polystyrene/Silica Composite Particles as Pickering Stabilizers, Langmuir. 32 (2016) 13159–13166. https://doi.org/10.1021/acs.langmuir.6b03285.

[73] W. Yi, H. Wu, H. Wang, Q. Du, Interconnectivity of Macroporous Hydrogels Prepared via Graphene Oxide-Stabilized Pickering High Internal Phase Emulsions, Langmuir. 32 (2016) 982–990. https://doi.org/10.1021/acs.langmuir.5b04477.

[74] I. Barbara, M. Dourges, Preparation of porous polyurethanes by emulsion-templated step growth polymerization, 132 (2017) 243–251. https://doi.org/10.1016/j.polymer.2017.11.018.

[75] W. Zhu, Y. Zhu, C. Zhou, S. Zhang, Pickering emulsion-templated polymers: Insights into the relationship between surfactant and interconnecting pores, RSC Adv. 9 (2019) 18909–18916. https://doi.org/10.1039/c9ra03186c.

[76] H. Shin, S. Kim, Y.K. Han, K.H. Kim, S.Q. Choi, Preparation of a monolithic and macroporous

superabsorbent polymer via a high internal phase Pickering emulsion template, J. Appl. Polym. Sci. 136 (2019) 1–7. https://doi.org/10.1002/app.48133.

[77] A. Kataruka, S.B. Hutchens, PDMS polymerized high internal phase emulsions (polyHIPEs) with closed-cell, aqueous-filled microcavities, Soft Matter. 15 (2019) 9665–9675. https://doi.org/10.1039/c9sm01732a.

[78] M. Agrawal, A. Yadav, B. Nandan, R.K. Srivastava, Facile synthesis of templated macrocellular nanocomposite scaffold: Via emulsifier-free HIPE-ROP, Chem. Commun. 56 (2020) 12604–12607. https://doi.org/10.1039/d0cc05331g.

[79] Y. Hua, S. Zhang, Y. Zhu, Y. Chu, J. Chen, Hydrophilic Polymer Foams with Well-Defined Open-Cell Structure Prepared from Pickering High Internal Phase Emulsions, (2013) 2181–2187. https://doi.org/10.1002/pola.26588.

[80] H. He, W. Li, M. Lamson, M. Zhong, D. Konkolewicz, C.M. Hui, K. Yaccato, T. Rappold, G. Sugar, N.E. David, K. Damodaran, S. Natesakhawat, H. Nulwala, K. Matyjaszewski, Porous polymers prepared via high internal phase emulsion polymerization for reversible CO2 capture, Polymer (Guildf). 55 (2014) 385–394. https://doi.org/10.1016/j.polymer.2013.08.002.

[81] D. Yin, B. Li, J. Liu, Q. Zhang, Structural diversity of multi-hollow microspheres via multiple Pickering emulsion co-stabilized by surfactant, Colloid Polym. Sci. 293 (2015) 341–347. https://doi.org/10.1007/s00396-014-3401-y.

[82] D. Yin, Y. Guan, B. Li, B. Zhang, Colloids and Surfaces A : Physicochemical and Engineering Aspects Antagonistic effect of particles and surfactant on pore structure of macroporous materials based on high internal phase emulsion, Colloids Surfaces A Physicochem. Eng. Asp. 506 (2016) 550–556. https://doi.org/10.1016/j.colsurfa.2016.06.060.

[83] U. Azhar, C. Huyan, X. Wan, C. Zong, A. Xu, J. Liu, J. Ma, S. Zhang, B. Geng, Porous multifunctional fluoropolymer composite foams prepared via humic acid modified Fe 3 O 4 nanoparticles stabilized Pickering high internal phase emulsion using cationic fluorosurfactant as co-stabilizer, Arab. J. Chem. 12 (2019) 559–572. https://doi.org/10.1016/j.arabjc.2018.04.003.

[84] I.H. Song, D.M. Kim, J.Y. Choi, S.W. Jin, K.N. Nam, H.J. Park, C.M. Chung, Polyimide-based polyHIPEs prepared via pickering high internal phase emulsions, Polymers (Basel). 11 (2019). https://doi.org/10.3390/polym11091499.

[85] R.T. Woodward, F. De Luca, A.D. Roberts, A. Bismarck, High-surface-area, emulsion-templated carbon foams by activation of polyhipes derived from pickering emulsions, Materials (Basel). 9 (2016). https://doi.org/10.3390/ma9090776.

[86] J.M. Blancas Flores, M.G. Pérez García, G. González Contreras, A. Coronado Mendoza, V.H. Romero Arellano, Polydimethylsiloxane nanocomposite macroporous films preparedviaPickering high internal phase emulsions as effective dielectrics for enhancing the performance of triboelectric nanogenerators, RSC Adv. 11 (2020) 416–424. https://doi.org/10.1039/d0ra07934k.

[87] I. Berezovska, K. Kapilov, P. Dhavalikar, E. Cosgriff-hernandez, M.S. Silverstein, Reactive Surfactants for Achieving Open-Cell PolyHIPE Foams from Pickering Emulsions, 2000825 (2021) 1–8. https://doi.org/10.1002/mame.202000825.

[88] A. Vílchez, C. Rodríguez-Abreu, A. Menner, A. Bismarck, J. Esquena, Antagonistic effects between magnetite nanoparticles and a hydrophobic surfactant in highly concentrated pickering emulsions, Langmuir. 30 (2014) 5064–5074. https://doi.org/10.1021/la4034518.

[89] Y. Zhu, Y. Hua, S. Zhang, J. Chen, C.P. Hu, Vinyl ester oligomer crosslinked porous polymers prepared via surfactant-free high internal phase emulsions, J. Nanomater. 2012 (2012). https://doi.org/10.1155/2012/307496.

[90] H. Xu, X. Zheng, Y. Huang, H. Wang, Q. Du, Interconnected Porous Polymers with Tunable Pore Throat Size Prepared via Pickering High Internal Phase Emulsions, Langmuir. 32 (2016) 38–45. https://doi.org/10.1021/acs.langmuir.5b03037.

[91] F. Yi, F. Xu, Y. Gao, H. Li, D. Chen, Macrocellular polymer foams from water in oil high internal phase emulsion stabilized solely by polymer Janus nanoparticles: Preparation and their application as support for Pd catalyst, RSC Adv. 5 (2015) 40227–40235. https://doi.org/10.1039/c5ra01859e.

[92] A. Menner, R. Verdejo, M. Shaffer, A. Bismarck, Particle-Stabilized Surfactant-Free Medium Internal Phase Emulsions as Templates for Porous Nanocomposite Materials :, (2007) 2398–2403.

[93] X. Zheng, Y. Zhang, H. Wang, Q. Du, Interconnected macroporous polymers synthesized from silica particle stabilized high internal phase emulsions, Macromolecules. 47 (2014) 6847–6855. https://doi.org/10.1021/ma501253u.

[94] Z. Zheng, X. Zheng, H. Wang, Q. Du, Macroporous graphene oxide-polymer composite

prepared through pickering high internal phase emulsions, ACS Appl. Mater. Interfaces. 5 (2013) 7974–7982. https://doi.org/10.1021/am4020549.

[95] B. Pang, H. Zhang, M. Schilling, H. Liu, X. Wang, F. Rehfeldt, K. Zhang, High-Internal-Phase Pickering Emulsions Stabilized by Polymeric Dialdehyde Cellulose-Based Nanoparticles, (2020). https://doi.org/10.1021/acssuschemeng.0c01116.

[96] T. Zhang, Z. Xu, Q. Guo, Closed-cell and open-cell porous polymers from ionomer-stabilized high internal phase emulsions, Polym. Chem. 7 (2016) 7469–7476. https://doi.org/10.1039/c6py01725h.

[97] Y. Hua, Y. Chu, S. Zhang, Y. Zhu, J. Chen, Macroporous materials from water-in-oil high internal phase emulsion stabilized solely by water-dispersible copolymer particles, Polymer (Guildf). 54 (2013) 5852–5857. https://doi.org/10.1016/j.polymer.2013.08.055.

[98] Y. Zhu, S. Huan, L. Bai, A. Ketola, X. Shi, X. Zhang, J.A. Ketoja, O.J. Rojas, High Internal Phase Oil-in-Water Pickering Emulsions Stabilized by Chitin Nanofibrils: 3D Structuring and Solid Foam, ACS Appl. Mater. Interfaces. 12 (2020) 11240–11251. https://doi.org/10.1021/acsami.9b23430.

[99] Y. Zhu, R. Zhang, S. Zhang, Y. Chu, J. Chen, Macroporous Polymers with Aligned Microporous Walls from Pickering High Internal Phase Emulsions, Langmuir. 32 (2016) 6083–6088. https://doi.org/10.1021/acs.langmuir.6b00794.

[100] M.S. Silverstein, H. Tai, A. Sergienko, Y. Lumelsky, S. Pavlovsky, PolyHIPE: IPNs, hybrids, nanoscale porosity, silica monoliths and ICP-based sensors, Polymer (Guildf). 46 (2005) 6682–6694. https://doi.org/10.1016/j.polymer.2005.05.022.

[101] K. Rohm, I. Manas-Zloczower, D. Feke, Poly(HIPE) morphology, crosslink density, and mechanical properties influenced by surfactant concentration and composition, Colloids Surfaces A Physicochem. Eng. Asp. 583 (2019) 123913. https://doi.org/10.1016/j.colsurfa.2019.123913.

[102] A. Barbetta, M. Dentini, E.M. Zannoni, M.E. De Stefano, Tailoring the porosity and morphology of gelatin-methacrylate polyHIPE scaffolds for tissue engineering applications, Langmuir. 21 (2005) 12333–12341. https://doi.org/10.1021/la0520233.

[103] E.C.C. Torquato, A.P.N. Brito, R.S. Trovão, M.A. Oliveira, N.S. Smith, M.C.C. Pinto, J.C. Pinto, E.P. Cipolatti, D.M.G. Freire, M.R.C. Marques, L.C. Costa, Synthesis of Porous Polymeric Supports with PolyHIPE Structures Based on Styrene-Divinylbenzene Copolymers, Macromol.

Symp. 394 (2020) 1–7. https://doi.org/10.1002/masy.202000109.

[104] Y. Luo, A.N. Wang, X. Gao, Pushing the mechanical strength of PolyHIPEs up to the theoretical limit through living radical polymerization, Soft Matter. 8 (2012) 1824–1830. https://doi.org/10.1039/c1sm06756g.

[105] A. Barbetta, N.R. Cameron, Morphology and surface area of emulsion-derived (PolyHIPE) solid foams prepared with oil-phase soluble porogenic solvents: Span 80 as surfactant, Macromolecules. 37 (2004) 3188–3201. https://doi.org/10.1021/ma0359436.

[106] N.R. Cameron, D.C. Sherrington, Synthesis and characterization of poly(aryl ether sulfone) PolyHIPE materials, Macromolecules. 30 (1997) 5860–5869. https://doi.org/10.1021/ma961403f.

[107] D. Golub, P. Krajnc, Emulsion templated hydrophilic polymethacrylates. Morphological features, water and dye absorption, React. Funct. Polym. 149 (2020) 104515. https://doi.org/10.1016/j.reactfunctpolym.2020.104515.

[108] R. Foudazi, B. Zhao, P. Gokun, I. Manas-Zloczower, S.J. Rowan, D.L. Feke, The Effect of Shear on the Evolution of Morphology in High Internal Phase Emulsions Used as Templates for Structural and Functional Polymer Foams, ACS Appl. Polym. Mater. 2 (2020) 1579–1586. https://doi.org/10.1021/acsapm.0c00003.

[109] R. Mravljak, O. Bizjak, M. Podlogar, A. Podgornik, Effect of polyHIPE porosity on its hydrodynamic properties, Polym. Test. 93 (2021). https://doi.org/10.1016/j.polymertesting.2020.106590.

[110] R. Riesco, L. Boyer, S. Blosse, P.M. Lefebvre, P. Assemat, T. Leichle, A. Accardo, L. Malaquin, Water-in-PDMS Emulsion Templating of Highly Interconnected Porous Architectures for 3D Cell Culture, ACS Appl. Mater. Interfaces. 11 (2019) 28631–28640. https://doi.org/10.1021/acsami.9b07564.

[111] A. Munive-Olarte, J.J. Hidalgo-Moyle, C. Velasquillo, K. Juarez-Moreno, J.D. Mota-Morales, Boosting cell proliferation in three-dimensional polyacrylates/nanohydroxyapatite scaffolds synthesized by deep eutectic solvent-based emulsion templating, J. Colloid Interface Sci. 607 (2022) 298–311. https://doi.org/10.1016/j.jcis.2021.08.149.

[112] S. Yang, Y. Wang, Y. Jia, X. Sun, P. Sun, Y. Qin, R. Li, H. Liu, C. Nie, Tailoring the morphology and epoxy group content of glycidyl methacrylate-based polyHIPE monoliths via radiation-induced polymerization at room temperature, Colloid Polym. Sci. 296 (2018) 1005–1016.

https://doi.org/10.1007/s00396-018-4307-x.

[113] I. Pulko, P. Krajnc, High internal phase emulsion templating - A path to hierarchically porous functional polymers, Macromol. Rapid Commun. 33 (2012) 1731–1746. https://doi.org/10.1002/marc.201200393.

[114] R. Owen, C. Sherborne, T. Paterson, N.H. Green, G.C. Reilly, F. Claeyssens, Emulsion templated scaffolds with tunable mechanical properties for bone tissue engineering, J. Mech. Behav. Biomed. Mater. 54 (2016) 159–172. https://doi.org/10.1016/j.jmbbm.2015.09.019.

[115] A. Menner, K. Haibach, R. Powell, A. Bismarck, Tough reinforced open porous polymer foams via concentrated emulsion templating, Polymer (Guildf). 47 (2006) 7628–7635. https://doi.org/10.1016/j.polymer.2006.09.022.

[116] S. Huš, P. Krajnc, PolyHIPEs from Methyl methacrylate: Hierarchically structured microcellular polymers with exceptional mechanical properties, Polymer (Guildf). 55 (2014) 4420–4424. https://doi.org/10.1016/j.polymer.2014.07.007.

[117] W.U. Ranting, A. Menner, A. Bismarck, Tough interconnected polymerized medium and high internal phase emulsions reinforced by silica particles, J. Polym. Sci. Part A Polym. Chem. 48 (2010) 1979–1989. https://doi.org/10.1002/POLA.23965.

[118] K. Haibach, A. Menner, R. Powell, A. Bismarck, Tailoring mechanical properties of highly porous polymer foams: Silica particle reinforced polymer foams via emulsion templating, Polymer (Guildf). 47 (2006) 4513–4519. https://doi.org/10.1016/j.polymer.2006.03.114.

[119] U. Azhar, Z. Huo, R. Yaqub, A. Xu, S. Zhang, B. Geng, Non-crosslinked fluorinated copolymer particles stabilized Pickering high internal phase emulsion for fabrication of porous polymer monoliths, Polymer (Guildf). 172 (2019) 160–169. https://doi.org/10.1016/j.polymer.2019.03.068.

[120] B. Jiang, Z. Wang, N. Zhao, Effect of pore size and relative density on the mechanical properties of open cell aluminum foams, Scr. Mater. 56 (2007) 169–172. https://doi.org/10.1016/j.scriptamat.2006.08.070.

[121] S. Huš, M. Kolar, P. Krajnc, Tailoring morphological features of cross-linked emulsion-templated poly(glycidyl methacrylate), Des. Monomers Polym. 18 (2015) 698–703. https://doi.org/10.1080/15685551.2015.1070503.

[122] B. Aldemir Dikici, C. Sherborne, G.C. Reilly, F. Claeyssens, Emulsion templated scaffolds manufactured from photocurable polycaprolactone, Polymer (Guildf). 175 (2019) 243–254.

https://doi.org/10.1016/j.polymer.2019.05.023.

[123] S. Kovačič, E. Žagar, C. Slugovc, Strength versus toughness of emulsion templated Poly(Dicyclopentadiene) foams, Polymer (Guildf). 169 (2019) 58–65. https://doi.org/10.1016/j.polymer.2019.02.045.

[124] T. Li, H. Liu, L. Zeng, S. Yang, Z. Li, J. Zhang, X. Zhou, Macroporous magnetic poly(styrene-divinylbenzene) nanocomposites prepared via magnetite nanoparticles-stabilized high internal phase emulsions, J. Mater. Chem. 21 (2011) 12865–12872. https://doi.org/10.1039/c1jm10799b.

[125] Q. Wang, H. Ma, J. Chen, Z. Du, J. Mi, Interfacial control of polyHIPE with nano-TiO2 particles and polyethylenimine toward actual application in CO2 capture, J. Environ. Chem. Eng. 5 (2017) 2807–2814. https://doi.org/10.1016/j.jece.2017.05.034.

[126] Y. Hu, X. Gu, Y. Yang, J. Huang, M. Hu, W. Chen, Z. Tong, C. Wang, Facile fabrication of poly(l -Lactic Acid)-Grafted hydroxyapatite/poly(lactic- co -glycolic Acid) scaffolds by pickering high internal phase emulsion templates, ACS Appl. Mater. Interfaces. 6 (2014) 17166–17175. https://doi.org/10.1021/am504877h.

[127] H. Dupont, C. Fouché, M.A. Dourges, V. Schmitt, V. Héroguez, Polymerization of cellulose nanocrystals-based Pickering HIPE towards green porous materials, Carbohydr. Polym. 243 (2020) 116411. https://doi.org/10.1016/j.carbpol.2020.116411.

[128] X. Li, G. Sun, Y. Li, J.C. Yu, J. Wu, G.H. Ma, T. Ngai, Porous TiO2 materials through pickering high-internal phase emulsion templating, Langmuir. 30 (2014) 2676–2683. https://doi.org/10.1021/la404930h.

[129] Y. Zhu, Y. Hua, S. Zhang, Y. Wang, J. Chen, Open-cell macroporous bead: a novel polymeric support for heterogeneous photocatalytic reactions, J. Polym. Res. 22 (2015). https://doi.org/10.1007/s10965-015-0703-9.

[130] E. Yüce, E.H. Mert, P. Krajnc, F.N. Parın, N. San, D. Kaya, H. Yıldırım, Photocatalytic Activity of Titania/Polydicyclopentadiene PolyHIPE Composites, Macromol. Mater. Eng. 302 (2017) 1–8. https://doi.org/10.1002/mame.201700091.

[131] J. Lee, J.Y. Chang, A hierarchically porous catalytic monolith prepared from a Pickering high internal phase emulsion stabilized by microporous organic polymer particles, Chem. Eng. J. 381 (2020) 122767. https://doi.org/10.1016/j.cej.2019.122767.

[132] Y. Sun, Y. Zhu, S. Zhang, B.P. Binks, Fabrication of Hierarchical Macroporous ZIF-8 Monoliths

Using High Internal Phase Pickering Emulsion Templates, Langmuir. 37 (2021) 8435–8444. https://doi.org/10.1021/acs.langmuir.1c00757.

[133] H. Gao, Y. Peng, J. Pan, J. Zeng, C. Song, Y. Zhang, Y. Yan, W. Shi, Synthesis and evaluation of macroporous polymerized solid acid derived from Pickering HIPEs for catalyzing cellulose into 5-hydroxymethylfurfural in an ionic liquid, RSC Adv. 4 (2014) 43029–43038. https://doi.org/10.1039/c4ra06870j.

[134] Y. Zhu, W. Wang, H. Yu, A. Wang, Preparation of porous adsorbent via Pickering emulsion template for water treatment: A review, J. Environ. Sci. (China). 88 (2020) 217–236. https://doi.org/10.1016/j.jes.2019.09.001.

[135] N. Vrtovec, S. Jurjevec, N. Zabukovec Logar, M. Mazaj, S. Kovačič, Metal Oxide-Derived MOF-74 Polymer Composites through Pickering Emulsion-Templating: Interfacial Recrystallization, Hierarchical Architectures, and CO2 Capture Performances, ACS Appl. Mater. Interfaces. 15 (2023) 18354–18361. https://doi.org/10.1021/acsami.3c01796.

[136] F. Lorignon, A. Gossard, S. Medjouel, M. Carboni, D. Meyer, Controlling polyHIPE Surface Properties by Tuning the Hydrophobicity of MOF Particles Stabilizing a Pickering Emulsion, ACS Appl. Mater. Interfaces. 15 (2023) 30707–30716. https://doi.org/10.1021/acsami.3c02987.

[137] T. Zhang, Q. Guo, Continuous preparation of polyHIPE monoliths from ionomer-stabilized high internal phase emulsions (HIPEs) for efficient recovery of spilled oils, Chem. Eng. J. 307 (2017) 812–819. https://doi.org/10.1016/j.cej.2016.09.024.

[138] N. Bizmark, X. Du, M.A. Ioannidis, High Internal Phase Pickering Emulsions as Templates for a Cellulosic Functional Porous Material, ACS Sustain. Chem. Eng. 8 (2020) 3664–3672. https://doi.org/10.1021/acssuschemeng.9b06577.

[139] M.W. Abebe, H. Kim, Methylcellulose/tannic acid complex particles coated on alginate hydrogel scaffold via Pickering for removal of methylene blue from aqueous and quinoline from non-aqueous media, Chemosphere. 286 (2022) 131597. https://doi.org/10.1016/j.chemosphere.2021.131597.

[140] X. Li, T. Zhang, J. Lu, Z. Xu, Y. Zhao, Emulsion-Templated, Magnetic, Hydrophilic–Oleophobic Composites for Controlled Water Removal, Langmuir. 38 (2022) 1422–1431. https://doi.org/10.1021/acs.langmuir.1c02583.

[141] N. Cohen, M.S. Silverstein, One-pot emulsion-templated synthesis of an elastomer-filled

hydrogel framework, Macromolecules. 45 (2012) 1612–1621. https://doi.org/10.1021/ma2027337.

[142] C. Warwar Damouny, M.S. Silverstein, Hydrogel-filled, semi-crystalline, nanoparticle-crosslinked, porous polymers from emulsion templating: Structure, properties, and shape memory, Polymer (Guildf). 82 (2016) 262–273. https://doi.org/10.1016/j.polymer.2015.11.040.

[143] T. Yang, Y. Hu, C. Wang, B.P. Binks, Fabrication of Hierarchical Macroporous Biocompatible Scaffolds by Combining Pickering High Internal Phase Emulsion Templates with Three-Dimensional Printing, ACS Appl. Mater. Interfaces. 9 (2017) 22950–22958. https://doi.org/10.1021/acsami.7b05012.

[144] H. Gui, T. Zhang, Q. Guo, Closed-cell, emulsionlated hydrogels for latent heat storage applications, Polym. Chem. 9 (2018) 3970–3973. https://doi.org/10.1039/c8py00785c.

[145] J. Lu, T. Zhang, Z. Xu, X. Yin, Y. Zhao, PolyHIPE Composites for Latent Heat Storage: Flexibility and Enhanced Light to Heat Conversion, ACS Appl. Polym. Mater. (2022). https://doi.org/10.1021/acsapm.2c01027.

[146] B. Li, Q. Chen, G. Dong, D. Yin, Close-cellar shape-stable phase change material monolith prepared by high internal phase Pickering emulsion polymerization, Compos. Part A Appl. Sci. Manuf. 163 (2022) 107143. https://doi.org/10.1016/j.compositesa.2022.107143.

[147] N. Rosen, H. Toledo, M.S. Silverstein, Encapsulating an inorganic phase change material within emulsion-templated polymers: Thermal energy storage and release, Polymer (Guildf). 276 (2023) 125947. https://doi.org/10.1016/j.polymer.2023.125947.

[148] X. Yin, T. Zhang, T. Zhao, K. Wang, Z. Xu, Y. Zhao, Cellulose-based, flexible polyurethane polyHIPEs with quasi-closed-cell structures and high stability for thermal insulation, Carbohydr. Polym. 302 (2023) 120385. https://doi.org/10.1016/j.carbpol.2022.120385.

[149] Y. Zhu, S. Zhang, Y. Hua, H. Zhang, J. Chen, Synthesis of latex particles with a complex structure as an emulsifier of pickering high internal phase emulsions, Ind. Eng. Chem. Res. 53 (2014) 4642–4649. https://doi.org/10.1021/ie404009x.

[150] X. Guan, T. Ngai, pH-Sensitive W/O Pickering High Internal Phase Emulsions and W/O/W High Internal Water-Phase Double Emulsions with Tailored Microstructures Costabilized by Lecithin and Silica Inorganic Particles, 25 (2021). https://doi.org/10.1021/acs.langmuir.0c03658.

[151] J. Liu, P. Wang, Y. He, K. Liu, R. Miao, Y. Fang, Polymerizable Nonconventional Gel Emulsions and Their Utilization in the Template Preparation of Low-Density, High-Strength Polymeric Monoliths and 3D Printing, Macromolecules. 52 (2019) 2456–2463. https://doi.org/10.1021/acs.macromol.8b02610.

[152] Z. Zheng, Y. Zhao, Z. Ye, J. Hu, H. Wang, Journal of Colloid and Interface Science Electrically conductive porous MXene-polymer composites with ultralow percolation threshold via Pickering high internal phase emulsion templating strategy, 618 (2022) 290–299. https://doi.org/10.1016/j.jcis.2022.03.086.

[153] A. Malayeri, C. Sherborne, T. Paterson, S. Mittar, I.O. Asencio, P. V. Hatton, F. Claeyssens, Osteosarcoma growth on trabecular bone mimicking structures manufactured via laser direct write, Int. J. Bioprinting. 2 (2016) 67–77. https://doi.org/10.18063/IJB.2016.02.005.

[154] A. Wang, T. Paterson, R. Owen, C. Sherborne, J. Dugan, J. Li, F. Claeyssens, Photocurable High Internal Phase Emulsions (HIPEs) Containing Hydroxyapatite for Additive Manufacture of Tissue Engineering Scaffolds with Multi-Scale Porosity, Mater. Sci. Eng. C. 67 (2016) 51–58. https://doi.org/10.1016/j.msec.2016.04.087.

[155] B. Aldemir Dikici, S. Dikici, G.C. Reilly, S. MacNeil, F. Claeyssens, A Novel Bilayer Polycaprolactone Membrane for Guided Bone Regeneration: Combining Electrospinning and Emulsion Templating, Materials (Basel). 12 (2019) 2643. https://doi.org/10.3390/ma12162643.

[156] B. Aldemir Dikici, G.C. Reilly, F. Claeyssens, Boosting the osteogenic and angiogenic performance of multiscale porous polycaprolactone scaffolds by in vitro generated extracellular matrix decoration, ACS Appl. Mater. Interfaces. 12 (2020) 12510–12524. https://doi.org/10.1021/acsami.9b23100.

[157] E.M. Christenson, W. Soofi, J.L. Holm, N.R. Cameron, A.G. Mikos, Biodegradable fumarate-based polyHIPEs as tissue engineering scaffolds, Biomacromolecules. 8 (2007) 3806–3814. https://doi.org/10.1021/bm7007235.

[158] G. Akay, M.A. Birch, M.A. Bokhari, Microcellular polyHIPE polymer supports osteoblast growth and bone formation in vitro., Biomaterials. 25 (2004) 3991–4000. https://doi.org/10.1016/j.biomaterials.2003.10.086.

[159] Y. Hu, H. Gao, Z. Du, Y. Liu, Y. Yang, C. Wang, Pickering high internal phase emulsion-based hydroxyapatite-poly(ε-caprolactone) nanocomposite scaffolds, J. Mater. Chem. B. (2015).

https://doi.org/10.1039/c5tb00093a.

[160] I. Gurevitch, M.S. Silverstein, Polymerized pickering HIPEs: Effects of synthesis parameters on porous structure, J. Polym. Sci. Part A Polym. Chem. 48 (2010) 1516–1525. https://doi.org/10.1002/pola.23911.

[161] R. Aveyard, B.P. Binks, J.H. Clint, Emulsions stabilised solely by colloidal particles, 102 (2003) 503–546.

[162] C.Y. Xie, S.X. Meng, L.H. Xue, R.X. Bai, X. Yang, Y. Wang, Z.P. Qiu, B.P. Binks, T. Guo, T. Meng, Light and Magnetic Dual-Responsive Pickering Emulsion Micro-Reactors, Langmuir. 33 (2017) 14139–14148. https://doi.org/10.1021/acs.langmuir.7b03642.

[163] N. Cai, C. Han, X. Luo, G. Chen, Q. Dai, F. Yu, Fabrication of Core/Shell Nanofibers with Desirable Mechanical and Antibacterial Properties by Pickering Emulsion Electrospinning, Macromol. Mater. Eng. 302 (2017) 1–10. https://doi.org/10.1002/mame.201600364.

[164] B.A. Bhanvase, D. V. Pinjari, S.H. Sonawane, P.R. Gogate, A.B. Pandit, Analysis of semibatch emulsion polymerization: Role of ultrasound and initiator, Ultrason. Sonochem. 19 (2012) 97–103. https://doi.org/10.1016/j.ultsonch.2011.05.016.

[165] V.O. Ikem, A. Menner, A. Bismarck, High Internal Phase Emulsions Stabilized Solely by Functionalized Silica Particles ** Zuschriften, (2008) 8401–8403. https://doi.org/10.1002/ange.200802244.

[166] A.R. Studart, H.C. Shum, D.A. Weitz, Arrested coalescence of particle-coated droplets into nonspherical supracolloidal structures, J. Phys. Chem. B. 113 (2009) 3914–3919. https://doi.org/10.1021/jp806795c.

[167] M. Kaganyuk, A. Mohraz, Impact of Particle Size on Droplet Coalescence in Solid-Stabilized High Internal Phase Emulsions, Langmuir. 35 (2019) 12807–12816. https://doi.org/10.1021/acs.langmuir.9b02223.

[168] T. Liu, S. Seiffert, J. Thiele, A.R. Abate, D.A. Weitz, W. Richtering, Non-coalescence of oppositely charged droplets in pH-sensitive emulsions, Proc. Natl. Acad. Sci. U. S. A. 109 (2012) 384–389. https://doi.org/10.1073/pnas.1019196109.

[169] A.M. Munshi, V.N. Singh, M. Kumar, J.P. Singh, Effect of nanoparticle size on sessile droplet contact angle, J. Appl. Phys. 103 (2008). https://doi.org/10.1063/1.2912464.

[170] S. Zhang, J. Chen, PMMA based foams made via surfactant-free high internal phase emulsion

templates, Chem. Commun. (2009) 2217–2219. https://doi.org/10.1039/b819101h.

[171] B.P. Binks, S.O. Lumsdon, Pickering emulsions stabilized by monodisperse latex particles: Effects of particle size, Langmuir. 17 (2001) 4540–4547. https://doi.org/10.1021/la0103822.

[172] H.H. Mert, PolyHIPE composite based-form stable phase change material for thermal energy storage, Int. J. Energy Res. 44 (2020) 6583–6594. https://doi.org/10.1002/er.5390.

[173] S. Dikici, B. Aldemir Dikici, S. Macneil, F. Claeyssens, Decellularised extracellular matrix decorated PCL PolyHIPE scaffolds for enhanced cellular activity, integration and angiogenesis, Biomater. Sci. 9 (2021) 7297–7310. https://doi.org/10.1039/d1bm01262b.

[174] B. Aldemir Dikici, M.C. Chen, S. Dikici, H.C. Chiu, F. Claeyssens, In Vivo Bone Regeneration Capacity of Multiscale Porous Polycaprolactone-Based High Internal Phase Emulsion (PolyHIPE) Scaffolds in a Rat Calvarial Defect Model, ACS Appl. Mater. Interfaces. 15 (2023) 27696–27705. https://doi.org/10.1021/acsami.3c04362.

[175] S. DİKİCİ, Ascorbic Acid Enhances the Metabolic Activity, Growth and Collagen Production of Human Dermal Fibroblasts Growing in Three-dimensional (3D) Culture, Gazi Univ. J. Sci. 36 (2022) 1–1. https://doi.org/10.35378/gujs.1040277.

[176] S.J. Pierre, J.C. Thies, A. Dureault, N.R. Cameron, J.C.M. Van Hest, N. Carette, T. Michon, R. Weberskirch, Covalent enzyme immobilization onto photopolymerized highly porous monoliths, Adv. Mater. 18 (2006) 1822–1826. https://doi.org/10.1002/adma.200600293.

[177] H. Bahmaee, R. Owen, L. Boyle, C.M. Perrault, A.A. Garcia-Granada, G.C. Reilly, F. Claeyssens, Design and Evaluation of an Osteogenesis-on-a-Chip Microfluidic Device Incorporating 3D Cell Culture, Front. Bioeng. Biotechnol. 8 (2020) 1–17. https://doi.org/10.3389/fbioe.2020.557111.

[178] J.P. Hooker, B. Parker, E. Wright, T. Junkers, N.R. Cameron, Photoresponsive Emulsion-Templated Porous Materials via Orthogonal Photoclick Chemistry, ACS Appl. Mater. Interfaces. 15 (2023) 11141–11149. https://doi.org/10.1021/acsami.2c22546.

[179] N. Sengokmen Ozsoz, S. Pashneh-Tala, F. Claeyssens, Optimization of a High Internal Phase Emulsion-Based Resin for Use in Commercial Vat Photopolymerization Additive Manufacturing, 3D Print. Addit. Manuf. (2023). https://doi.org/10.1089/3dp.2022.0235.

[180] N. Sengokmen-Ozsoz, R. Boston, F. Claeyssens, Investigating the Potential of Electroless Nickel Plating for Fabricating Ultra-Porous Metal-Based Lattice Structures Using PolyHIPE Templates, ACS Appl. Mater. Interfaces. 15 (2023) 30769–30779.

https://doi.org/10.1021/acsami.3c04637.

[181] A.F. Stalder, T. Melchior, M. Müller, D. Sage, T. Blu, M. Unser, Low-bond axisymmetric drop shape analysis for surface tension and contact angle measurements of sessile drops, Colloids Surfaces A Physicochem. Eng. Asp. 364 (2010) 72–81. https://doi.org/10.1016/j.colsurfa.2010.04.040.

[182] B. Aldemir Dikici, S. Dikici, F. Claeyssens, Synergistic effect of type and concentration of surfactant and diluting solvent on the morphology of highly porous emulsion templated tissue engineering scaffolds, Colloids Surfaces B Biointerfaces. (2022).

[183] R. Foudazi, I. Masalova, A.Y. Malkin, The rheology of binary mixtures of highly concentrated emulsions: Effect of droplet size ratio, J. Rheol. (N. Y. N. Y). 56 (2012) 1299. https://doi.org/10.1122/1.4736556.

[184] E.S. Lee, D.G. Kim, K.H. Kim, Distinctive rheological properties of Pickering emulsions: from their origin to the applications, Korea Aust. Rheol. J. 34 (2022) 91–103. https://doi.org/10.1007/s13367-022-00018-x.

[185] V.N. Kazakov, E.L. Barkalova, L.A. Levchenko, T.M. Klimenko, V.B. Fainerman, R. Miller, Dilation rheology as medical diagnostics of human biological liquids, Colloids Surfaces A Physicochem. Eng. Asp. 391 (2011). https://doi.org/10.1016/j.colsurfa.2011.03.028.

[186] H. Wang, X. Wei, Y. Du, D. Wang, Experimental investigation on the dilatational interfacial rheology of dust-suppressing foam and its effect on foam performance, Process Saf. Environ. Prot. 123 (2019). https://doi.org/10.1016/j.psep.2019.01.027.

[187] L. Yue, W. Pu, T. Zhao, J. Zhuang, S. Zhao, A high performance magnetically responsive Janus nano-emulsifier: Preparation, emulsification characteristics, interfacial rheology, and application in emulsion flooding, J. Pet. Sci. Eng. 208 (2022). https://doi.org/10.1016/j.petrol.2021.109478.

[188] S. Reynaert, P. Moldenaers, J. Vermant, Interfacial rheology of stable and weakly aggregated two-dimensional suspensions, Phys. Chem. Chem. Phys. 9 (2007). https://doi.org/10.1039/b710825g.

[189] J. Wang, F. Yang, J. Tan, G. Liu, J. Xu, D. Sun, Pickering emulsions stabilized by a lipophilic surfactant and hydrophilic platelike particles, Langmuir. 26 (2010). https://doi.org/10.1021/la903817b.

[190] R. Van Hooghten, V.E. Blair, A. Vananroye, A.B. Schofield, J. Vermant, J.H.J. Thijssen,

Interfacial Rheology of Sterically Stabilized Colloids at Liquid Interfaces and Its Effect on the Stability of Pickering Emulsions, Langmuir. (2017). https://doi.org/10.1021/acs.langmuir.6b04365.

[191] E. Guzmán, L. Liggieri, E. Santini, M. Ferrari, F. Ravera, Effect of hydrophilic and hydrophobic nanoparticles on the surface pressure response of DPPC monolayers, J. Phys. Chem. C. 115 (2011). https://doi.org/10.1021/jp207713x.

[192] M. Zhou, R. Foudazi, Effect of Cosurfactant on Structure and Properties of Polymerized High Internal Phase Emulsions (PolyHIPEs), Langmuir. 37 (2021). https://doi.org/10.1021/acs.langmuir.1c00419.

[193] V. Nozari, C. Calahoo, J.M. Tuffnell, D.A. Keen, T.D. Bennett, L. Wondraczek, Ionic liquid facilitated melting of the metal-organic framework ZIF-8, Nat. Commun. 12 (2021) 1–13. https://doi.org/10.1038/s41467-021-25970-0.

[194] B. Zhang, J. Zhang, C. Liu, L. Peng, X. Sang, B. Han, X. Ma, T. Luo, X. Tan, G. Yang, High-internal-phase emulsions stabilized by metal-organic frameworks and derivation of ultralight metal-organic aerogels, Sci. Rep. 6 (2016) 1–9. https://doi.org/10.1038/srep21401.

[195] K.S. Park, Z. Ni, A.P. Côté, J.Y. Choi, R. Huang, F.J. Uribe-Romo, H.K. Chae, M. O'Keeffe, O.M. Yaghi, Exceptional chemical and thermal stability of zeolitic imidazolate frameworks, Proc. Natl. Acad. Sci. U. S. A. 103 (2006) 10186–10191. https://doi.org/10.1073/pnas.0602439103.

[196] H.U. Escobar-Hernandez, L.M. Pérez, P. Hu, F.A. Soto, M.I. Papadaki, H.C. Zhou, Q. Wang, Thermal Stability of Metal-Organic Frameworks (MOFs): Concept, Determination, and Model Prediction Using Computational Chemistry and Machine Learning, Ind. Eng. Chem. Res. 61 (2022) 5853–5862. https://doi.org/10.1021/acs.iecr.2c00561.

[197] J. Wang, J. Yang, H. Zhu, B.G. Li, S. Zhu, In-situ construction of hierarchically porous MOF monoliths using high internal phase emulsion templates, Chem. Eng. J. 456 (2023) 141026. https://doi.org/10.1016/j.cej.2022.141026.

[198] H. yan Niu, L. qin Cao, X. le Yang, K. nan Liu, L. Liu, J. de Wang, In situ growth of the ZIF-8 on the polymer monolith via CO2-in-water HIPEs stabilized using metal oxide nanoparticles and its photocatalytic activity, Polym. Adv. Technol. 32 (2021) 3194–3204. https://doi.org/10.1002/pat.5331.

[199] M.G. Schwab, I. Senkovska, M. Rose, M. Koch, J. Pahnke, G. Jonschker, S. Kaskel, MOF@PolyHIPEs, Adv. Eng. Mater. 10 (2008) 1151–1155.

https://doi.org/10.1002/adem.200800189.

[200] L.D. O'Neill, H. Zhang, D. Bradshaw, Macro-/microporous MOF composite beads, J. Mater. Chem. 20 (2010) 5720–5726. https://doi.org/10.1039/c0jm00515k.

[201] X. Jiang, H. Pan, G. Ruan, H. Hu, Y. Huang, Z. Chen, Wettability tunable metal organic framework functionalized high internal phase emulsion porous monoliths for fast solid-phase extraction and sensitive analysis of hydrophilic heterocyclic amines, J. Hazard. Mater. 431 (2022) 128565. https://doi.org/10.1016/j.jhazmat.2022.128565.

[202] J. Wang, J. Qin, H. Zhu, B.G. Li, S. Zhu, Hierarchically Porous Monolith with High MOF Accessibility and Strengthened Mechanical Properties using Water-in-Oil High Internal Phase Emulsion Template, Adv. Mater. Interfaces. 8 (2021) 1–8. https://doi.org/10.1002/admi.202100620.

[203] J. Luo, L. Jiang, G. Ruan, C. Li, F. Du, Fabrication and application of a MIL-68(In)-NH2incorporated high internal phase emulsion polymeric monolith as a solid phase extraction adsorbent in triazine herbicide residue analysis, RSC Adv. 11 (2021) 20439–20445. https://doi.org/10.1039/d1ra02619d.

[204] V. Alejandro, C. Rodr, A. Menner, A. Bismarck, J. Esquena, Antagonistic E ff ects between Magnetite Nanoparticles and a Hydrophobic Surfactant in Highly Concentrated Pickering Emulsions, (2014).

[205] D.N. Ta, H.K.D. Nguyen, B.X. Trinh, Q.T.N. Le, H.N. Ta, H.T. Nguyen, Preparation of nano-ZIF-8 in methanol with high yield, Can. J. Chem. Eng. 96 (2018) 1518–1531. https://doi.org/10.1002/cjce.23155.

[206] U. Azhar, M. Arif, M.S. Bashir, M. Babar, M. Sagir, G. Yasin, Functionalized Fe3O4-based methyl methacrylate Pickering PolyHIPE composites costabilized by fluorinated block copolymer for oil/water separation, Chemosphere. 309 (2022) 136526. https://doi.org/10.1016/j.chemosphere.2022.136526.